

2

NUCLEAR MAGNETIC RESONANCE STUDIES
OF
NATURAL PRODUCTS AND RIBONUCLEIC ACIDS

By

DONALD WILLIAM HUGHES, B.Sc.

A Thesis

Submitted to the School of Graduate Studies
in Partial Fulfilment of the Requirements
for the Degree
Doctor of Philosophy

McMaster University

September, 1978

NMR OF NATURAL PRODUCTS AND RIBONUCLEIC ACIDS

DOCTOR OF PHILOSOPHY (1978)
(Chemistry)

McMASTER UNIVERSITY
Hamilton, Ontario

TITLE: Nuclear Magnetic Resonance Studies of Natural Products
and Ribonucleic Acids

AUTHOR: Donald William Hughes, B.Sc. (McMaster University)

SUPERVISORS: Professors D.B. MacLean and R.A. Bell

NUMBER OF PAGES: xv, 156

ABSTRACT

Nuclear magnetic resonance (NMR) spectroscopy has been applied to a number of problems in natural products chemistry and biochemistry.

Natural abundance ^{13}C NMR spectra were used to differentiate the relative stereochemistry of several naturally occurring diastereomers in the phthalideisoquinoline, protoberberine and spirobenzylisoquinoline alkaloids. The data acquired from this study aided the structural elucidation of 10-oxocantrine which is a new compound in the cularine-morphine dimer group of alkaloids.

In order to assess the factors which influence the conformation and base stacking of a dinucleotide, an NMR investigation of the diastereomers of 2'-O-tetrahydropyranylyl[3'-phenyl-5'] and [3'-(2,2,2-trichloroethyl)-5']2'-O-tetrahydropyranylyluridine was undertaken. The steric effect of large substituents on the ribose 2' oxygen was found to be the dominant factor. In addition there is an indication of a stacking interaction between the phenyl ester group and the 5' uracil ring.

Proton nuclear magnetic resonance was utilized to probe the factors which affect the helix-coil transition of several synthetic oligoribonucleotides. The complementary tetranucleotides GpApGpC:GpCpUpC were examined to confirm the correlation between the duplex melting temperature (T_m) obtained by NMR and that from the extrapolation of the UV data. This was also the first ^1H NMR study of a non-self-complementary duplex formed by synthetic tetra-ribonucleotides. The self-complementary

sequences CpApUpG, CpApUpGpU and CpApUpGpA were examined to investigate the effect of unpaired terminal dangling bases on duplex stability. From the T_m of $24 \pm 1^\circ\text{C}$ for CpApUpG, the dangling U in CpApUpGpU causes an increase of $+5.5^\circ\text{C}$ and the dangling A in CpApUpGpA causes an increase of $+11^\circ\text{C}$. A dangling U is similar in effectiveness at stabilizing a short duplex as an internal A-U hydrogen bonded base pair, while a dangling A is more effective. This work represents the first attempt to quantify the effect of a dangling base on ribonucleotide double helix formation.

Much of the work presented in this thesis has been previously reviewed and appears in the literature under the following references:

1. ^{13}C magnetic resonance spectra of some isoquinoline alkaloids and related model compounds.
D.W. Hughes, H.L. Holland, and D.B. MacLean, *Can. J. Chem.*, 54, 2252 (1976).
2. ^{13}C nuclear magnetic resonance spectra of the spirobenzylisoquinoline alkaloids and related model compounds.
D.W. Hughes, B.C. Nalliah, H.L. Holland, and D.B. MacLean, *Can. J. Chem.*, 55, 3304 (1977).
3. Cancentrine V: The ^{13}C magnetic resonance spectra of cancentrine and some derivatives; the structure of 10-oxocancentrine.
Can. J. Chem. In press.
4. Proton magnetic resonance studies on short duplexes. I. Helix formation in the duplex set GpApGpC:GpCpUpC.
D.W. Hughes, R.A. Bell, T.E. England, and T. NEILSON, *Can. J. Chem.*, 56, 2243 (1978).

5. Proton magnetic resonance studies on short duplexes. II.
The self-complementary oligoribonucleotide CpApUpG.
P.J. Romaniuk, T. Neilson, D.W. Hughes, and R.A. Bell.
Can. J. Chem., 56, 2249 (1978).
6. The stabilizing effect of dangling bases on a short RNA double
helix as determined by proton nuclear magnetic resonance
spectroscopy.
P.J. Romaniuk, D.W. Hughes, R.J. Gregoire, T. Neilson, and
R.A. Bell, J. Am. Chem. Soc., 100, 3971 (1978).

ACKNOWLEDGEMENTS

I would like to express my gratitude and appreciation to the following people who have contributed to this thesis.

My parents for their support and encouragement.

Dr's. D.B. MacLean, R.A. Bell, and T. Neilson for their advice and guidance during this project.

Brian G. Sayer for his technical assistance with the NMR spectrometers.

Dr's. Herbert L. Holland and Bala C. Nalliah for their collaboration with the isoquinoline alkaloid work.

Dr. Thomas E. England, Paul J. Romaniuk, and René J. Gregoire of the Department of Biochemistry for their collaboration with the oligoribonucleotide studies.

Fadjar Ramelan for recording the mass spectra and for providing many of the diagrams and photoreductions of the NMR spectra.

Pauline Horridge for typing this manuscript.

The financial assistance of the Department of Chemistry is also acknowledged.

TABLE OF CONTENTS

	Page
DESCRIPTIVE.....	ii
ABSTRACT.....	iii
ACKNOWLEDGEMENTS.....	vi
1. PULSED FOURIER TRANSFORM NMR	
1.1 Historical Introduction.....	1
1.2 Theory of Pulsed NMR.....	3
2. CARBON-13 NMR	
2.1 Introduction.....	
2.2 ¹³ C Chemical Shifts.....	17
2.2.1 ¹³ C Substituent Effects.....	19
2.2.2 Representative ¹³ C Chemical Shifts..	21
2.3 Assignment Techniques in ¹³ C NMR.....	25
3. ¹³ C NMR OF THE ISOQUINOLINE ALKALOIDS	
3.1 Introduction.....	27
3.2 Results and Discussion	
3.2.1 Simple Isoquinolines.....	28
3.2.2 Phthalideisoquinoline Alkaloids.....	33
3.2.3 Protoberberine Alkaloids.....	39
3.2.4 Spirobenzylisoquinoline Alkaloids...	45
3.2.5 Cancentrine Alkaloids.....	59
4. NMR STUDY OF 2'-O-TETRAHYDROPYRANYLURIDYL[3'- PHENYL-5'] AND [3'-(2,2,2-TRICHLOROETHYL)-5'] 2'-O-TETRAHYDROPYRANYLURIDINE	
4.1 Introduction.....	72
4.2 Results and Discussion	
4.2.1 2'-O-Tetrahydropyranyluridine.....	73
4.2.2 2'-O-Tetrahydropyranyluridyl [3'-Phenyl-5'] and [3'-(2,2,2-Tri- chloroethyl)-5'] 2'-O-Tetrahydro- pyranyluridine.....	81

	PAGE
5. PROTON MAGNETIC RESONANCE STUDIES ON SHORT DUPLEXES OF OLIGORIBONUCLEOTIDES	
5.1 Helix Formation in the Duplex Set of GpApGpC:GpCpUpC	
5.1.1 Introduction.....	95
5.1.2 Results.....	97
5.1.3 Discussion.....	104
5.2 The Stabilizing Effect of Dangling Bases on a Short RNA Double Helix	
5.2.1 Introduction.....	109
5.2.2 CpApUpG.....	111
5.2.3 CpApApUpG and CpApUpUpG.....	119
5.2.4 CpApUpGpA and CpApUpGpU.....	128
EXPERIMENTAL.....	140
CONCLUSIONS.....	145
REFERENCES.....	147

LIST OF TABLES

TABLE	PAGE
1. Properties of various magnetic nuclei	16
2. Substituent effects for acyclic hydrocarbons	22
3. Substituent effects in methylcyclohexanes	23
4. Substituent effects in monosubstituted benzenes	24
5. ^{13}C chemical shifts of the simple isoquinolines	30
6. ^{13}C chemical shifts of the phthalideisoquinoline alkaloids	35
7. ^{13}C chemical shifts of phthalide and its derivatives	37
8. ^{13}C chemical shifts of the protoberberine alkaloids	42
9. ^{13}C chemical shifts of the indanones and indandiones	49
<u>34a-39</u>	49
10. ^{13}C chemical shift of the spiro-diones <u>40</u> and <u>41</u>	51
11. ^{13}C chemical shifts of the spirobenzylisoquinoline alkaloids	54
12. ^{13}C chemical shifts of the cancentrine alkaloids	61
13. ^{13}C chemical shifts of the cancentrine model compounds	63
14. 220 MHz ^1H chemical shifts and coupling constants for cancentrine (<u>53a</u>) and 10-oxocancentrine (<u>53b</u>).	67
15. 220 MHz ^1H NMR data for the diastereomers of 2'-O-tetrahydropyranyluridine in DMSO-d_6	75
16. ^{13}C chemical shifts of the diastereomers of 2'-O-tetrahydropyranyluridine and uridine (106)	79
17. Vicinal coupling constants and torsion angles for <u>57</u> , <u>58</u> , and uridine (107)	80

	PAGE
18. ^1H chemical shifts of the phosphotriesters in DMSO- d_6	83
19. ^1H coupling constants (Hz) of the phosphotriesters	84
20. ^{13}C chemical shifts of the phosphotriesters in acetone- d_6	87
21. ^{13}C - ^{31}P coupling constants of the phosphotriesters	88
22. Phosphate torsion angles for the triesters	92
23. Chemical shifts and coupling constants for the derivatives of GAGC, GCUC and duplex at 65°C	99
24. GAGC ribose ring $J_{1',2'}$ coupling constant changes with respect to temperature	101
25. Chemical shifts of the oligoribonucleotides in D_2O at 70°C	112
26. Coupling constants ($J_{1',2'}$) for the oligoribo- nucleotides at 70°C	113
27. Chemical shifts of the oligoribonucleotides in D_2O at 70°C	121
28. Coupling constants ($J_{1',2'}$) of the oligoribo- nucleotides at 70°C	122
29. Chemical shifts of the oligoribonucleotides in D_2O at 70°C	130
30. Coupling constants ($J_{1',2'}$) of the oligoribonucleo- tides at 70°C	131
31. Melting temperatures and concentrations of the base paired duplexes	135

LIST OF FIGURES

FIGURE	PAGE
1. Larmor precession of the nuclear magnetic moment	5
2. The effect of an rf pulse on the magnetization M_0 in the rotating frame	10
3. Block diagram of the Bruker WH-90 pulsed spectrometer with quadrature detection	15
4. ^{13}C chemical shifts	18
5. Structures of the simple isoquinolines	29
6. Structures of the phthalideisoquinoline alkaloids	34
7. Structure of phthalide (<u>16</u>) and its derivatives	36
8. (a) Structures of the protoberberine alkaloids (b) The reduction of berberine chloride to (+)-canadine-8,14- d_2	41
9. Comparison of the ^{13}C chemical shifts of the aliphatic carbons of mesocorydaline (<u>25</u>) and compound <u>28</u> (<u>60</u>)	44
10. ^{13}C chemical shifts of the indanes <u>29-33</u> and methylene-cyclopentane (<u>31</u>) (<u>74</u>)	47
11. Structures of the indanones and indandiones <u>34a-39</u>	48
12. Structures of the spiro-diones <u>40</u> and <u>41</u>	51
13. Structures of the spirobenzylisoquinoline alkaloids <u>43-52</u>	53
14. Structures of cancentrine (<u>53a</u>), 10-oxocancentrine (<u>53b</u>) and 9,10-dihydrocancentrine methine-O-methylether (<u>54</u>)	60

FIGURE	PAGE
15. Structures of codeine (<u>55a</u>), codeinone (<u>55b</u>), 10-oxocodeinone (<u>55c</u>), and cularine (<u>56</u>)	62
16. Mass spectrum fragmentation scheme for 10-oxo- cancetrine	69
17. Structures of the S _a (<u>57</u>) and R _a (<u>58</u>) diastereomers of 2'-O-tetrahydropyranyluridine	74
18. Conformations of the ribose ring	77
19. Structures of the UpU triesters	82
20. Staggered conformations of the C ₃ -O ₃ and C ₅ -O ₅ bonds	90
21. Calculated positions of the phosphorus atoms for the tg conformations of the C ₃ -O ₃ bond of the triesters <u>60</u> and <u>62</u>	93
22. Watson-Crick base-pairs in ribonucleic acids	96
23. Variable temperature versus chemical shift plots for the base protons of (a) GAGC and (b) GCUC	100
24. Assignment of the base resonances in the 90 MHz ¹ H NMR spectrum of the mixture of GAGC - GCUC at 65°C	102
25. Variable temperature plots for (a) the non-exchangeable and (b) the exchangeable protons of the bases in the mixture of GAGC - GCUC	103
26. Chemical shift correlation of the ¹ H resonances for GA, GAG, and GAGC	105
27. The assignment of the base and anomeric protons in the 90 MHz ¹ H NMR spectrum of CAUG at 70°C	114

FIGURE	PAGE
28. Chemical shift versus temperature plots for (a) CAU and (b) AUG	115
29. Chemical shift versus temperature plots for (a) the base and (b) the ribose anomeric protons of CAUG (concentration $9.2 \times 10^{-3} M$)	116
30. The 90 MHz 1H NMR spectra of (a) CAAUG and (b) CAUUG in D_2O at $70^\circ C$	123
31. The 90 MHz 1H NMR spectrum of the mixture of CAAUG and CAUUG at $70^\circ C$	124
32. Chemical shift versus temperature plot for the purine base protons of the duplex formed by CAAUG and CAUUG	125
33. Difference spectra of (a) CAAUG and (b) CAUUG obtained by computer subtraction of the corresponding pentaribonucleotide spectra in Figure 30 from the mixture spectrum in Figure 31	127
34. The 90 MHz 1H NMR spectra of (a) CAUGA and (b) CAUGU in D_2O at $70^\circ C$	132
35. Chemical shift versus temperature plot for the base and ribose anomeric protons of (a) CAUGA and (b) CAUGU	133
36. Diagrammatic representation of the base stacking interaction between the dangling base and terminal G-C base pair in (a) CAUGA and (b) CAUGU	137

SYMBOLS AND ABBREVIATIONS

Symbols

ΔE	separation between two energy levels
H_0	dc magnetic field
ΔH_0	inhomogeneity of H_0
H_1	macroscopic rf field
H_2	decoupling rf field
H_{eff}	an effective magnetic field (equation 1.16)
h	Planck's constant
\hbar	Planck's constant divided by 2π
I	spin quantum number
i	square root of minus one
J_{AB}	spin coupling constant between A and B separated by n bonds
k	Boltzmann constant
M	macroscopic magnetization
M_0	value of M at equilibrium
$M_{x,y,z}$	components of M in laboratory frame
$M_{x',y',z'}$	components of M in rotating frame
$M(\omega)$	magnetization as a function of angular frequency
$M(t)$	magnetization as a function of time
N_{eq}	equilibrium population of lower Zeeman energy level
N_2, N_1	populations of upper and lower energy levels, respectively
P	angular momentum
R_f	term used in adsorption chromatography expressing the ratio of the distance moved by a compound to the distance travelled by the solvent front.

T	temperature
T_1	spin-lattice relaxation time
T_2	spin-spin relaxation time
T_2^*	time for decay of FID in presence of field inhomogeneity
T_m	temperature at which equal amounts of double stranded and single stranded oligoribonucleotides exist in equilibrium
t_p	time duration of a pulse
t	time
x, y, z	x, y and z axes in laboratory frame
x', y', z'	x', y' and z' axes in rotating frame
γ	magnetogyric ratio
Δ	chemical shift range
δ	chemical shift of a nucleus in ppm
θ	angle
μ	nuclear magnetic moment
ν_0	resonance or Larmor frequency in hertz
$\nu_{1/2}$	line width at half-maximum intensity
τ	time between pulses in a pulse sequence
ω_0	$2\pi\nu_0$, resonance frequency in radians per second

Abbreviations

cw	continuous wave
FID	free induction decay
NOE	nuclear Overhauser enhancement

1. PULSED FOURIER TRANSFORM NMR

1.1 HISTORICAL INTRODUCTION:

Nuclear magnetic resonance (NMR) is a branch of spectroscopy that deals with the radio-frequency induced transitions between magnetic energy levels of atomic nuclei. NMR evolved from the concept of nuclear spin since a spinning nucleus would possess both an angular momentum and a magnetic moment. These magnetic properties were initially postulated by Pauli in 1924 to explain the hyperfine splitting of atomic spectra. Further evidence for the model of nuclear spin was provided by the Stern-Gerlach experiments for determining electron magnetic moments. Rabi and co-workers (1) in 1939 modified this approach to measure nuclear magnetic moments. A beam of hydrogen molecules was first passed through an inhomogeneous magnetic field and then a radio-frequency was applied to the beam in a homogeneous field. It was found that energy was absorbed at a specific frequency and this resulted in a deflection of the beam. This was the first observation of the NMR phenomena but was restricted to molecular beams in high vacuum.

The more familiar experiments on the nuclear magnetic resonance of bulk materials were first conducted by Bloch (2,3,4) and Purcell (5) in 1945. Initially the technique seemed to have little applicability to chemical problems but this situation radically changed in 1949 when it became evident that the resonance frequency of a nucleus is dependent on its local electronic environment (6). This observation became known as the chemical shift and its significance was demonstrated when the proton NMR spectrum of ethanol appeared as three distinct peaks (7).

Under conditions of higher resolution the ethanol signals displayed a fine structure which was attributed to a spin-spin interaction or coupling of neighbouring nuclei (8). These developments culminated in the NMR spectrometer becoming commercially available in the mid 1950's. With the instrumental advances that followed, proton magnetic resonance assumed a major role in the identification, characterization and structural analysis of organic molecules.

Several methods were developed to perform high resolution NMR experiments with the most common being the slow passage continuous wave (cw) approach. This consists of placing the sample in a fixed magnetic field and slowly sweeping the radio-frequency (rf) field while observing the absorption of energy from the rf field. The principal limitation of this method is its inability to provide a suitable signal/noise ratio for samples of low concentration or samples which contain nuclei of low isotopic abundance or sensitivity such as ^{13}C .

One solution was a variation of the cw experiment known as adiabatic rapid passage in which a strong rf field is swept rapidly through a particular spectral region. These fast sweep rates resulted in a loss of resolution and consequently limited the usefulness of the method.

In the 1960's the most widely employed means of increasing the sensitivity of NMR was time averaging of slow passage cw spectra. The spectrum is repeatedly scanned and the data is then stored in digital form in a computer of average transients. Successive accumulation of these spectra improves the signal/noise by a factor of the square root of the number of scans. Although computer averaging has made a significant contribution to NMR spectroscopy, particularly in ^{13}C NMR, the considerable time required in some cases to produce a spectrum makes

the technique extremely slow.

An alternative method for obtaining an NMR signal which was originally proposed by Bloch (3,4) and first used by Hahn (9) is pulsed NMR. A very short and powerful rf pulse is applied to the sample and the resulting signal is observed once the rf pulse is switched off. The pulse technique has existed almost as long as the cw method but the lack of the appropriate instrumentation caused its slow development. It was not until 1966 that Ernst and Anderson (10) demonstrated that the response of a nucleus to an rf pulse is the Fourier transform of a slow passage cw spectrum. Pulsed Fourier transform NMR was also shown to have two major advantages over the slow passage method in that it improves the sensitivity by an order of magnitude and requires a much shorter time to obtain a spectrum.

Since the introduction of the commercially available Fourier transform spectrometer in 1969, there has been a substantial growth in many areas of NMR spectroscopy, in particular ^{13}C NMR and in relaxation studies. As instrumental advances are made, pulsed Fourier transform NMR should surpass conventional methods in its ability to provide solutions to both chemical and biochemical problems.

1.2 THEORY OF PULSED NMR:

The spin of a nucleus corresponds to an angular momentum p which can only assume values that are multiples of \hbar , where \hbar is Planck's constant h , divided by 2π . The maximum possible value of p is

$$p = I\hbar = \frac{Ih}{2\pi} \quad (1.1)$$

The quantity I is the nuclear spin quantum number which is either integral or half-integral in value. A nucleus of spin I will have $2I + 1$ energy levels. Those nuclei with $I=0$ do not possess angular momentum and thus do not show magnetic properties. Nuclear magnetic resonance therefore deals with nuclei that have $I \neq 0$. These nuclei also possess a magnetic moment μ which is a result of the angular momentum of a charged particle. This magnetic moment is aligned along the angular momentum vector as expressed by the equation

$$\mu = \gamma p = \frac{\gamma I h}{2\pi} \quad (1.2)$$

where γ is the magnetogyric ratio. It is the interaction of this magnetic moment with a radio-frequency field that allows the observation of magnetic resonance.

In the classical mechanical description of NMR, a nucleus that is placed in a magnetic field H_0 will have its magnetic moment μ inclined at an angle θ relative to the direction of H_0 . The interaction of μ and H_0 creates a torque L which is a force acting perpendicular to the plane containing μ and H_0 and is determined by the change in angular momentum

$$L = \frac{dp}{dt} = \mu \times H_0 \quad (1.3)$$

Due to the combined effects of the torque and the spinning of the nucleus, the magnetic moment will be pulled in the direction of the torque force resulting in a precessional motion about H_0 as illustrated in Figure 1.

This motion of μ can be described by the following equation

$$\frac{d\mu}{dt} = \frac{\gamma dp}{dt} = \gamma \mu \times H_0 \quad (1.4)$$

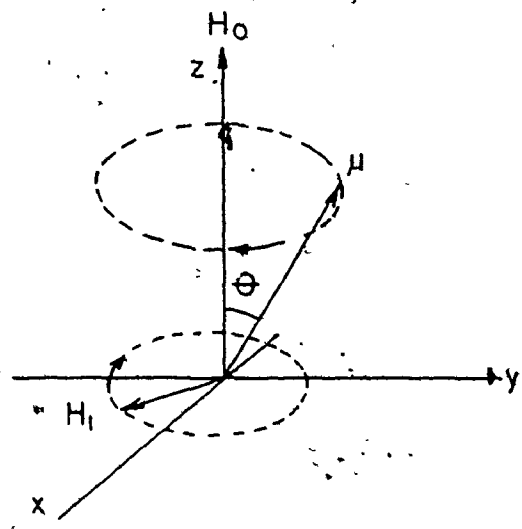


FIGURE 1. Larmor precession of the nuclear magnetic moment.

The angular velocity of this precession is given by

$$\frac{d\mu}{dt} = \omega_0 \times \mu \quad (1.5)$$

where
$$\omega_0 = \gamma H_0 \quad (1.6)$$

while the frequency is determined from the Larmor equation

$$\nu_0 = \frac{|\omega_0|}{2\pi} = \frac{\gamma H_0}{2\pi} \quad (1.7)$$

It should also be noted that the energy of interaction between the magnetic moment $\hat{\mu}$ and H_0 is dependent on the angle θ

$$E = -\mu \cdot H_0 = -\mu H_0 \cos\theta \quad (1.8)$$

During the NMR experiment a radio-frequency field H_1 is applied in a plane perpendicular to H_0 such that the magnetic vector of H_1 will rotate about H_0 (Figure 1). The resonance condition is achieved when the frequency of rotation of this magnetic vector equals the Larmor frequency of the spinning nucleus and an absorption of energy from H_1 will occur. This causes the magnetic moment to tip to a different angle θ but it still maintains a constant precessional frequency. The NMR spectrum can therefore be obtained by continuously applying H_1 and scanning the excitation radio-frequency through the nuclear precessional frequencies and measuring the absorption of energy. This is the slow passage continuous wave technique.

Quantum mechanics also produces the same equation for the precessional frequency which is derived as follows from the energy difference ΔE between adjacent nuclear spin energy levels

$$\Delta E = \frac{\mu H_0}{I} = \frac{\gamma h H_0}{2\pi} \quad (1.9)$$

$$\Delta E = h\nu_0 = \frac{\gamma h H_0}{2\pi} \quad (1.10)$$

$$\frac{\Delta E}{h} = \nu_0 = \frac{\gamma H_0}{2\pi} \quad (1.11)$$

For ^1H and ^{13}C with a spin of $1/2$ there are two of these energy levels whose relative populations are determined from the Boltzmann equation

$$\frac{N_2}{N_1} = \exp(-\Delta E/kT) \quad (1.12)$$

where N_2 and N_1 are the populations of the upper and lower energy levels respectively.

When a sample is placed in the magnetic field there is initially no net magnetization because the nuclear energy levels are equally populated. As the nuclei interact amongst themselves and with their surroundings an equilibrium situation is achieved where there is a slight excess of nuclei in the lower energy level with their magnetic moments aligned along H_0 . The equilibrium population of the lower energy level is given by

$$n \text{ eq.} = \frac{N_1 - N_2}{N_1} = \frac{2\mu H_0}{kT} \quad (1.13)$$

The precession of this group of magnetic moments about H_0 can be readily interpreted by adding the moments vectorially and thus producing a net magnetization vector M along the z axis. At equilibrium this magnetization is designated as M_0 .

Bloch (3,4) developed the following series of differential equations in order to describe the motion of this net magnetization in an applied field.

$$\begin{aligned} \frac{dM_x}{dt} &= \gamma(MyH_0 + M_z H_1 \sin wt) - \frac{M_x}{T_2} \\ \frac{dM_y}{dt} &= \gamma(M_z H_1 \cos wt - M_x H_0) - \frac{M_y}{T_2} \end{aligned} \quad (1.14)$$

$$\frac{dM_z}{dt} = -\gamma(M_x H_1 \sin \omega t + M_y H_1 \cos \omega t) - \frac{(M_z - M_0)}{T_1}$$

M_x, M_y, M_z : magnetization in the x, y and z directions, respectively.

T_1, T_2 : spin-lattice and spin-spin relaxation time, respectively.

The solution of these equations predicts the observed line shape of the NMR signal which is either the normal Lorentzian absorption signal or the dispersion signal.

Bloch also incorporated into these equations the rates for the relaxation of these magnetization vectors back to their equilibrium values after perturbation by the radio-frequency field. It was formulated that these rates followed a simple exponential decay.

Pulsed NMR utilizes a high energy and extremely short (1-100 μ sec) radio-frequency pulse. The effect this has on the magnetization M is interpreted by using a coordinate system that rotates at the nuclear precessional frequency corresponding to the magnetic field H_0 .

In the rotating frame the motion of M is defined by the equation

$$\left(\frac{dM}{dt}\right)_{\text{rot.}} = \gamma M \times H_{\text{eff}} \quad (1.15)$$

$$\text{where the effective field } H_{\text{eff}} = H_0 + \frac{\omega}{\gamma} \quad (1.16)$$

The quantity ω/γ , which arises from the effect of rotation, has the dimensions of the magnetic field and is often termed a "fictitious" field.

Therefore in the rotating frame the magnetization will precess about H_{eff} rather than H_0 .

When the rf pulse is applied, the H_1 field vector is fixed along the x' axis since H_1 also rotates at the same frequency as the frame. The contribution of H_1 to H_{eff} is given by

$$H_{\text{eff}} = H_0 + \frac{\omega}{\gamma} + H_1 \quad (1.17)$$

At resonance $\omega = -\gamma H_0$ and this will cancel H_0 along the z axis

$$H_{\text{eff}} = H_0 + \frac{(-\gamma H_0)}{\gamma} + H_1 = H_1 \quad (1.18)$$

$$\left(\frac{dM}{dt}\right)_{\text{rot}} = \gamma M \times H_1 \quad (1.19)$$

since M can now interact only with H_1 , M will begin to precess about the x' axis with an angular frequency of γH_1 (Figure 2a). In a time t_p (sec), the angle θ through which M precesses is determined by

$$\theta = \gamma H_1 t_p \quad (\text{radians}) \quad (1.20)$$

The H_1 pulse is applied for a period of time long enough to tip M towards the y' axis and is then switched off. Originally, there was no component of M in the $x'y'$ plane due to the lack of phase coherence of the magnetic moments in this plane. However, as a result of precession about H_1 , a component of M is generated along the y' axis ($M_{y'}$ in Figure 2b). The moments comprising M now begin to exchange energy and dephase in the $x'y'$ plane (Figure 2c). $M_{y'}$ will then decay to zero in a time T_2 . This is defined as the spin-spin or transverse relaxation time. Another factor contributing to the reduction of $M_{y'}$ is that the magnetic field H_0 is not perfectly homogeneous. Therefore nuclei in different parts of the sample will experience a range of values for the magnetic field ΔH_0 and precess at different Larmor frequencies. This results in some nuclei precessing at a frequency either faster or slower than that of the rotating frame. Overall $M_{y'}$ will decrease as a function of T_2^* where

$$\frac{1}{T_2^*} = \frac{1}{T_2} + \frac{\gamma \Delta H_0}{2} \quad (1.21)$$

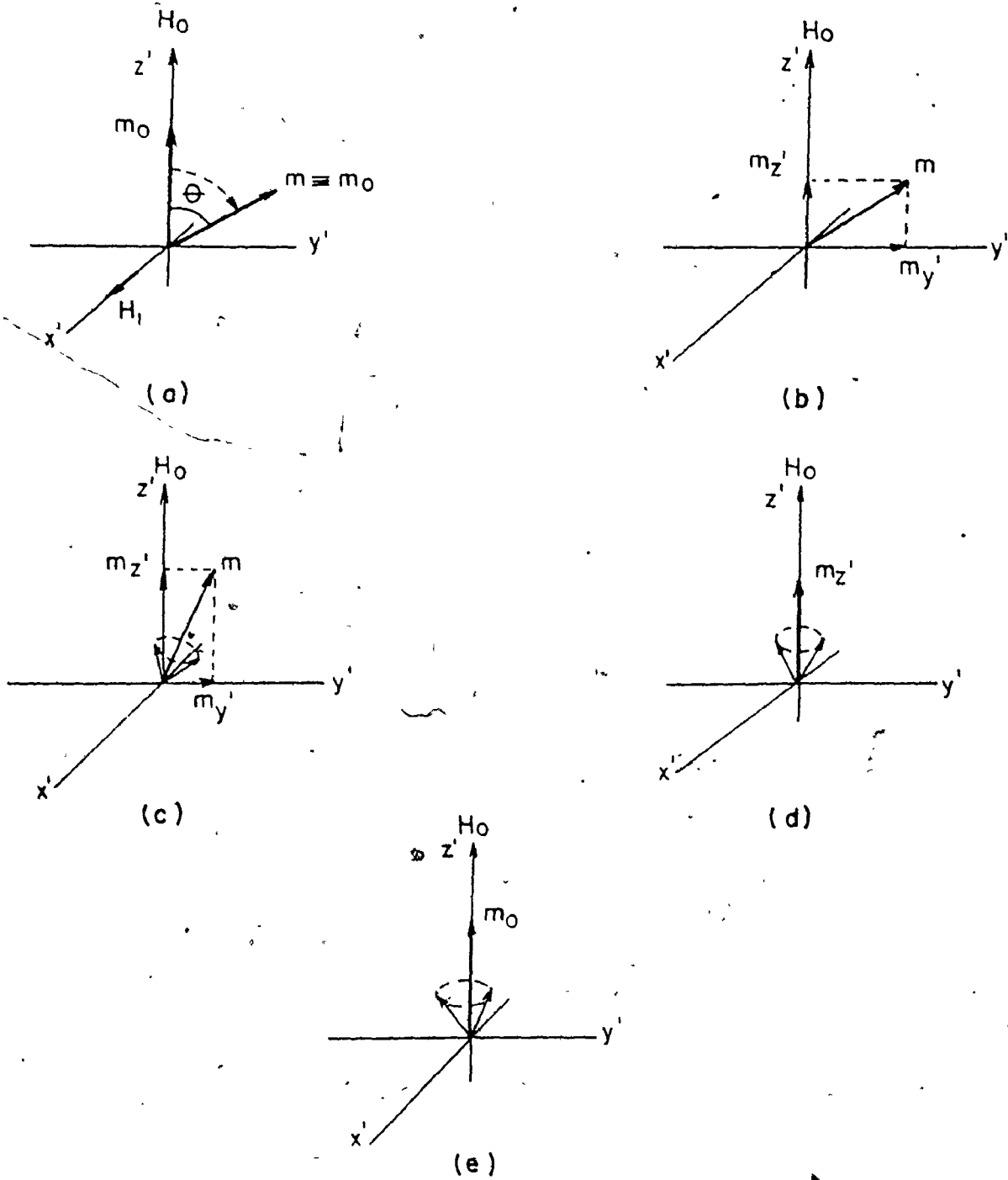


FIGURE 2. The effect of an rf pulse on the magnetization M_0 in the rotating frame.

The nuclear moments also lose energy to their surroundings and relax toward the z' axis. The component M_z' will relax toward the equilibrium value M_0 (Figure 2d-e) in a time T_1 known as the spin-lattice or longitudinal relaxation time. When the nuclear moments have returned to equilibrium there is no component of M left in the $x'y'$ plane. Thus T_2 or T_2^* are never longer than or can be shorter than T_1 : $T_2^* \leq T_2 \leq T_1$. The relaxation time T_1 can be considered as an enthalpy process while T_2 is an entropy process:

The signal that is detected by the spectrometer is the net magnetization in the $x'y'$ plane along the y' axis only. The magnitude of $M_{y'}$ determines the intensity of the signal which is known as the free induction decay or FID. If a 90° radio-frequency pulse is applied at the resonance frequency of a single type of nucleus the signal will decay exponentially in a time T_2^* . The decay pattern is a direct measure of the decrease in $M_{y'}$ since the instrument uses a phase sensitive detector referenced in phase to the applied radio frequency.

Consider the situation where a 90° pulse is applied at a frequency different from the precessional frequency of the nucleus. Since the frame rotates at the applied radio frequency, the magnetization $M_{y'}$ will rotate relative to the frame. The detector will show not only the exponential decay but also an interference pattern similar in appearance to a damped sine wave as $M_{y'}$ and the reference frequency alternate in and out of phase with each other.

The experiment discussed above is totally analogous to a system that contains several of the same type of nuclei which have different precessional frequencies arising from differences in chemical shifts and spin-spin coupling. This means that some nuclei precess at frequencies

different from that of the rotating frame and the interference patterns that result are quite complex.

Since the FID contains all the spectral information it must be converted into a form that can be utilized by the chemist. This is achieved by Fourier analysis in which a complex waveform is separated into its spectral components. The FID is a plot of intensity vs time and is known as a time domain function whereas the corresponding spectrum is a frequency domain function. Fourier analysis makes it possible to transform data from one domain into the other. The mathematical expression for this transformation is:

$$f(x) = \int_{-\infty}^{+\infty} f(y) e^{-ixy} dy \quad (1.22)$$

where $f(x)$ is the Fourier transform of $f(y)$ and the inverse relation is

$$f(y) = \frac{1}{2\pi} \int_{-\infty}^{+\infty} f(x) e^{ixy} dx \quad (1.23)$$

When applied to NMR it is found that the magnetization expressed as a function of angular frequency $M(\omega)$ is the Fourier transform of $M(t)$ which is the magnetization as a function of time (the FID signal).

$$M(\omega) = \int_{-\infty}^{+\infty} M(t) e^{-i\omega t} dt \quad (1.24)$$

Thus Fourier transformation of the FID gives a spectrum identical with that obtained by continuous wave techniques.

Pulse methods are usually applied to a system where the nuclei have precessional frequencies covering a wide range of chemical shifts. The rf pulse is applied outside the region of chemical shifts. As mentioned previously a pulse can tip nuclear moments precessing at a frequency different from the radio frequency. In order to gain further understanding

of this point one must again consider the behaviour of the magnetization in a frame rotating at the radio frequency ω . The magnetization resulting from nuclei with Larmor frequencies ω_i precess about an effective field given by

$$|H_{\text{eff}}| = \frac{1}{\gamma} [(\omega_i - \omega)^2 + (\gamma H_1)^2]^{1/2} \quad (1.25)$$

since the H_1 field is quite large, the term $(\omega_i - \omega)$ can be neglected for any value of ω_i

$$\gamma H_1 \gg |\omega_i - \omega| \quad (1.26)$$

$$\gamma H_1 \gg 2\pi\Delta \quad (\text{Hz}) \quad (1.27)$$

where Δ is the entire range of chemical shifts. This results in $H_{\text{eff}} = H_1$ which means that the magnetization precess about H_1 for all nuclei with Larmor frequencies contained within Δ . When a 90° pulse is used

$$\frac{\pi}{2} = \gamma H_1 t_p \quad (1.28)$$

$$t_p = \frac{\pi}{2} \frac{1}{\gamma H_1} \quad (1.29)$$

Combining equations (1.27) and (1.29) results in

$$t_p \ll \frac{1}{4} \Delta \quad (\text{Hz}) \quad (1.30)$$

Therefore nuclei with a large frequency range require the pulse time to be short and the pulse power to be strong.

Ernst and Anderson (10) showed that Fourier transformation of the FID would provide spectral information more efficiently than the continuous wave experiment. The increase in sensitivity in a single pulse experiment is proportional to $\left(\frac{\Delta}{\nu_{1/2}}\right)^{1/2}$ where Δ is the total chemical shift range and $\nu_{1/2}$ is the width of the narrowest signal. Theoretically, the increase in sensitivity for ^{13}C is given by $\frac{(5000 \text{ Hz})^{1/2}}{(0.5 \text{ Hz})} = 100$. However in practice a

sensitivity enhancement of $\gt 10$ is achieved.

The primary advantage of Fourier transform NMR is the short time required to attain a specified signal/noise. Generally a spectrum with a given sensitivity can be obtained approximately 100 times faster than by continuous wave methods. This saving in time can be utilized in the following ways:

- (a) improvement of the signal/noise by repeating a pulse and coherently adding successive FID's before Fourier transformation.
- (b) optimum field homogeneity can be maintained during the shorter pulse experiment.
- (c) spectra of short lived species can be obtained.
- (d) measurement of the decaying magnetization of individual spectral lines to yield T_1 and T_2 values which are useful for chemical shift assignments and provide information about molecular motion.

The instrumental requirements for pulsed Fourier transform NMR are described in the following block diagram which outlines the essential features of the Bruker WH-90 spectrometer used in this work. For more detailed information concerning both the instrumentation and operation of the pulsed spectrometer and the theory of pulsed NMR these leading references should be consulted: 10, 11, 12, 13, 14.

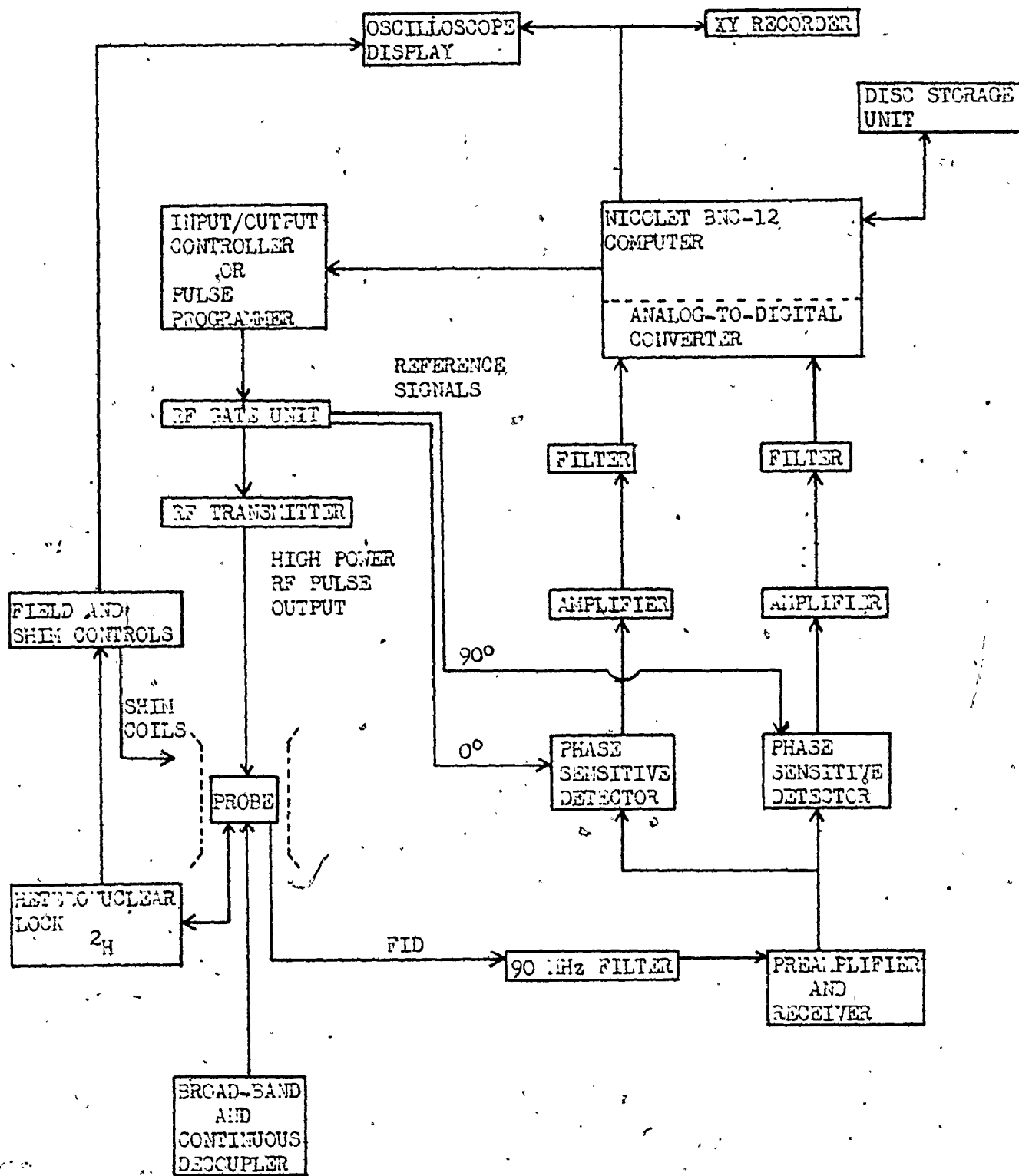


FIGURE 3. Block diagram of the Bruker WH-90 pulsed spectrometer with quadrature detection.

2. CARBON-13 NMR

2.1 INTRODUCTION:

Natural abundance carbon-13 nuclear magnetic resonance was initially reported by Lauterbur (15) and Holm (16) in 1957. Although this provided the means of directly observing the carbon framework of a molecule, the growth of ^{13}C NMR was impeded by the limited instrumentation. The advent of both field/frequency controlled spectrometers and computer averaging produced a significant amount of progress in the 1960's largely by the efforts of P.C. Lauterbur, D.M. Grant, J.D. Roberts and J.B. Stothers.

Two instrumental breakthroughs which essentially revolutionized the study of ^{13}C NMR occurred in 1966 when Ernst (15) developed broad-band heteronuclear decoupling and with Anderson (10) conducted the first pulsed Fourier transform NMR experiments. When the pulsed spectrometer was first commercially produced in 1969, ^{13}C NMR could then be utilized as a routine analytical device.

In order to understand why ^{13}C NMR has taken far longer to develop than ^1H NMR one must consider the factors that influence the sensitivity of the NMR experiment.

TABLE 1. Properties of various magnetic nuclei

Nucleus	I	% Natural Abundance	$\gamma \times 10^{-3}$ (rad G ⁻¹ sec ⁻¹)	Frequency (MHz) in 21.14 KG Field	Relative Sensitivity ^a
^1H	1/2	99.985	26.753	90.00	1.00
^{13}C	1/2	1.108	6.728	22.62	1.59×10^{-2}
^{19}F	1/2	100	25.179	84.67	0.83
^{31}P	1/2	100	10.840	36.43	6.63×10^{-2}

^a Sensitivity at constant field = $7.652 \times 10^{-3} \gamma^3 (I + 1)$

The first is the natural isotopic abundance (Table 1). Carbon-13 is the only isotope of carbon that has a nuclear spin of $1/2$ and has an abundance of 1.108%. Although this appears quite small it is sufficient for the NMR experiment. The low abundance has the advantage of eliminating homonuclear spin-spin coupling in unenriched samples.

Secondly, the sensitivity is directly proportional to the cube of the magnetogyric ratio. Considering the ratio $(\gamma^{13}\text{C}/\gamma^1\text{H})^3$, it can be determined that the signal from the ^{13}C nucleus is approximately 1/64 of that of the proton at resonance. A combination of the low isotopic abundance and magnetogyric ratio as well as the fact that adjacent ^1H nuclei are spin coupled to the ^{13}C nucleus results in a signal that is nearly 6000 times smaller in ^{13}C NMR than in ^1H NMR when obtained under identical experimental conditions.

This problem of low sensitivity has been largely overcome by the use of pulsed Fourier transform NMR which allows spectra to be obtained routinely on samples of 50-100 mg. The recent development of quadrature detection (18,19,20) has produced a sensitivity improvement by a factor of 1.4. When quadrature detection is used with the newly designed microprobes, ^{13}C spectra can be recorded on samples at the microgram level.

2.2 ^{13}C CHEMICAL SHIFTS:

Carbon chemical shifts cover approximately 600 ppm but most compounds resonate over a 220 ppm range. With Fourier transform spectrometers the natural abundance ^{13}C signal from tetramethylsilane (TMS) is used as a reference in a manner analogous to the ^1H δ scale.

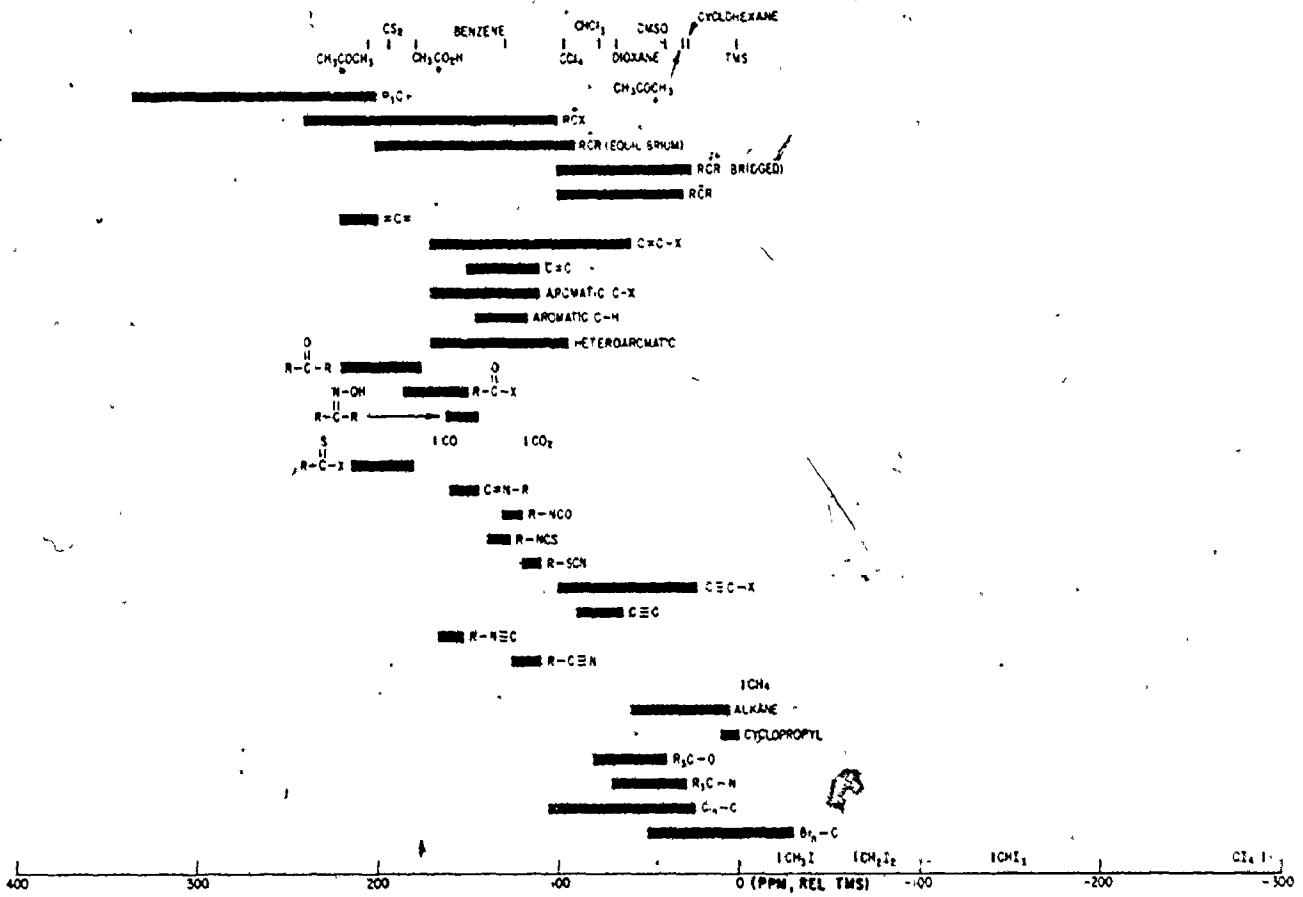


FIGURE 4. ¹³C chemical shifts.

The accompanying chart (Figure 4) serves to illustrate the range of ^{13}C chemical shifts for a variety of compounds. Some general trends that are readily observed are sp^3 carbons resonate at high field, sp^2 carbons at low field and sp carbons appear at intermediate field. Substituents with increasing electronegativity cause downfield shifts.

2.2.1 ^{13}C SUBSTITUENT EFFECTS:

Much of the work in ^{13}C NMR has been devoted to the examination of the influence of substituents on carbon chemical shifts. Analysis of the empirical results have led to both a correlation of the chemical shift with the molecular electronic structure and the derivation of substituent parameters for predicting chemical shifts for closely related compounds. Coincidentally, several theoretical interpretations of carbon shieldings have been developed but these have not been entirely successful. A detailed discussion of chemical shift theory will not be presented, however, this information can be found in the reviews of Stothers (21) and Ditchfield (22).

In dealing with substituent effects three factors can perturb the electronic environment of a nucleus and cause a chemical shift. The following equation illustrates the contribution of these factors to the ^{13}C chemical shift

$$\delta^{13}\text{C} = \delta_{\text{EL}} + \delta_{\text{A}} + \delta_{\text{inter}} \quad (2.1)$$

The electronic term δ_{EL} corresponds to changes in the electronic structure around a nucleus, δ_{A} is the anisotropy term which accounts for the effects of magnetic fields generated by the circulation of electrons on neighbouring nuclei and δ_{inter} is the small intermolecular contribution arising from

changes in the magnetic fields associated with the nuclei of the medium surrounding the molecule being observed. The electronic term which makes the largest contribution can be elaborated further

$$\delta_{EL} = \delta_E + \delta_{EF} + \delta_{ST} + \delta_{MIS} \quad (2.2)$$

where

δ_E is associated with changes in substituent or structure which through resonance or inductive effects can influence the electronic distribution of a nucleus.

δ_{EF} is the electric field effect resulting from the through space polarization of the electron density in the sigma or π bonds.

δ_{ST} accounts for the increase or decrease in shielding of the ^{13}C nucleus as a result of steric interactions. The most common example of δ_{ST} is the γ -gauche shielding effect initially observed in hydrocarbons. Carbons in a γ -gauche conformation are shielded as a result of the polarization of the electron density in the C-H bonds towards carbon which is caused by the nonbonded repulsions between the sterically crowded hydrogens bound to these carbons (23).

δ_{MIS} is any miscellaneous contribution not accounted for by the previous terms such as a transannular interaction of functional groups within a molecule. The effect of changes in either solvent or molecular geometry when a group is replaced by a different substituent (24) has been neglected. Although the above substituent effects are well documented in the literature, they are currently undergoing extensive re-investigation (25,26) in order to improve the theoretical understanding of the origin of these effects.

2.2.2 REPRESENTATIVE ^{13}C CHEMICAL SHIFTS:

A survey of carbon shieldings for the compounds and functional groups pertinent to this work is outlined in this section. More complete discussions of these data are available in references 21, 27 and 28.

ALKANES:

In their study of acyclic hydrocarbons Grant and Paul (29) found that these compounds have chemical shifts over the range of -2 to 43 ppm. Regression analysis of this data indicated that the carbon shielding could be determined from the following equation

$$\delta_{\text{C}i} = B + \sum_j A_j N_{ij} \quad (2.3)$$

where $\delta_{\text{C}i}$ is the i th carbon shielding, B is a constant with a value of -2.6, A_j is an additive shift parameter for position j , and N_{ij} is the number of substituents at position j . In linear alkanes only five values of A are required and these are designated as the α , β , γ , δ and ϵ substituent effects. These parameters represent the change in chemical shift upon replacement of a hydrogen by a methyl group at the α , β , γ , δ , and ϵ positions along the carbon chain (Table 2).

Branched hydrocarbons caused deviations from this additivity relationship and additional variables had to be included in order to correlate accurately the observed and calculated carbon shieldings. This work was later modified by Lindeman and Adams (30) who derived a more simplified equation based on the analysis of chemical shift data from 59 hydrocarbons.

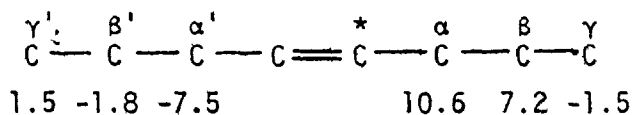
Additivity parameters for substituents other than methyl have been determined in a similar fashion and some examples are also included in Table 2.

TABLE 2. Substituent effects for acyclic hydrocarbons (28)

Substituent	α	β	γ	δ	ϵ
CH ₃	9.1	9.4	-2.5	0.3	0.1
Cl	31.2	10.5	-4.6	0.1	0.5
1°NH ₂	28.9	11.4	-4.6	0.7	-0.1
1°OH	48.3	10.2	-5.8	0.3	0.1

ALKENES:

Alkenes resonate in the 80-165 ppm region of the ¹³C spectrum with ethylene appearing at 123.3 ppm. Using ethylene as a reference, Roberts and co-workers (31) derived the following additivity parameters to calculate the chemical shifts of the olefinic carbons.



$$\delta_{13\text{C}}^* = 123.3 + \alpha + \beta + \gamma + \alpha' + \beta' + \gamma'$$

For a cis alkene the factor -1.1 is included in the above summation.

Alkyl substituents on the double bond can convey their effect either through the sigma bonds and deshield the substituted carbon relative to ethylene or through the π system and shield the adjacent unsaturated carbon. Similar trends were found for polar substituents with unpaired electrons such as oxygen or nitrogen. Resonance interactions of the type $\text{CH}_2 = \text{CH} - \ddot{\text{X}} \longleftrightarrow \text{CH}_2^- - \text{CH} = \text{X}^+$ were used to rationalize these results. Electron withdrawing groups such as C=O or C \equiv N reversed the above trends.

CYCLOALKANES AND CYCLOALKENES:

The ^{13}C spectra of cycloalkanes showed very little deviation from the chemical shift of cyclohexane (27.8 ppm) with the exception being cyclopropane (-2.6 ppm). From the study of various methyl substituted cyclohexanes (34), additivity parameters were obtained (Table 3) and subsequently verified from the low temperature spectrum of methylcyclohexane (35).

TABLE 3. Substituent effects in methylcyclohexanes (34).

Substituent	α	β	γ	δ
equat. CH_3	5.6	8.9	0.0	-0.3
axial CH_3	1.1	5.2	-5.4	-0.1
gem $(\text{CH}_3)_2$	-3.4	-1.2		
vic $(\text{CH}_3)_2(\text{e,e})$	-2.3			
(a,e)	-3.1			

These parameters take on increased significance because their value is directly related to the geometry and conformation of the ring system. Substituent effects for other groups have also been determined (36,37, 38).

Investigations of cyclic olefins (21) revealed that ring size has relatively little effect on the sp^2 carbon shieldings which are usually 130-135 ppm. The exception is cyclohexene (127.2 ppm). Alkyl substituents on cyclohexene exert their greatest effect on the double bond shieldings when they are directly attached to an unsaturated carbon.

AROMATICS:

Substituted aromatics cover a wide chemical shift range of 100-170 ppm, with benzene appearing at 128.6 ppm. The early studies by Lauterbur (39,40) demonstrated that the substituent effects on the aromatic shieldings were additive. Substituent parameters for numerous monosubstituted benzenes were subsequently determined (21) and some examples are provided in Table 4. The correlation between calculated and observed chemical shifts is quite good, however, deviations occur in ortho substituted benzenes.

Closer examination of the data in Table 4 indicates the sensitivity of the aromatic chemical shifts to the electronic effects of polar substituents. The chemical shift changes observed for C-1 are a reflection of the inductive effect of the substituent. Resonance interactions between the substituent and the aromatic π system account for the shielding changes at the ortho and para positions while the meta carbon is essentially unaffected.

TABLE 4. Substituent effects in monosubstituted benzenes.

Substituent	C-1	ortho	meta	para
CH ₃	10.0	0.8	0.0	-2.5
OH	29.5	-12.6	1.8	-7.6
OCH ₃	32.2	-14.0	1.6	-7.1
COCH ₃	9.9	0.4	0.4	4.7
NO ₂	20.1	-4.7	1.0	6.6

Aromatic chemical shifts are also influenced by changes in concentration and solvent (41).

CARBONYL CARBONS:

Carbonyl carbons resonate at lower field (150-230 ppm) because of the polarization of the electron density in the π -bond towards oxygen. The following results illustrate the chemical shifts of some typical carbonyl compounds: ketones, 170-225 ppm; aldehydes, 170-205 ppm; carboxylic acids, 165-185 ppm; esters and amides, 160-180 ppm (21,27).

Conjugation of a carbonyl group with a double bond or aromatic ring causes an upfield shift of the carbonyl resonance and a deshielding of the β carbon. The contribution of the canonical structure $\text{>C}^{\oplus}=\overset{\ominus}{\text{C}}-\text{O}^{\ominus}$, was used to explain this observation (42).

2.3 ASSIGNMENT TECHNIQUES IN ^{13}C NMR:

Several procedures have been developed in ^{13}C NMR to provide unambiguous chemical shift assignments and the most commonly used methods are summarized below.

1. Broad-band or proton noise decoupling. This produces a singlet for each carbon and gives the spectrum that provides the ^{13}C chemical shifts (17,43,44).

2. Coherent single-frequency off-resonance decoupling. This allows the observation of a residual coupling, J_R which assigns quaternary carbons, methines, methylenes and methyl groups as singlets, doublets, triplets and quartets, respectively. The value of J_R is given by

$$J_R = \frac{J^{13\text{C},1\text{H}} \nu_{\text{H}}}{\nu_{\text{H}_2}} \quad (2.4)$$

where $J^{13\text{C},1\text{H}}$ is the actual $^{13}\text{C}-^1\text{H}$ coupling constant, $\Delta\nu$ (in Hz) is the frequency difference between the decoupling field frequency and the particular proton resonance frequency and γH_2 is the decoupling field strength (17,43,45).

3. Selective enhancement of quaternary carbons (46).
4. Model compound studies (43).
5. Isotopic labelling (^2H , ^{13}C , ^{12}C , ^{15}N). Substitution of a hydrogen by deuterium can essentially remove the signal from the directly bonded carbon due to a combination of the spin coupling with deuterium and saturation of the carbon signal caused by the increase in the spin-lattice relaxation time of that carbon (43,44,47).
6. Gated decoupling. This technique measures the actual $^{13}\text{C}-^1\text{H}$ coupling constant without the loss of the nuclear Overhauser enhancement (43,44,48,49,50).
7. Selective ^1H decoupling. Irradiation of a specific ^1H frequency results in a singlet for the directly bonded carbon while the remaining carbons exhibit a residual coupling (43,44).
8. $^{13}\text{C}-^1\text{H}$ chemical shift cross-correlation. A plot of the residual coupling J_R vs the decoupling frequency permits the determination of the ^1H chemical shifts from the carbon shifts (43,44,51).
9. Spin-lattice relaxation time (T_1). The T_1 correlates the molecular motion and the number of neighbouring protons with the molecular structure (43,44,52,53,54,55).
10. Overhauser suppression. This determines both the ^{13}C nuclear Overhauser enhancement and peak integrations (43,44,52,56).

3. ^{13}C NMR OF THE ISOQUINOLINE ALKALOIDS

3.1 INTRODUCTION

Since the late 1950's proton NMR spectroscopy has contributed immensely to many areas of natural products chemistry. With the availability of Fourier transform spectrometers ^{13}C NMR is rapidly approaching the level of ^1H NMR in its application to natural products structural elucidation and conformational analysis. In the case of the isoquinoline alkaloids several classes have been investigated by ^{13}C NMR. Early reports were made on the Amaryllidaceae (57) and protopine alkaloids (58). More recently Wenkert et al. have reviewed work on the aporphines and tetrahydroprotoberberines, the pavine alkaloid argemonine and cularine (59). Other publications have appeared on the tetrahydroprotoberberines (60) and the reduced proaporphines (61).

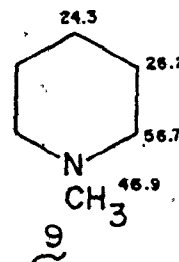
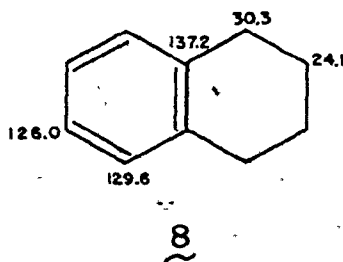
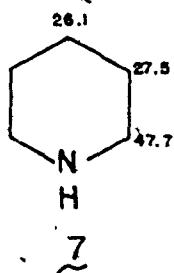
One aspect of the application of ^{13}C NMR to the structural analysis of the isoquinoline alkaloids not dealt with in these previous studies is that several alkaloids exist as pairs of diastereomers in nature. Thus the objective of this work was to utilize ^{13}C NMR spectroscopy in the differentiation and assignment of the relative stereochemistry of a number of diastereomeric phthalideisoquinolines, 13-methyltetrahydroprotoberberines and spirobenzylisoquinoline alkaloids. Although the relative stereochemistry of these compounds can be determined by other physical methods, ^{13}C NMR was found to be as effective as the other techniques because of its sensitivity to structural changes. Several model compounds were also examined in order to assist in the chemical shift assignments of the alkaloids.

The final section on the isoquinoline alkaloids will illustrate the contribution made by ^{13}C NMR in the structural elucidation of a new alkaloid in the canconine series.

3.2. RESULTS AND DISCUSSION

3.2.1 SIMPLE ISOQUINOLINES

These studies began with an examination of several simple isoquinolines since this structural unit is common to all of these alkaloids. Spectra were initially obtained on the 6,7-dimethoxy-1,2,3,4-tetrahydroisoquinolines 1 and 2, and 6,7-dimethoxy-3,4-dihydroisoquinolines 3 and 4 (Figure 5 and Table 5). The assignment of the aliphatic carbons of 1 follows readily by comparison with the results for piperidine (7) and tetralin (8) (21,62). Of the two carbons adjacent to nitrogen in 1, C-1 is at lower field because of the slightly larger α effect of the phenyl group (21). The specific assignment of C-5 and C-8 was achieved by selective



proton decoupling. Although the proton resonance frequencies are separated by only 8 Hz, C-5 and C-8 were differentiated by running a series of spectra in which the proton decoupling frequency was progressively increased over the relevant frequency range. The deshielding effect of the ortho-methoxy

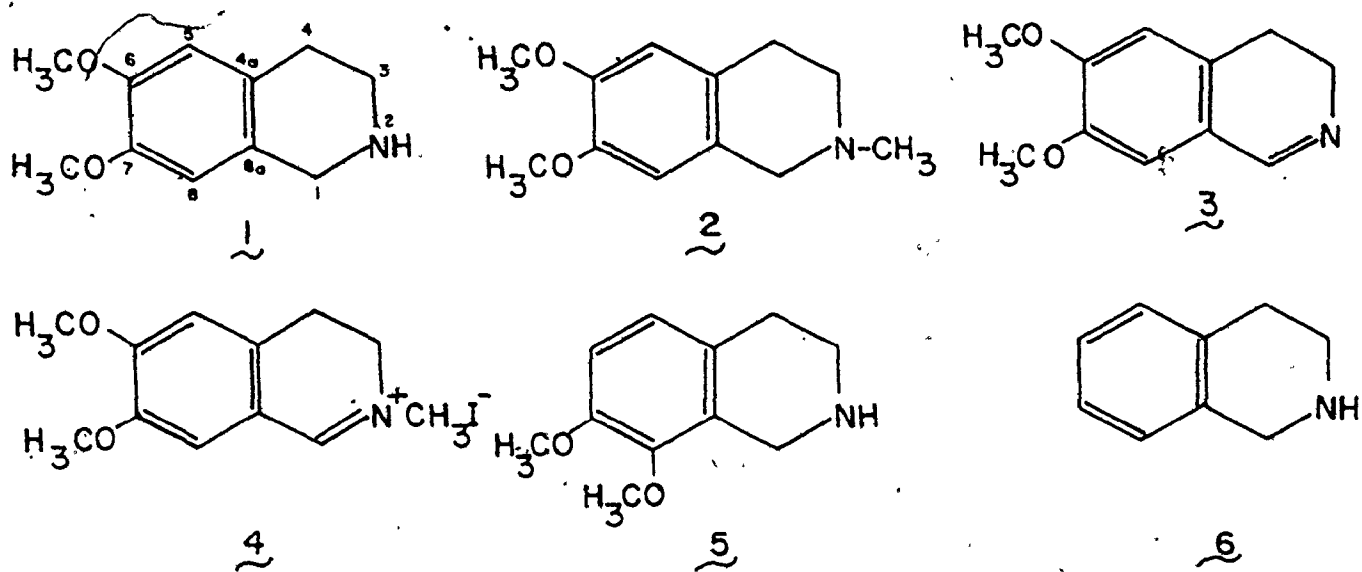


FIGURE 5. Structures of the simple isoquinolines.

TABLE 5. ^{13}C chemical shifts^a of the simple isoquinolines.

Carbon	<u>1</u>	<u>2</u>	<u>3</u>	<u>4</u>	<u>5</u>	<u>6</u>
1	47.8	57.6	159.5	164.6	43.6	48.2
3	43.9	53.0	47.4	50.5	43.6	43.8
4	28.6	28.8	24.7	25.5	28.5	29.1
4a	127.9	126.7	129.8	132.3	129.9	136.1
5	112.2	111.6	110.5	111.3	124.4	129.2
6	147.5	147.7	151.3	157.6	110.8	125.6
7	147.3	147.3	147.9	148.8	145.5	125.9
8	109.3	109.5	110.5	115.7	150.3	126.1
8a	126.6	125.8	121.6	117.2	128.0	134.8
6 OCH ₃	55.9	55.9	56.0	57.0		
7 OCH ₃	55.9	55.9	56.1	57.2	55.9	
8 OCH ₃					60.0	
NCH ₃		46.0		48.1		

^a Chemical shifts in ppm from internal TMS (± 0.1 ppm). Samples were dissolved in CDCl_3 to a concentration range of 0.16 M to 0.45 M.

groups readily distinguishes the substituted aromatic carbons 6 and 7 from C-4a and C-8a. Because of the nearly identical chemical shifts of C-4a and C-8, and C-6 and C-7, unambiguous assignments could not be made.

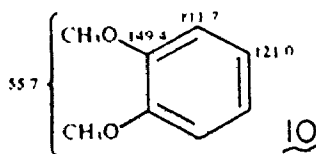
The spectrum of 2 revealed that the aromatic carbons undergo very little change in chemical shift from those of 1, whereas C-1 and C-3 are shifted downfield by 9.8 and 9.1 ppm, respectively, because of the β N-methyl group (34). Similar results have been observed for piperidine (7) and N-methylpiperidine (9) (21).

The assignment of the C-3 and C-4 resonances of 3 and 4 are apparent from the previous discussion, and those of C-1 by virtue of its unsaturated character. Again C-5 and C-8 are readily differentiated from the substituted aromatic carbons. Because of charge delocalization through resonance in 4, carbons 4a, 6 and 8 should appear at lower field than their counterparts 8a, 7 and 5, respectively. It is for this reason that the assignments shown in Table 5 have been made. Although 3 does not bear a formal positive charge the same resonance arguments may be applied in assigning the aromatic signals.

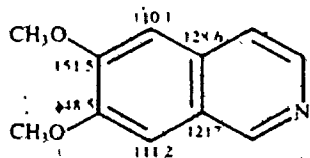
Since many isoquinoline alkaloids, notably the protoberberines, contain the 7,8-disubstituted 1,2,3,4-tetrahydroisoquinoline unit, 7,8-dimethoxy-1,2,3,4-tetrahydroisoquinoline (5) was examined. With the exception of C-8a, the chemical shifts of the aromatic carbons of 5 correlate with those calculated by applying the shift parameters for ortho-dimethoxy groups to the observed spectrum of tetrahydroisoquinoline (6). The nature of the deviation of the calculated shift for C-8a is discussed at the conclusion of section 3.2.3. The assignments in 6 were made by comparison with 7 and 8 and have not been verified by other methods. Regardless of the assignments made in 6, the differences in shift parameters are sufficiently large that the calculated spectrum always leads to the same order of chemical shifts for C-5, C-6, C-4a and C-8a. It is noteworthy that C-1 of 5 is shielded relative to 6 (-4.6 ppm) as a result of the steric perturbation at C-1 caused by the C-8 methoxy group. Assignment of the signal at 60.0 ppm to the C-8 methoxy group was based on analogous results obtained by Dhimi and Stothers on ortho-disubstituted anisoles (63). Experimental verification of this assignment is provided

by the similar system in rings C and D of canadine in the protoberberine section.

The calculation that was mentioned in the previous paragraph was based on additivity parameters derived from comparison of the chemical shifts of benzene (128.6 ppm) and veratrole (10) (C-1, + 20.8; C-2, -16.9; C-3, -7.6 ppm). In almost all cases studied, these parameters expressing



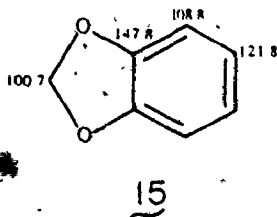
the combined effect of two ortho-methoxy groups gave a closer fit with the observed chemical shifts than those calculated using parameters derived from anisole. As an example, further support for the assignments in 3 is provided by applying the ortho-dimethoxy substituent parameters to the reported spectrum of isoquinoline (21). The resulting calculated carbon shieldings for the benzenoid ring of 6,7-dimethoxyisoquinoline are very similar to those observed for 3.



3.2.2 PHTHALIDEISOQUINOLINE ALKALOIDS

The phthalideisoquinolines were the first group of alkaloids to be considered. Naturally occurring β -hydrastine (11) and its diastereomer α -hydrastine (12), and the pair of natural diastereomeric bases, corlumine (13) and adlumine (14) were examined (Figure 6 and Table 6).

The carbon resonances of rings A and B of 11 were tentatively assigned by comparison with the previous data (compounds 1 and 2 in Table 5) and with the spectrum of methylenedioxybenzene, 15. Phthalide (16) and meconin (19) were used as models in the assignment of the resonances of ring D (Figure 7 and Table 7). The spectrum of phthalide was interpreted as follows. By comparison with the calculated chemical shifts of



2-carbomethoxybenzyl alcohol (C-1, 143.4; C-2, 130.2; C-3, 130.4; C-4, 128.0; C-5, 134.3; C-6, 127.8) it was possible to assign C-3a and C-7a with some certainty and C-5 and C-7 tentatively. The absence of the signal at 128.5 ppm in the spectrum of 6-deuteriophthalide (16b) confirmed the assignment of C-6. Selective decoupling experiments on 16b assigned C-7 since the proton on C-7 is downfield from the other protons in the ^1H spectrum. The observed chemical shifts of 6-nitrophthalide (17) and 6-aminophthalide (18) agreed closely with those calculated by applying the appropriate shift parameters to the resonances of phthalide, and so strengthened the assignments of phthalide.

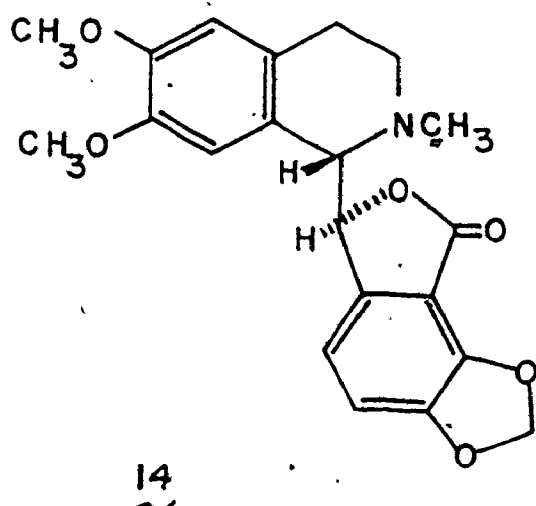
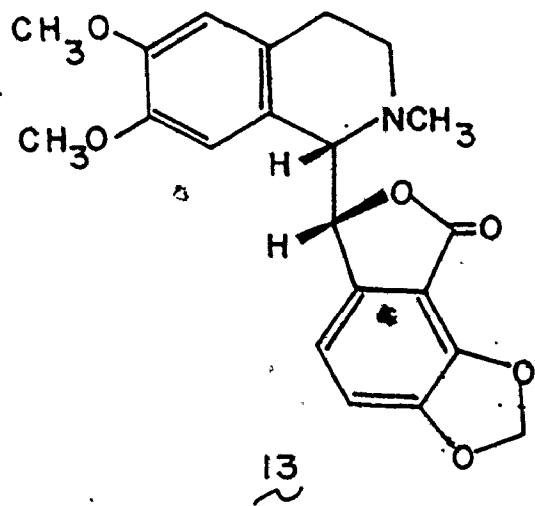
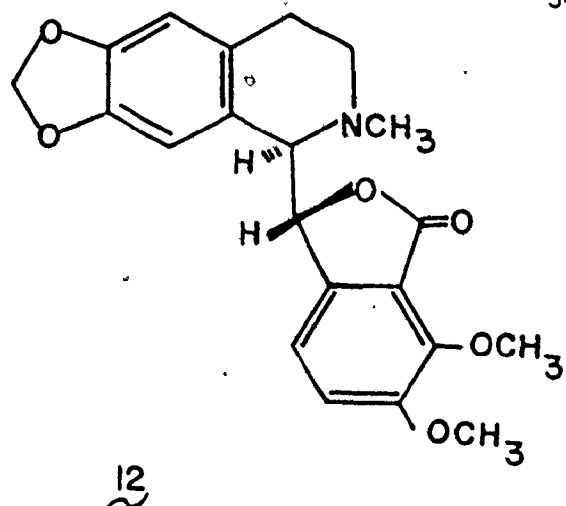
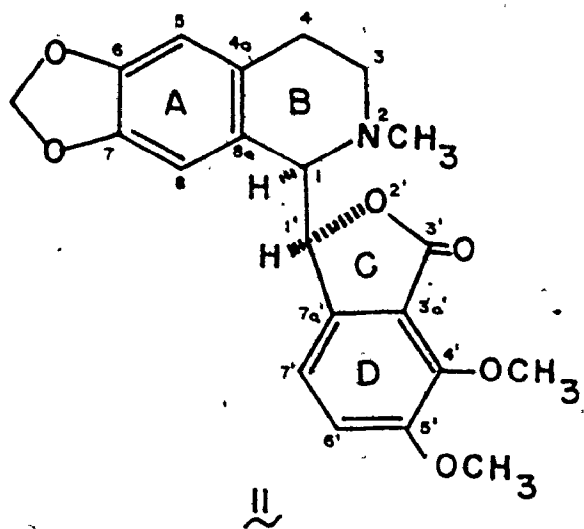
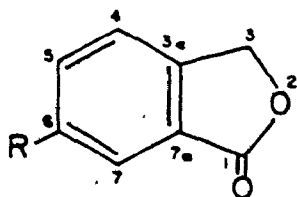


FIGURE 6. Structures of the phthalideisoquinoline alkaloids.

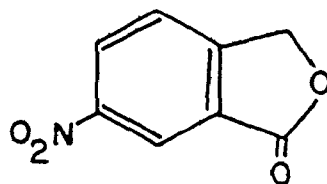
TABLE 6. ^{13}C chemical shifts of the phthalideisoquinoline alkaloids.

Carbon	β -Hydrastine (11)	α -Hydrastine (12)	Corlumine (13)	Adlumine (14)
1	66.0	66.2	65.7	65.7
3	49.0	51.3	49.5	51.7
4	26.7	29.3	26.5	29.1
4a	124.5	125.3	123.4	123.9
5	108.1	108.2	111.3	111.0
6	146.3	146.3	148.2	147.4
7	145.4	145.8	147.2	146.9
8	107.3	107.4	110.7	110.0
8a	130.0	130.0	129.5	128.4
1'	82.7	81.8	84.9	82.1
3''	167.0	168.0	167.2	167.7
3'a	119.4	119.3	110.3	109.7
4'	147.5	147.6	144.5	144.1
5'	152.6	152.3	149.1	148.8
6'	118.5	118.4	113.1	112.8
7'	117.3	118.1	115.5	116.1
7'a	140.4	141.1	140.8	140.9
NCH ₃	44.7	44.9	45.1	44.9
6,7 OCH ₂ O	100.5	100.7		
4' OCH ₃	62.0	62.2		
5' OCH ₃	56.7	56.7		
6 OCH ₃			55.9	55.6
7 OCH ₃			55.9	55.9
4',5' OCH ₂ O			103.3	103.1

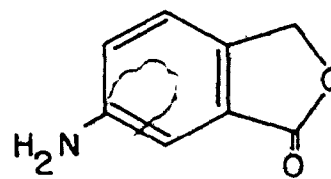


16a R=H

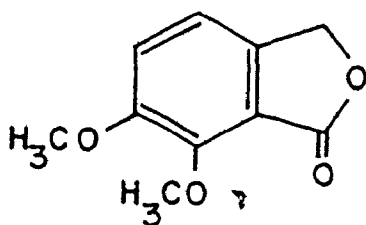
16b R=D



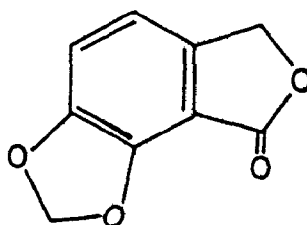
17



18



19



20

FIGURE 7. Structure of phthalide (16) and its derivatives.

TABLE 7. ^{13}C chemical shifts of phthalide and its derivatives.

Carbon	<u>16</u>	<u>17^a</u>	<u>18^a</u>	<u>19</u>	<u>20</u>
1	170.4	169.0	171.4	168.7	171.7
3	69.5	70.5	69.6	68.5	71.8
3a	146.3	153.4	134.4	139.6	139.4
4	122.0	125.0	123.0	116.7	115.1
5	133.6	128.9	121.0	119.9	114.7
6	128.5	148.5	149.8	152.6	149.5
7	124.9	120.1	107.3	148.6	145.6
7a	125.2	126.7	125.9	118.1	108.0
6 OCH ₃				57.0	
7 OCH ₃				62.3	
6,7 OCH ₂ O					103.8

^a Solvent: DMSO-d₆

Assignment of the aromatic carbons of meconin (19) was achieved by comparison with chemical shifts calculated using the ortho-dimethoxy shift parameters. Carbons 4 and 5 were verified by selective proton decoupling. Although the protons at C-4 (6.976) and C-5 (7.136) form an AB quartet, the C-4 proton was identified by long-range coupling to the C-3 benzylic protons.

In the alkaloids 11 and 12 the pattern observed for meconin is preserved. C-1' in both alkaloids is downfield relative to the corresponding carbon of meconin, while C-6' and C-7' have become more nearly equal in chemical shift. The signals of the methoxy groups in 11, 12 and 19 were assigned in analogy with those made for the model compound 5.

the more hindered methoxy group being at lower field.

Similar reasoning was used in assigning the signals in the spectra of 13 and 14. For the phthalide portion of these molecules, 6,7-methylenedioxyphthalide (20) was used as a model whose calculated chemical shifts (C-3a, 139.5; C-4, 115.2; C-5, 113.8; C-6, 147.7; C-7, 144.1; C-7a, 105.4 ppm) correlated well with the observed shifts (Table 7). This calculation was based on additivity parameters derived from methylenedioxybenzene (15) (C-1, +19.2; C-2, -19.8; C-3, -6.8) and applying these to the phthalide assignments. Selective proton decoupling confirmed the C-4 and C-5 assignments. The corresponding protons appear as an AB quartet ($J = 8.0$ Hz) at 7.27δ and 7.00δ with the C-4 proton being long-range coupled to the C-3 hydrogens.

Verification of the assignments of the unsubstituted aromatic carbons in 11, 13 and 14 was provided by selective decoupling experiments. In the case of 11 the protons on C-5 and C-7' were differentiated from C-8 and C-6', respectively, by virtue of their long-range coupling to benzylic protons. The assignments in 12 were made by comparison with 11. In corlumine (13) the protons on C-6' and C-7' form an AB quartet at 6.90δ and 6.14δ while the corresponding adlumine (14) protons appear at 6.84δ and 7.13δ . Again the C-7' proton in both compounds is long-range coupled to the C-1' hydrogen allowing the differentiation of C-6' and C-7'. Similar experiments established carbons 5 and 8.

A close examination of the diastereomeric pairs 11 and 12, and 13 and 14 shows that the isomers may be distinguished by ^{13}C NMR. In 12 and 14 both C-3 and C-4 are deshielded relative to the corresponding carbons in 11 and 13 whereas the opposite effect is observed at C-1'. The chemical

shifts at C-3 and C-4 are therefore diagnostic of the relative stereochemistry of these systems and ^{13}C NMR may thus be used to assign the relative configuration to a pair of diastereomeric phthalideisoquinolines. It should be pointed out that similar stereochemical assignments have been made from analysis of proton spectra (64) and that the ^{13}C NMR results are in agreement.

Comparison of the spectra of 11 or 12 with those of 13 or 14 demonstrates that structural elucidation of the phthalideisoquinoline alkaloids is facilitated by ^{13}C NMR. For example, the chemical shift of C-3'a is characteristic of the presence of either methylenedioxy or ortho-dimethoxy substitution at C-4' and C-5'. In 11 or 12, the appearance of the C-3'a resonance at ca. 10 ppm lower field than the corresponding carbon of 13 or 14 may be attributed to a steric perturbation by the C-4' and C-5' methoxy substituents. Such steric crowding is absent when the substituent at C-4' and C-5' is methylenedioxy. This effect is elaborated on further at the end of the protoberberine alkaloid section.

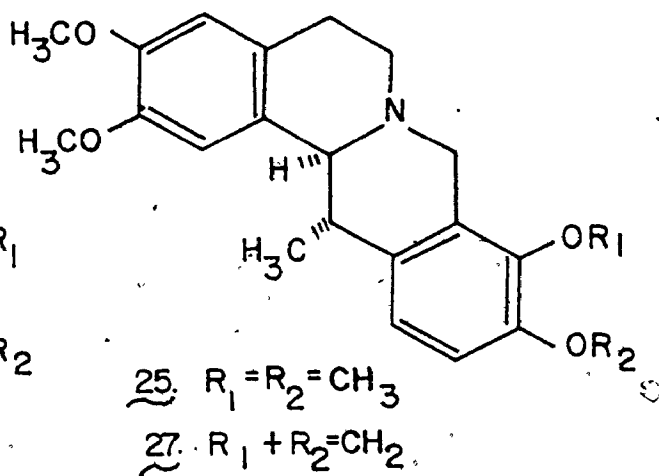
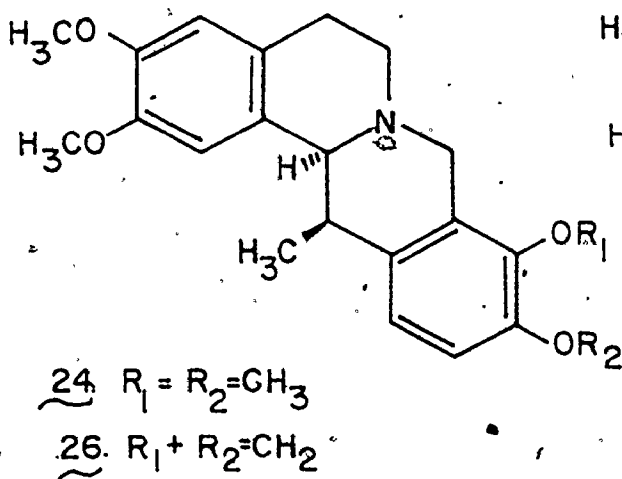
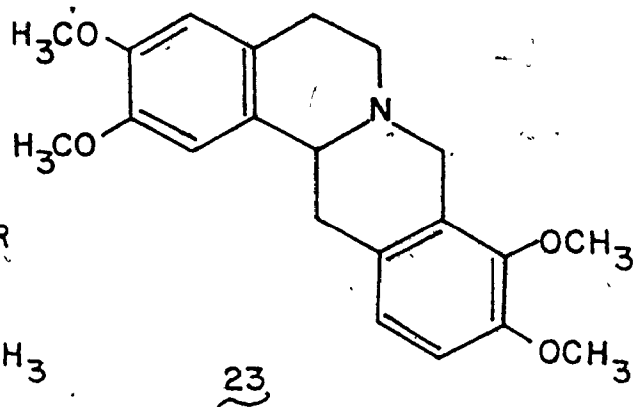
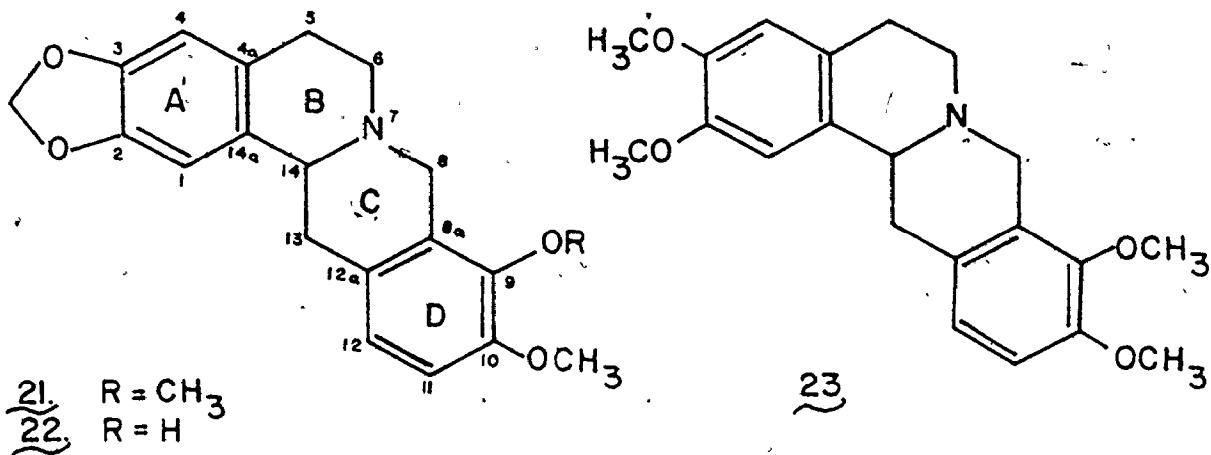
3.2.3 PROTOBERBERINE ALKALOIDS

The protoberberines are tetracyclic alkaloids that are derivatives of the dibenzo (a,g) quinolizidine system. The majority of compounds in this group carry oxygen substituents on the aromatic rings but are otherwise unsubstituted. There is however a small group of compounds with a methyl group at C-13. These alkaloids exist as diastereomers and several examples were examined to determine if their stereochemistry could be assigned by ^{13}C NMR.

The assignments for canadine (21) (Figure 8(a) and Table 8) were made by comparison with the model systems in section 3.2.1 and the phthalideisoquinolines, and also through the study of several deuterated derivatives. Reduction of berberine chloride with NaBD_4 yielded (+)-canadine labelled with deuterium at C-8 and C-14 (Figure 8(b)). In the spectrum of the labelled compound the signals at 59.6 and 53.4 ppm were virtually absent and these were assigned to C-14 and C-8, respectively. Canadine bearing deuterium in the 9-methoxy group was prepared by treatment of nandinine (22) with diazomethane and D_2O . This removed the resonance at 60.1 ppm confirming the assignment of the C-9 methoxy in canadine. There was not sufficient information to differentiate C-2 from C-3, C-4a from C-14a, or C-8a from C-12a. The spectrum of nandinine differs from that of canadine only in the aromatic signals of ring D, particularly those of C-8a and C-9. It is noteworthy that the signal from C-8 remains unaffected despite removal of the methyl group from the methoxy of C-9. The shift of C-8a to higher field may be attributed in part to a release from steric crowding, discussed above, caused by the C-9 methoxy group of (21). Tetrahydropalmatine (23) served as a model for the corydalines discussed below and its assignments are in accord with those of canadine.

Corydaline (24) and mesocorydaline (25) (Figure 8(a)) are diastereomeric 13-methyltetrahydroprotoberberines. It is known from ^1H NMR studies (65) that corydaline is a trans-quinolizidine and mesocorydaline a cis-quinolizidine, in which the methyl groups are axial and equatorial, respectively, in ring C. The change from a trans to a cis configuration in going from 24 to 25 is evident in the upfield shift of carbons 5,6,8

(a)



(b)

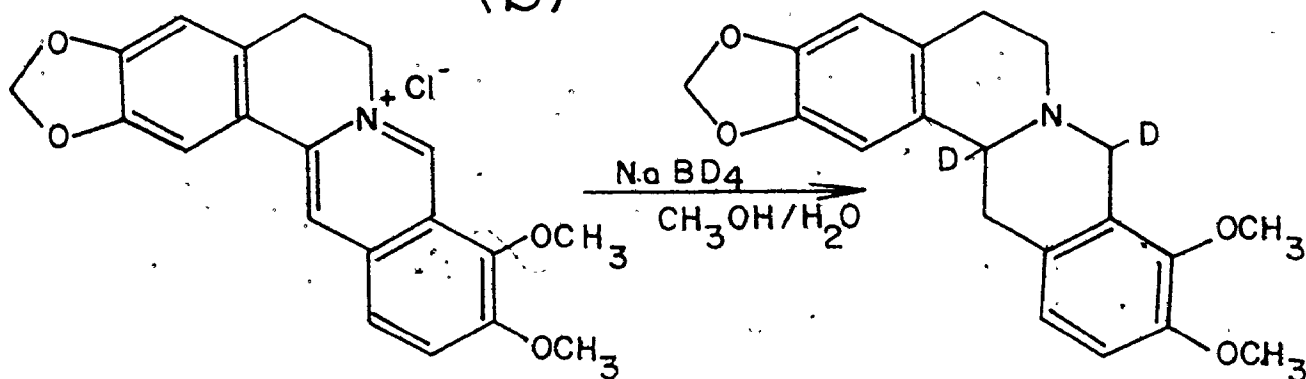


FIGURE 8. (a) Structures of the protoberberine alkaloids. (b) The reduction of berberine chloride to (+)-canadine-8,14-d₂.

TABLE 8. ^{13}C chemical shifts of the protoberberine alkaloids.

Carbon	<u>21</u>	<u>22</u>	<u>23</u>	<u>24</u>	<u>25</u>	<u>26</u>	<u>27</u>
1	105.5	105.7	108.9	109.0	112.1	108.8	112.0
2	146.0	146.1	147.6	147.3	146.7	147.3	146.6
3	146.2	146.2	147.6	147.8	148.0	147.9	148.0
4	108.4	108.5	111.5	111.3	111.1	111.3	110.9
4a	127.8	128.0	127.8	128.5	127.7	128.5	126.3
5	29.5	29.7	29.1	29.4	28.1	29.3	27.6
6	51.4	51.4	51.5	51.5	47.0	51.3	46.9
8	53.4	53.5	54.0	54.5	51.1	53.4	49.8
8a	127.8	121.4	126.9	128.6	126.5	116.9	115.8
9	150.3	141.7	150.3	150.2	150.2	144.8	144.8
10	145.2	144.2	145.2	145.1	145.4	143.2	143.7
11	111.1	109.1	111.1	111.7	111.1	106.8	106.8
12	123.8	119.4	123.7	124.1	123.2	121.3	120.3
12a	128.7	128.1	128.7	135.1	133.0	136.1	133.5
13	36.4	36.5	36.4	38.4	34.6	38.7	34.2
14	59.6	59.7	59.3	63.1	64.2	63.2	63.8
14a	130.9	131.1	129.9	128.6	130.7	128.5	130.3
2,3 OCH ₂ O	100.7	100.8					
9 OCH ₃	60.1		60.1	60.1	60.4		
10 OCH ₃	55.8	56.2	56.1	56.2	56.4		
2 OCH ₃			55.8	55.8	55.9	55.9	55.9
3 OCH ₃			55.8	55.9	55.9	56.1	56.1
9,10 OCH ₂ O						101.1	101.1
13 CH ₃				18.4	22.4	18.5	22.4

and 13 and is attributed to γ -gauche interactions (33,66,67) in the cis compound. Carbon-14, however, moves slightly downfield, a trend also observed in the quinolizidine systems of the Nuphar and Lycopodium alkaloids (68,69). The methyl group also moves downfield as it changes from an axial to an equatorial position. A similar shift is observed at C-1. It is of interest that the same downfield shift is observed in the proton spectrum for the methyl group. This is a reflection of a change in both the steric environment and anisotropic shielding of the methyl group.

The analogous diastereomeric pair, cavidine (26) and thalictrofoline (27) were also examined and gave similar results. It is apparent then that ^{13}C NMR may be used to assign the relative configuration to the 13-methyltetrahydroprotoberberines.

Kametani *et al.* (60) have used ^{13}C NMR as a probe to study the effect of substituents at C-1 on the stereochemistry of the quinolizidine system of alkaloids of the protoberberine group. When a methoxy was present at C-1 they concluded that the quinolizidine system was preferentially in the cis form. This conclusion was based on the upfield shift of the signal for C-6. Comparison of the published results of 28 (Figure 9) with those of 24, 25, 26, and 27 reveals some interesting differences. In the cis 13-methyltetrahydroprotoberberines C-5, C-6, C-8, and C-13 all undergo upfield shifts relative to the trans compounds but only C-6 and C-13 are appreciably affected in 28. Carbon 14 in 28 is shifted upfield relative to 23 in a manner analogous to that discussed previously for C-1 in compound 6 and this steric effect probably outweighs any change associated with a cis-trans interconversion. Interestingly, C-5 and C-8 of 28 do not experience an upfield shift as they do in the 13-methyl compounds. Although the nature of these differences has not undergone a detailed

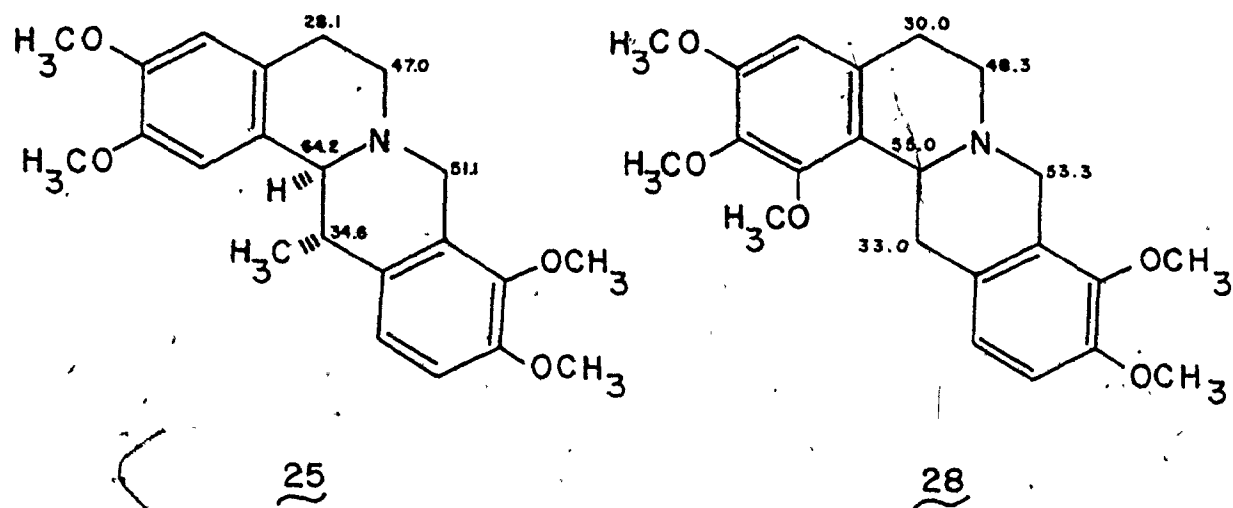


FIGURE 9. Comparison of the ^{13}C chemical shifts of the aliphatic carbons of mesocorydaline (25) and compound 28 (60).

investigation, it can be concluded that the conformations of the cis compounds resulting from C-1 methoxy substitution must differ from the cis C-13 methyl compounds.

Throughout this work use has been made of calculations based on the shift parameters for ortho-dimethoxy or methylenedioxy substituents. Chemical shifts calculated from these parameters are generally in good agreement with observed values, with the exception of the calculated shifts for a substituted aromatic carbon ortho to two adjacent methoxy groups. Examples are C-8a of 5, C-3'a of 11 and 12, C-7a of 19 and C-8a of 21 - 25, where the values calculated as described above are ca. 10 ppm lower than those observed. A similar discrepancy has been noted by Dhimi and Stothers (63) in the case of ortho-disubstituted anisoles and attributed to steric perturbations. The observation that the less bulky methylenedioxy substituent gives calculated shifts which are in close agreement with observed values at a substituted ortho carbon, such as C-7a of 20, and C-8a of 26 and 27 supports this conclusion. As noted previously, this difference between the ortho-dimethoxy and methylenedioxy substituents is of diagnostic value in structural assignments.

3.2.4 SPIROBENZYLISOQUINOLINE ALKALOIDS

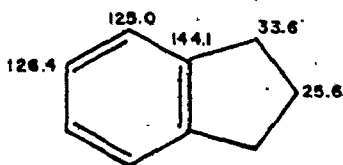
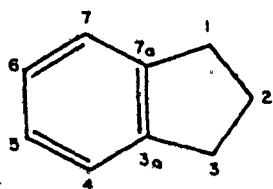
The spirobenzylisoquinoline alkaloids are a relatively small group of compounds within the isoquinoline family. Their structure and chemistry were recently reviewed (70,71). Ochotensimine (43) was the first member of this group to be investigated and it and ochotensine (70,71) are the only alkaloids that carry an exocyclic methylene on the spiro ring. More common are the alkaloids that are oxygenated in the five-membered ring and carry these oxygens in the form of carbonyl, hydroxy, or acetoxy groups

on one or both of carbons 8 or 13. The structures of the alkaloids of this group and synthetic analogues used in this study are shown as the formulas 43-52 in Figure 13.

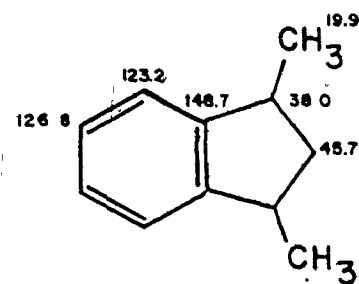
The appropriately substituted 1,2,3,4-tetrahydroisoquinolines served as models for rings A and B. Several indane derivatives were prepared and their spectra aided the assignment of the ^{13}C resonances in rings C and D of the spiro compounds.

Chemical shifts for both indane (29) and 1,3-dimethylindane (30) (Figure 10) have been published (21,72), and the indane results were recently verified (73). Using indane and methylenecyclopentane (31) (74) as models, the shift assignments for 1-methyleneindane (32) were made. Of the two substituted aromatic carbons in 32, C-7a was assigned at lower field because of β -substitution at C-1. In dealing with the unsubstituted aromatic carbons, the signal at 120.6 ppm was assigned to C-7 because of the γ -steric effect of the C-1 substituent. While the signal at 125.3 ppm could not be unambiguously differentiated from that at 126.4, it was assigned to C-4 since this carbon is in an environment analogous to that in indane. Of the two remaining signals, that at lower field is tentatively assigned to C-5 because it is para to the double bond system. The aromatic chemical shifts of 4,5-methylenedioxy-1-methyleneindane (33) (Figure 10) were then calculated using the substituent parameters for a methylenedioxy group and it served as a model for rings C and D of ochotensimine.

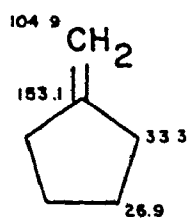
Several derivatives of 1-indanone (34a) were examined to serve as models for the alkaloids bearing a carbonyl group in ring C (Figure 11 and Table 9). In the case of 1-indanone itself, C-3a is at lower field.



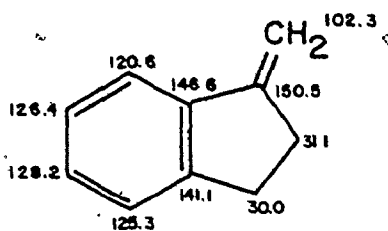
29



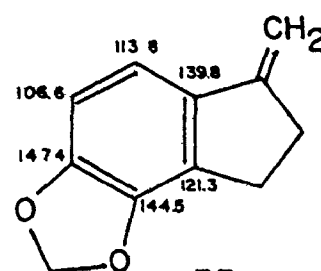
30



31

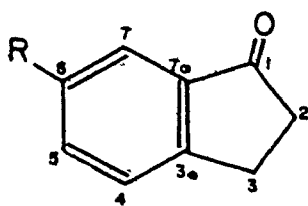


32



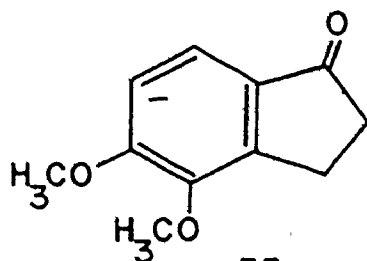
33

FIGURE 10. ^{13}C chemical shifts of the indanes 29-33 and methylenecyclopentane (31) (74).

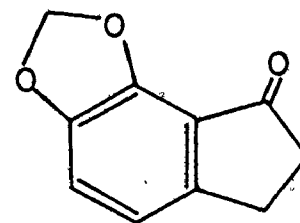


34a. R=H

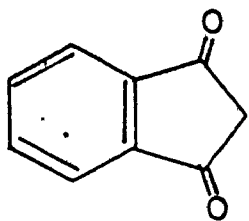
34b. R=D



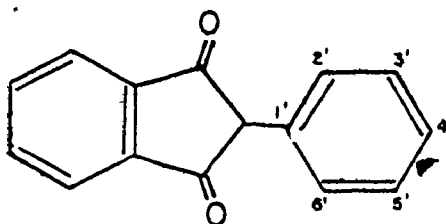
35



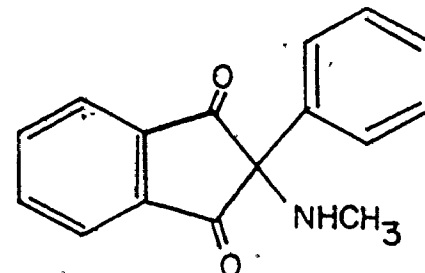
36



37



38



39

FIGURE 11. Structures of the indanones and indandiones 34a-39.

TABLE 9. ^{13}C chemical shifts of the indanones and indandiones 34a-39.

Carbon	<u>34a</u>	<u>35</u>	<u>36</u>	<u>37</u>	<u>38</u>	<u>39</u>
1	206.5	205.2	204.1	197.3	198.2	200.8
2	36.0	36.4	37.3	45.0	59.8	73.5
3	25.5	22.5	25.8	197.3	198.2	200.8
3a	155.0	145.6	148.3	141.5	142.8	142.8
4	126.6	147.9	118.9	123.8	123.8	123.1
5	134.4	157.6	114.3	136.4	136.0	136.4
6	127.1	112.5	147.4	136.4	136.0	136.4
7	123.4	120.0	143.6	123.8	123.8	123.8
7a	137.0	131.2	120.4	141.5	142.8	142.8
4 OCH ₃		60.3				
5 OCH ₃		56.3				
6,7 OCH ₂ O			103.0			
1'					133.2	136.3
2',6'					125.5	127.5
3',5'					128.4	129.0
4'					127.9	128.8
NHCH ₃						31.6

than C-7a due to the electron withdrawing effect of the carbonyl group. The assignments of the unsubstituted carbons were verified by examination of the spectrum of 6-deuterio-1-indanone (34b). In 34b the signal at 127.1 ppm had virtually disappeared so that the assignment at C-6 was secure. Carbon 5 follows from consideration of the substituent effect for a carbonyl group on a para carbon. The remaining positions C-4 and C-7 were determined from the gated decoupled spectrum since deuterium substitution at C-6 removes the 7.0 Hz meta coupling between C-4 and the C-6 hydrogen. With the spectrum of 1-indanone established, the resonances in the substituted 1-indanones 35 and 36 could be assigned by making use of the substituent parameters for o-dimethoxy and methylenedioxy groups. The calculated chemical shifts showed a reasonable agreement with observed values except for the expected deviation at C-3a in the dimethoxy compound. The assignments of the protonated aromatic carbons were verified in all cases by selective proton decoupling.

Another series of models, the 1,3-indandiones, were also studied. The diones have been prepared as intermediates in several synthetic approaches to the spiro alkaloids (70,71) and their spectral data is also included. The compounds examined are shown in Figures 11 and 12. In two of them (40 and 41) the complete skeleton of the spiro alkaloids is present.

The spectra of the 1,3-indandiones 37, 38, and 39 were used in the interpretation of the spectra of the spiro compounds 40 and 41. Assignment of the resonances of 37 was made without difficulty because of the symmetry of this molecule and by taking into account the substituent effects of the two carbonyl groups (Table 9). As C-2 becomes more substituted in going from 37 to 39, its chemical shift moves downfield as expected. Substitution at C-2 also deshields the carbonyl carbons but has very little influence on

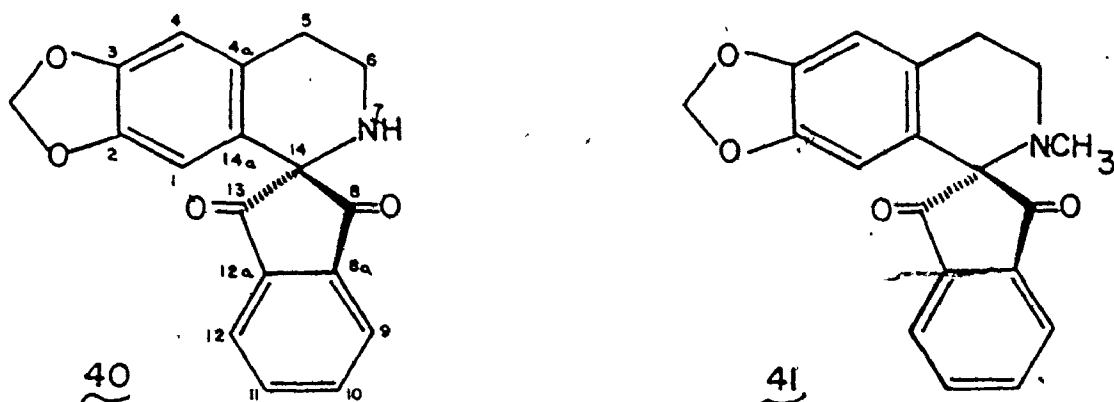


FIGURE 12. Structures of the spiro-diones **40** and **41**.

TABLE 10. ¹³C chemical shifts of the spiro-diones **40** and **41**.

Carbon	40	41
1	105.3	105.2
2	146.4	146.3
3	147.3	147.2
4	110.1	109.5
4a	131.0	129.9
5	29.4	29.1
6	40.1	48.1
8, 13	200.0	202.8
8a, 12a	142.0	142.4
9, 12	124.5	123.8
10, 11	136.3	136.6
14	66.2	71.7
14a	136.1	137.7
2, 3 OCH ₂ O	101.6	101.1
NCH ₃		40.5

the aromatic carbons of the indandione system.

In the spiro compounds, 40 and 41, the indandione part of the molecule retains its symmetry and chemical shifts are observed which are similar to the models 37, 38 and 39. The resonances of the ring A carbons are very similar to those found in other tetrahydroisoquinolines. The assignments made for C-4a and C-14a are based on the argument that C-14a has the greater number of β -substituents. In the proton spectrum of 41 the hydrogen at C-1 is shielded relative to that at C-4 (75) and it was through selective proton decoupling that the resonances of these carbons were established. The major difference between 40 and 41 lies in the chemical shifts of C-6 and C-14, both of which are deshielded in the N-methyl relative to the N-H compound. Calculations, using the β equatorial methyl parameter derived from methylcyclohexane (34), work well for C-6 but because of the highly substituted nature of C-14 there was a deviation between the observed and calculated chemical shift.

Turning now to (+)-ochotensimine (43 in Figure 13), this alkaloid is distinguished from the others examined in this study by the presence of an exocyclic methylene at C-13. The assignments (Table 11) in rings A and B were made by comparison with the spectrum of 2 (Figure 5 and Table 5). Carbons 1, 2, 3, 4, and 4a are not greatly different from the model and the assignments of C-1 and C-4 were differentiated from C-11 and C-12 by selective proton decoupling. Since carbons 2 and 3 are separated by only 0.2 ppm unambiguous assignments could not be made. C-14a and C-12 cannot be differentiated but it is noteworthy that relative to the model C-14a has shifted considerably downfield. This shift is attributed to the greater β substitution at C-14 in 43 relative to 2.

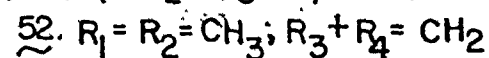
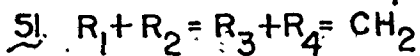
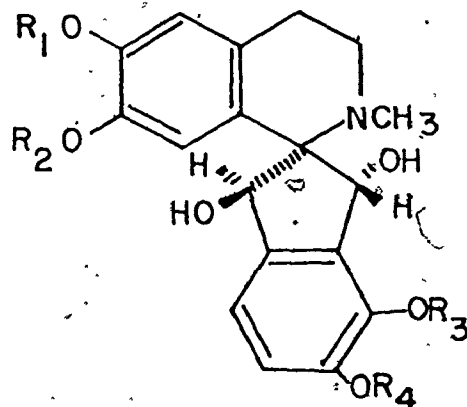
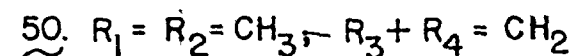
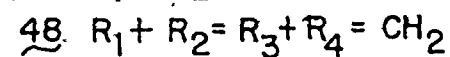
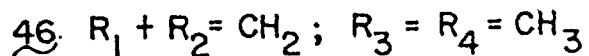
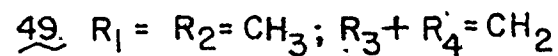
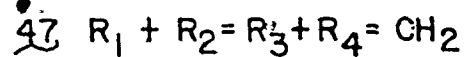
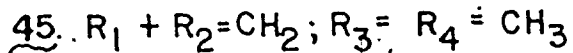
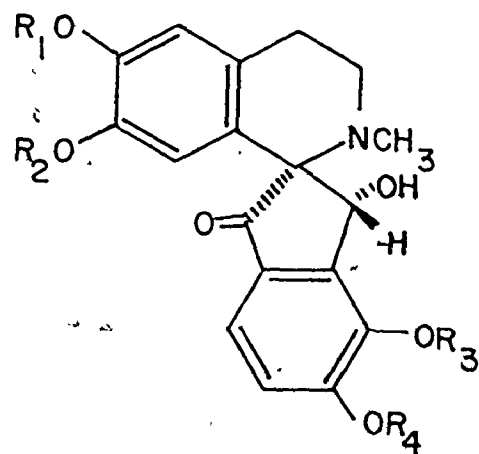
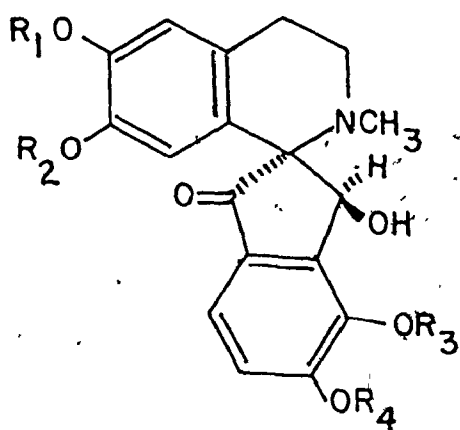
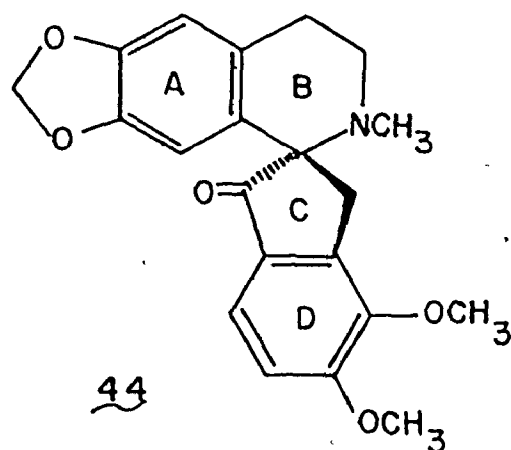
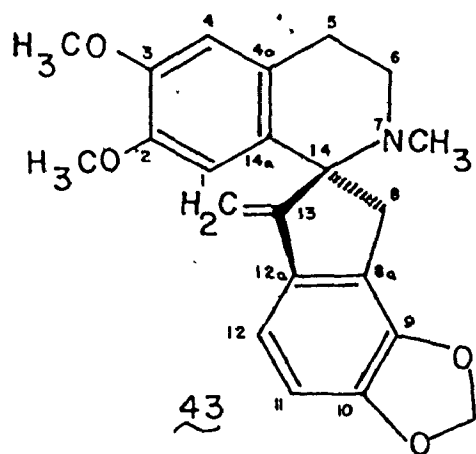


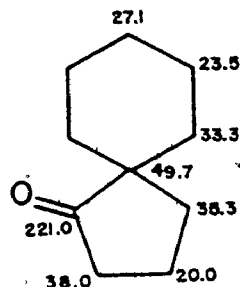
FIGURE 13. Structures of the spirobenzylisoquinoline alkaloids 43-52.
(The absolute stereochemistry is not implied in this figure).

TABLE 11. ^{13}C Chemical Shifts of the Spirobenzylisoquinoline Alkaloids

Carbon	43	44	45	46	47	48	49	50	51	52
1	110.5	104.8	107.2	105.7	106.9	105.8	110.7	110.7	109.7	110.1
2	147.5	146.5	146.9	146.8	147.4	146.9	147.2	148.5	146.2	147.3
3	147.7	146.5	146.9	146.8	147.4	146.9	148.9	148.6	146.8	148.3
4	110.5	108.5	109.1	108.2	109.6	108.2	112.5	111.4	110.0	113.0
4a	126.1	128.3	125.9	129.3	125.0	129.3	124.0	128.7	126.0	124.9
5	29.1	29.4	28.9	29.4	29.2	29.5	28.5	29.3	22.8	22.0
6	48.1	48.4	48.7	50.3	48.9	50.2	48.9	50.3	47.6	47.8
8	37.0	37.3	70.5	75.9	70.3	75.0	70.1	75.1	73.4	73.4
8a	123.8	145.4	145.4	146.7	132.7	134.3	132.9	134.6	121.5	121.5
9	143.0	145.6	145.5	147.0	146.1	144.4	145.0	144.4	144.7	144.9
10	148.2	158.5	159.2	159.3	154.8	154.5	154.5	154.6	148.6	148.4
11	108.0	113.8	114.5	114.3	110.9	110.6	110.4	109.5	107.1	109.7
12	113.6	121.1	120.6	120.4	119.9	119.6	119.5	119.6	116.1	115.7
12a	136.1	131.0	130.0	130.1	132.5	131.2	132.5	131.3	140.0	140.9
13	155.5	206.4	202.4	202.7	201.5	202.2	201.7	202.7	79.5	79.0
14	71.9	71.2	76.8	72.0	77.2	72.0	76.9	72.0	75.2	75.2
14a	137.2	131.8	130.9	130.1	130.6	129.8	129.7	128.7	129.5	128.3
NCH ₃	39.0	39.2	39.4	41.8	39.7	41.7	39.6	41.9	37.7	37.9
2,3 OCH ₂ O	100.9	100.9	100.9	101.0	101.3	101.1			101.0	
9,10 OCH ₂ O	101.3				103.2	103.1	103.1	103.2	101.9	101.8
2* OCH ₃	56.1						56.1	56.1		56.0
3* OCH ₃	55.8						56.0	56.5		55.5
9 OCH ₃		60.4		61.3						
10 OCH ₃		56.3		56.4						
13 = CH ₂	106.7									

* These assignments may be reversed.

In ring B the changes between 2 and 43 are as follows: C-14, +14.3; C-6, -4.9; C-5, +0.3; N-CH₃, -7.0. The shielding of both C-6 and the N-methyl group may be attributed to the γ -gauche effect of both C-8 and C-13. Geminal substitution to create the spiro ring junction at C-14 causes a significant deshielding in a manner analogous to that observed for the spiro carbon in spiro[4.5]decan-1-one (42) (76) relative to cyclohexane.



42

Chemical shift assignments for rings C and D were determined with the aid of model compounds 32 and 33, already discussed. The calculated shifts of 33 served as a guide in assigning the substituted aromatic carbons of ring D. Selective proton decoupling differentiated between C-11 and C-12. Identification of the exocyclic methylene of ring C was provided by a gated decoupling experiment. This carbon appears as a triplet centered at 106.7 ppm with $^1J_{13C,1H} = 160.6$ Hz.

The synthetic spiro ketone 44 was examined as a model for the sibiricine type alkaloids where three diastereomeric pairs were studied, the compounds 45 and 46, sibiricine 47 (77) and corydaine 48 (78), and raddeanone 49 (79) and yenusomidine 50 (80), all of established

stereochemistry (Figure 13 and Table 11). The carbon resonances of rings A and B in 44 were assigned through comparison with other isoquinoline alkaloids that carry methylenedioxy substitution in ring A, e.g. β -hydrastine (11) and canadine (21). Selective proton decoupling confirmed the assignments at C-1 and C-4. The fact that C-1 and C-4 are not equivalent as they are in ochotensimine may be a reflection of the difference in anisotropic shielding between the exocyclic methylene in 43 and the carbonyl in 44. Carbons 4a and 14a follow the same trend observed in 43 but C-14a is less deshielded.

The chemical shifts of the aliphatic carbons of 44 are essentially identical with those of 43. The indanone 35 serves as an excellent model for the carbons of rings C and D of 44; however, one cannot differentiate between C-8a and C-9 because of their similar shifts.

Alkaloids of the sibiricine group differ from 44 by the presence of a hydroxy function at C-8 and these may exist in diastereomeric forms. Chemical shift assignments for the synthetic compounds, 45 and 46 follow directly from the model 44. The ring D assignments for the pairs 47 and 48 and 49 and 50 were made by selective proton decoupling and by comparison to chemical shifts calculated for 4,5-methylenedioxy-1-indanone; C-3a, 135.2; C-4, 145.8; C-5, 153.6; C-6, 107.3; C-7, 116.6; C-7a, 130.2.

In 45, C-8 and C-14 show the expected downfield shifts relative to 44 because of the α - and β -OH substituent effects, respectively. The carbonyl group is shielded by -4.0 ppm. There are a number of significant changes in 46 relative to its diastereomer. Hydrogen bonding between the hydroxy group and the nitrogen (78) causes slight conformational and electronic changes in the system resulting in a deshielding of C-8, C-6, and the N-methyl. At the same time C-14 is appreciably shielded.

Differences of similar sign and magnitude are also observed between sibiricine (47) and corydaine (48) and raddeanone (49) and yenusomidine (50).

Ochrobirine 51 and yenusomine 52 (80) carry hydroxy groups on each of C-8 and C-13 and they represent another structural variation. The problem here was to determine if ^{13}C NMR could differentiate between C-8 and C-13 in these compounds and be used to assign the configuration of the hydroxy groups.

The data presented in Table II shows that several important chemical shift changes occur when corydaine (48) is transformed into ochrobirine (51). Upon replacement of the carbonyl function by hydroxy, the aromatic carbon C-1 is deshielded by 3.9 ppm relative to corydaine while C-12 is shielded by -3.5 ppm. Examination of the aliphatic carbons of 51 indicates a distinct difference between C-8 and C-13. Selective proton decoupling was used to resolve these assignments since in the ^1H NMR spectrum of 51 the C-8 and C-13 hydrogens appear at 4.88 and 5.42 ppm, respectively (70,81). Although C-8 is shielded relative to that in corydaine (48), C-8 is still downfield from the corresponding carbon in sibiricine (47) which indicates a retention of the corydaine relative configuration.

Of the ring B carbons of ochrobirine (51), only C-14 has undergone a downfield shift whereas C-5, C-6, and the N-methyl are shielded by -6.7, -2.6, and -4.0 ppm respectively, relative to corydaine. The γ steric effect of the sp^3 centre at C-13 accounts for the shielding of C-6 and the N-methyl. Examination of molecular models demonstrates that the C-13 hydrogen and both the N-methyl and pseudo-axial C-6 hydrogen are quite

sterically crowded when ring B adopts a half-chain conformation. Distortion of the B ring half-chain to a slightly more flattened conformation partially relieves these steric interactions while maintaining the internal hydrogen bond. This conformational change may contribute to the upfield shift of C-5.

Yenusomine (52) is a trans diol like ochrobirine with the hydroxy at C-8 hydrogen-bonded to nitrogen. The changes that occur in going from yenusomidine (50) to yenusomine exactly parallel those that take place in the corydaine to ochrobirine transformation. These results demonstrate the value of ^{13}C NMR in the assignment of the relative stereochemistry of the spirobenzylisoquinoline alkaloids.

3.2.5 CANCENTRINE ALKALOIDS

The cancentrine alkaloids were first isolated by Manske in 1932 (82) and in 1970 the structure of cancentrine 53a was elucidated (83). It is composed of a morphine-derived unit and a cularine-like unit which are fused together as shown in Figure 14. Other alkaloids in this series are the dehydrocantrines, A and B (84). The former has a double bond between C-8 and C-14 while the B compound has a double bond between C-31 and C-32. The data obtained from the ^{13}C spectra of cancentrine, the derivative 54 and the codeine model compounds 55a-c was used to elucidate the structure of the new alkaloid 10-oxocancentrine 53b.

The interpretation of the ^{13}C spectrum of cancentrine (Table 12) was aided by reference to the published spectra of codeine 55a and cularine 56 (Figure 15 and Table 13). Comparison of the aliphatic region of the codeine (55a) spectrum (85) with that of cancentrine (53a) allowed the assignment of resonances for C-10, C-15, C-16, and N-CH₃ which were substantiated by the off-resonance spectrum. The high field resonance of C-10, a benzylic carbon, has been ascribed to a γ -steric interaction with the N-CH₃ (85). The other high field signal in the spectrum of 53a at 29.0 ppm has been assigned to C-31 by reference to the cularine 56 spectrum (59). The off-resonance spectrum of 53a showed a singlet at 51.4 ppm, a doublet at 46.2 ppm, and a triplet at 40.2 ppm that are attributed to carbon atoms 13, 14, and 8, respectively. The transformation of the six-membered ring C of codeine to the five-membered alicyclic spiro ring present in cancentrine has caused a deshielding of C-13 and C-14 relative to the corresponding carbon atoms of codeine.

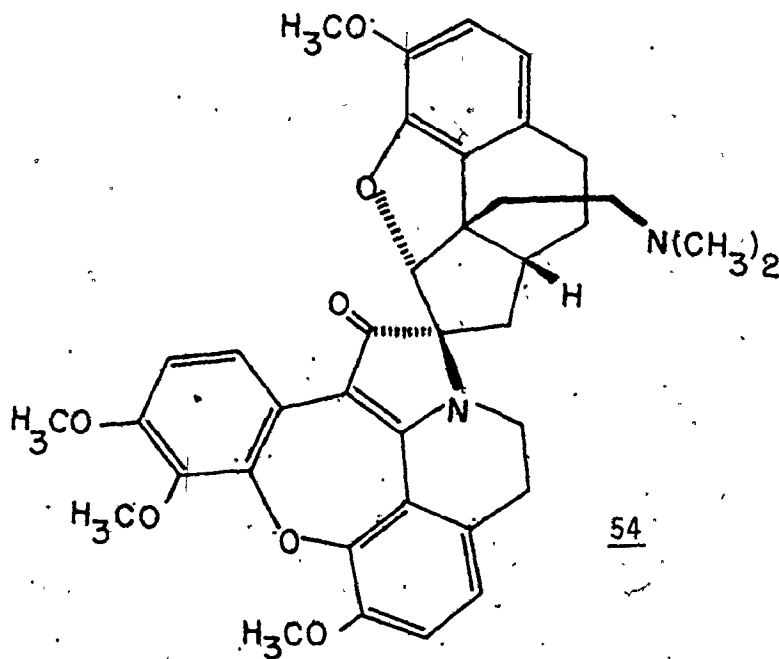
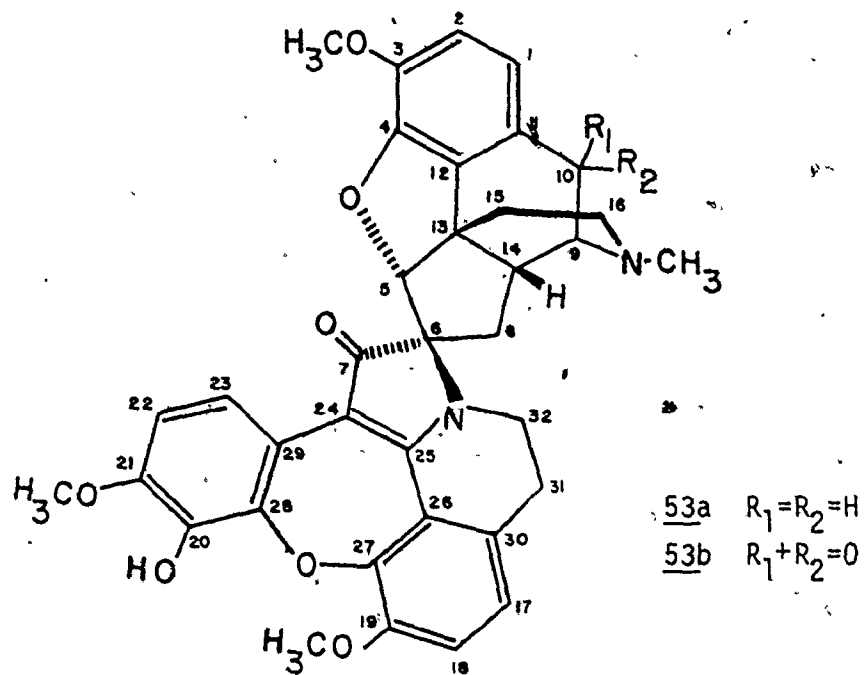
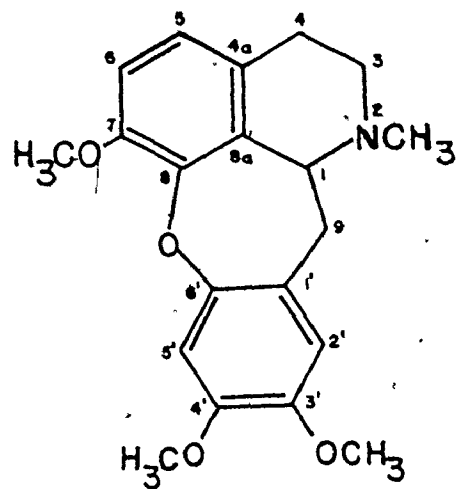
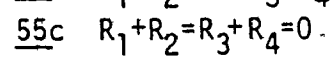
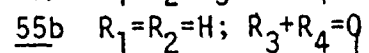
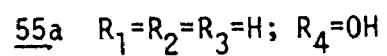
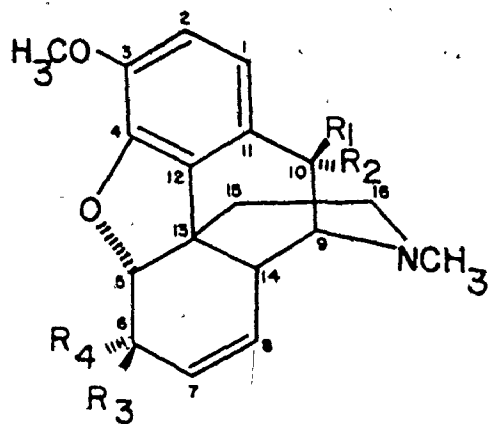


FIGURE 14. Structures of cancentrine (53a), 10-oxocancentrine (53b), and 9,10-dihydrocancentrine methine-o-methylether (54).

TABLE 12. ^{13}C chemical shifts of the cancontrine alkaloids

Carbon	53a	53b	54
1	119.7	120.2	119.9
2	115.3	115.3	116.0
3	142.7	146.6	142.5
4	145.1	143.3	146.9
5	97.5	96.7	99.3
6	79.1	78.3	79.2
7	194.0	193.2	193.3
8	40.2	40.0	40.1
9	58.8	68.0	23.7
10	20.4	196.3	26.2
11	127.4	124.4	127.3
12	127.7	135.6	128.8
13	51.4	52.5	56.4
14	46.2	48.9	41.9
15	33.2	32.1	33.3
16	46.6	47.3	45.5
17	124.3	124.2	124.2
18	116.3	115.9	116.8
19	149.8	149.5	152.3
20	138.0	137.8	147.8
21	146.8	146.6	151.2
22	109.2	108.9	109.1
23	116.6	115.9	121.1
24	104.3	104.3	104.2
25	160.1	160.4	160.6
26	121.4	121.0	121.8
27	147.7	146.8	147.6
28	140.7	140.5	141.7
29	119.7	119.2	121.0
30	127.8	127.5	128.1
31	29.0	28.8	29.4
32	57.8	57.3	55.8
3 OCH ₃	56.5	56.3	56.4
19 OCH ₃	56.5	56.3	57.7
20 OCH ₃			61.5
21 OCH ₃	56.5	56.3	56.7
NCH ₃	43.2	43.3	



56

FIGURE 15. Structures of codeine (55a), codeinone (55b), 10-oxocodeinone (55c) and cularine (56).

TABLE 13. ^{13}C chemical shifts of the cancentrine model compounds.

Carbon	<u>55a</u> ^a	<u>55b</u> ^a	<u>55c</u>	Carbon	<u>56</u> ^b
1	119.3	119.7	120.0	1	56.7
2	112.8	114.7	115.0	3	47.5
3	142.0	142.3	149.6	4'	26.0
4	146.2	144.6	144.9	4a	126.3
5	91.3	88.0	87.7	5	124.3
6	66.4	194.1	193.2	6	110.4
7	133.2	132.2	132.7	7	148.9
8	128.1	149.1	148.3	8	144.8
9	58.7	58.9	68.5	8a	132.5
10	20.4	20.4	190.4	9	35.3
11	127.0	126.1	125.1	1'	118.3
12	130.9	129.0	137.1	2'	113.6
13	43.0	43.1	44.6	3'	144.8
14	40.7	41.4	44.4	4'	147.3
15	35.8	33.9	33.9	5'	105.1
16	46.4	46.7	47.2	6'	148.4
3 OCH ₃	56.2	56.7	56.3	7 OCH ₃	55.8
NCH ₃	43.0	42.9	43.4	3' OCH ₃	56.0
				4' OCH ₃	56.0
				NCH ₃	42.4


^a Assignments from reference 85

^b Assignments from reference 59

A similar effect is observed at C-5. Although the splitting patterns of C-9 and C-32 in the off-resonance spectrum are partially obscured by the overlapping methoxyl resonances at 56.5 ppm, C-9 was assigned to 58.8 ppm and C-32 to 57.8 ppm. The remaining signal at 79.1 ppm is assigned to the spiro carbon, C-6.

The oxygenated aromatic carbons of cancertrine all fall in the range, 135-150 ppm while the remaining aromatic carbons, whether substituted with H or carbon, resonate in the 100-130 ppm region. By off-resonance decoupling it was possible in most cases to differentiate the protonated from the non-protonated carbons. For those cases where overlap of signals made this difficult or impossible the technique of selective enhancement of quaternary carbon signals (46) was used. A low power and modulated decoupling field was applied to the sample, producing essentially a broad-band spectrum composed only of the quaternary carbons. From a combination of the low-power decoupled and off-resonance spectra, the signal at 119.7 ppm was found to result from the overlap of both a protonated and carbon-substituted aromatic carbon.

The aromatic carbons of the morphine half of cancertrine (53a) were assigned by comparison to codeine. The assignment of C-4 to 145.1 ppm rather than 146.8 ppm was based on the correlation noted by Terui et al. (85) between peak intensity and the spin-lattice relaxation times, the latter determined by Wehrli for codeine (52). Carbon-4 of 53a does not have any neighbouring protons to provide dipolar relaxation and therefore should have a longer T_1 and a lower intensity because of saturation. The similarity in chemical shifts for carbons 11, 12, and 30 did not allow unambiguous assignments to be made.



Reference to the cularine (56) data in Table 13 allowed the tentative assignment of the remaining aromatic signals. The chemical shifts of C-30 and C-26 were assigned in reverse order to the corresponding cularine carbon atoms, 8a and 4a. Since C-26 does not have any neighbouring hydrogens this would account for the low intensity of the peak at 121.4 ppm. Of the carbon atoms containing oxygen substituents, C-20 was assigned to 138.0 ppm because the hydroxy group deshields the directly bonded carbon atom less than a methoxy group (21, 43). The signals at 194.0, 160.1, and 104.3 ppm are attributed to the carbon atoms of the α,β -unsaturated carbonyl system, C-7, C-25, and C-24, respectively.

Further evidence for the cancentrine chemical shift assignments was provided by an examination of the spectrum of 9,10-dihydrocancetrine methine-o-methyl ether (54) (86). Fission of the bond to nitrogen caused C-9 to shift upfield from 58.8 ppm in cancentrine (53a) to 23.7 ppm in 54. Carbon 14 was also shielded relative to 53a because of the elimination of the β nitrogen substituent effect. Carbon 10 was assigned to 26.2 ppm; it is deshielded relative to cancentrine because of removal of the γ -steric interaction with the N-CH₃. The chemical shift equivalence of C-16 and the N(CH₃)₂ group was confirmed by the off-resonance spectrum in which the methylene triplet of C-16 was centered in the methyl quartet. The off-resonance spectrum also enabled the peak at 61.5 ppm to be assigned to the C-20 methoxy group. This assignment is consistent with the previously discussed alkaloids containing a sterically crowded methoxy group. Carbon-32 could only be tentatively assigned to 55.8 ppm because of the overlap of its coupling pattern with those of the methoxy carbons in the off-resonance spectra. By the technique of selective enhancement of

quaternary carbons the signal at 56.4 ppm was assigned to C-13!

Using the procedure described in the analysis of the aromatic region of the cancentrine spectrum, the corresponding aromatic carbons of the morphine part of 54 were readily assigned. Similarly in the cularine portion of 54 the carbon atoms of the ring containing the single methoxy substituent at C-19 remain essentially unchanged relative to 53a except for C-19 itself which is deshielded. The conversion of the hydroxy group at C-20 to a methoxy shifted the peak at 138.0 ppm in the spectrum of 53a to 147.8 ppm in 54. There was also a deshielding of the resonance for C-23 which now appears at 121.1 ppm. The signals at 151.2 and 152.3 ppm can be assigned to either C-21 or C-19; these signals were more intense than the signals of the other oxygenated carbons because of the dipolar relaxation provided by the neighbouring protons on carbons 22 and 18, respectively.

DISCUSSION

10-Oxocancentrine

The new cancentrine alkaloid, designated 10-oxocancentrine had the following spectral properties. In the 220 MHz ^1H NMR spectrum there were no signals at 2.0 and 3.18 ppm corresponding to the 10α and 10β protons, respectively, in cancentrine (83) (Table 14). There was also a simplification of the multiplet coupling for the C-9 proton now appearing at 3.39 ppm. The aromatic region of the ^1H spectrum of cancentrine (53a) contains three pairs of AB quartets whose chemical shift assignments were determined by both NOE experiments and acetylation shifts (83,86). In cancentrine the two high field aromatic doublets at 6.65 ($J=8.8$ Hz) and 6.70 ppm ($J=8.4$ Hz) were assigned to H-1 and H-22, respectively. The

TABLE 14. 220 MHz ^1H chemical shifts and coupling constants for
 cancentrine (53a) and 10-oxocancentrine (53b).

Proton	<u>53a</u>	<u>53b</u>
H-5	4.88	4.84
H-9	3.41	3.39
H-10 α	2.37	
H-10 β	3.18	
3-OCH ₃	3.97	4.02
19-OCH ₃	3.93	3.98
21-OCH ₃	3.86	3.85
H-1	6.65	7.45
H-2	6.86	7.00
H-17	6.97	7.03
H-18	7.04	7.09
H-22	6.70	6.67
H-23	7.49	7.49
NCH ₃	2.50	2.53
J _{10α,10β}	18.5	
J _{1,2}	8.8	8.7
J _{1,18}	8.5	8.7
J _{22,23}	8.4	8.6

spectrum of 10-oxocancentrine (53b) has only one doublet at 6.67 ppm ($J=8.6$ Hz) and a new doublet centered at 7.45 ppm ($J=8.7$ Hz). This new low field doublet is attributed to H-1 because it is now deshielded by the carbonyl group considered to be situated at C-10. The remaining aromatic resonances of 53b show the same spectral pattern as cancentrine except for a slight deshielding (Table 14).

The mass spectrum of 53b shows a molecular ion at m/e 620 with a composition of $C_{36}H_{32}N_2O_8$. This ion loses CH_3 (m/e 605, $C_{35}H_{29}N_2O_8$) and OH (m/e 603, $C_{36}H_{31}N_2O_7$). Peaks which provided important structural information occurred at m/e 257 and 363 with compositions $C_{15}H_{15}NO_3$ and $C_{21}H_{17}NO_5$, respectively. These fragments in analogy with the mass spectrum of cancentrine, are considered to correspond to the morphine (m/e 257) and cularine (m/e 363) portions of the molecule and result from a fission of the bonds marked a and b in Figure 16. Cancentrine undergoes an identical fragmentation (86) to produce ions at m/e 243 ($C_{15}H_{17}NO_2$) and m/e 363 ($C_{21}H_{17}NO_5$). This difference of 14 mass units in the morphine fragment can be accounted for by the presence of a carbonyl oxygen in 53b replacing the C-10 methylene of cancentrine.

The IR spectrum was similar to the other cancentrine alkaloids (83,84,86): a phenolic OH stretch at 3450 cm^{-1} and a carbonyl absorption at 1668 cm^{-1} . The single absorption at 1668 cm^{-1} indicates that if two carbonyl groups are present both must be adjacent to either a double bond or aromatic ring. Since the 1H and mass spectrum data clearly show a change in functionality only at C-10, structure 53b was proposed for 10-oxocancentrine.

In order to gain further evidence for structure 53b, a ^{13}C spectrum was obtained as well as a spectrum of the model compound 10-oxocodentrine (55c). The chemical shift assignments of 55c were made by comparison to the published data for codeinone (55b) (85). The new carbonyl signal of 55c appears at 190.4 ppm indicative of a conjugative interaction with the aromatic ring and this substantiated by both the IR carbonyl absorption of 1675 cm^{-1} and a deshielding of carbons 3 and 12. The only aliphatic carbons that show a significant change relative to 55b are C-9 and C-14 which are deshielded as a result of the α and β substituent effects of the C-10 carbonyl group.

Examination of the aliphatic region of the ^{13}C spectrum of 53b showed the absence of a signal at 20.4 ppm corresponding to that of C-10 in cancentrine. There was also a deshielding of the C-9 resonance at 58.8 ppm in cancentrine to 68.0 ppm in 53b. The other aliphatic carbons of 10-oxocandentrine are essentially unchanged relative to cancentrine except for a deshielding of C-14 to 48.9 ppm. The deshielding of carbons 9 and 14 is similar in magnitude to that experienced by the corresponding carbons in 55c. These results correlate with the proton data in locating the carbonyl at C-10.

Because of the limited quantities of material the microprobe spectrum of 10-oxocandentrine had a relatively low signal/noise ratio for the substituted aromatic carbons and as a result only tentative assignments were made. At the low field end of the spectrum a pair of signals of approximately equal intensity appear above the noise at 193.2 and 196.3 ppm. Since the peak at 193.2 ppm correlates with the chemical shift of C-7 in 53a and 54, the other signal of 196.3 ppm was assigned to C-10 even though it is deshielded relative to C-10 in the model 55c.

The aromatic carbon chemical shift assignments for the aromatic portion of 10-oxococentrine were determined by comparison to 53a. The shifts for the codeine substituted aromatic carbons could not be accurately assigned but are expected to show a trend similar to those of 55c because of the effect of the C-10 carbonyl group.

These spectroscopic studies support the proposed structure 53b for 10-oxococentrine.

4. NMR STUDY OF 2'-O-TETRAHYDOPYRANYLURIDYL [3'-PHENYL-5'] AND
[3'-(2,2,2-TRICHLOROETHYL)-5'] 2'-O-TETRAHYDOPYRANYLURIDINE

4.1 INTRODUCTION

The current interest in the structure of nucleic acids has resulted in the widespread application of NMR spectroscopy in the study of the conformation of dinucleoside monophosphates in solution. Dinucleotides serve as models for the interactions experienced at the nearest neighbour level in polyribonucleotides. Early publications have reported on the conformation (87) and intramolecular base-stacking (88) of several ribodinucleotides. More recently, Sarma and co-workers (89), through the use of high-frequency Fourier transform NMR and computer simulations have completely assigned and analyzed the ^1H spectra of all the dinucleotides except GpG. Carbon-13 (90-93) and ^{31}P (94,95) NMR are now providing additional conformational data.

A further understanding of the factors that influence dinucleotide conformation and base-stacking can be obtained from studies of modified systems. Examples of the modifications that have been used are changing the phosphate linkage from the natural $3' \rightarrow 5'$ to $2' \rightarrow 5'$, esterification of the phosphate and placing substituents on the ribose C-2' oxygen. The phosphate triesters are of particular interest because the addition of an ester group causes the phosphorus to become chiral and generate a pair of diastereomers. Esterification also produces a neutral molecule which eliminates any intermolecular electrostatic interactions. Ts'o and co-workers have used the ^1H NMR of the triesters of dTpdT and dApdA (96-99) to show that the reduction of the phosphate shielding provides evidence

for the anti-conformation of the base in the 5' half of the dinucleotide and that the chemical shift differences between the esterified and non-esterified dinucleotides gives information on base-stacking.

The phenyl and 2,2,2-trichloroethyl esters of UpU were examined to determine if any stacking exists between the phenyl and uracil rings and to observe the effects of sterically bulky groups on the conformation of the dinucleotide. These dinucleotides were further modified by the presence of tetrahydropyranyl (THP) groups bonded to both C-2' oxygens. Because of the numerous substituents it was necessary to study initially the effect of the THP group on the conformation of the uridine mononucleoside and then use this system as a model for the triesters.

4.2 RESULTS AND DISCUSSION

4.2.1 2'-O-TETRAHYROPYRANYLURIDINE

2'-O-Tetrahydropyranyluridine exists as a pair of S (57) and R (58) diastereomers (Figure 17) with the new chiral centre being C-1 of the THP ring. These compounds are characterized by quite different NMR spectra and chromatographic behaviour. The 220 MHz ^1H NMR data are given in Table 15. Chemical shifts and coupling constants were determined by comparison to the reported shifts for uridine (100), double irradiation experiments and by computer simulations. The absolute stereochemistry was established previously by both NOE experiments (101) and by X-ray crystallography (102).

Examination of the uracil resonances reveals a deshielding of H-6 in the R isomer (58) relative to the S (57) by +0.068 ppm. This appears to indicate a change in the glycosyl torsion angle defining the relative orientation of the base and ribose ring (more conclusive results are provided in the ^{13}C discussion). In cases where dry DMSO- d_6 was used as

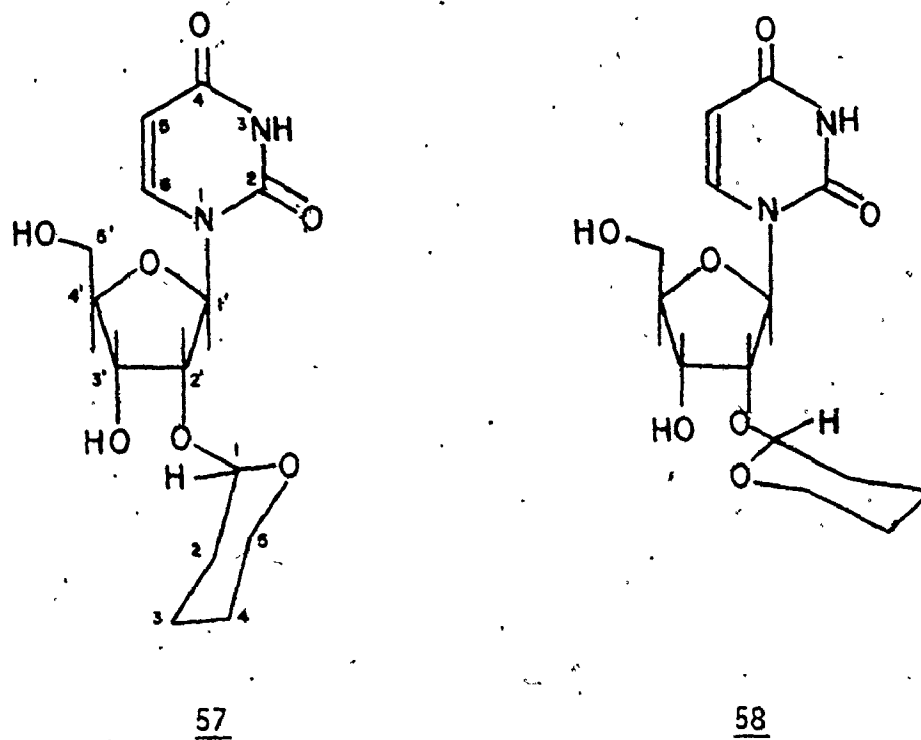


FIGURE 17. Structures of the S (57) and R (58) diastereomers of 2'-O-tetrahydropyranyluridine. (The absolute stereochemistry is not implied in this figure).

TABLE 15. 220 MHz ^1H NMR data for the diastereomers of 2'-O-tetrahydro-pyranyluridine⁸ in $\text{DMSO-d}_6^{\text{a}}$.

Proton	Chemical Shifts ^b (ppm)			Coupling Constants ^c (Hz)	
	<u>57</u>	<u>58</u>		<u>57</u>	<u>58</u>
NH	11.400	11.390	$J_{5,6}$	8.0	8.0
H-5	5.695	5.668	$J_{1',2'}$	6.6	4.5
H-6	7.943	8.011	$J_{2',3'}$	5.2	4.6
			$J_{3',4'}$	2.8	5.1
H-1'	5.999	5.872	$J_{4',5'}$... ^d	... ^d
H-2'	4.220	4.188	$J_{4',5''}$
H-3'	4.147	4.101	$J_{5',5''}$...	-11.3
H-4'	3.918	3.928			
H-5'	3.618	3.700	$J_{5',\text{NH}}$	2.5	2.5
H-5''	3.584	3.613	$J_{3',\text{OH}}$	5.1	5.1
			$J_{5',\text{OH}}$	4.8	...
3'-OH	5.218	5.033	$J_{5'',\text{OH}}$	4.8	...
5'-OH	5.173	5.241			
THP H-1	4.609	4.761			
THP H-2,-3,-4	1.432, 1.625	1.455, 1.795			
THP H-5	3.355	3.386			

^a Concentration: 0.2 M

^b Chemical shifts are in ppm relative to internal TMS and are accurate to ± 0.005 ppm.

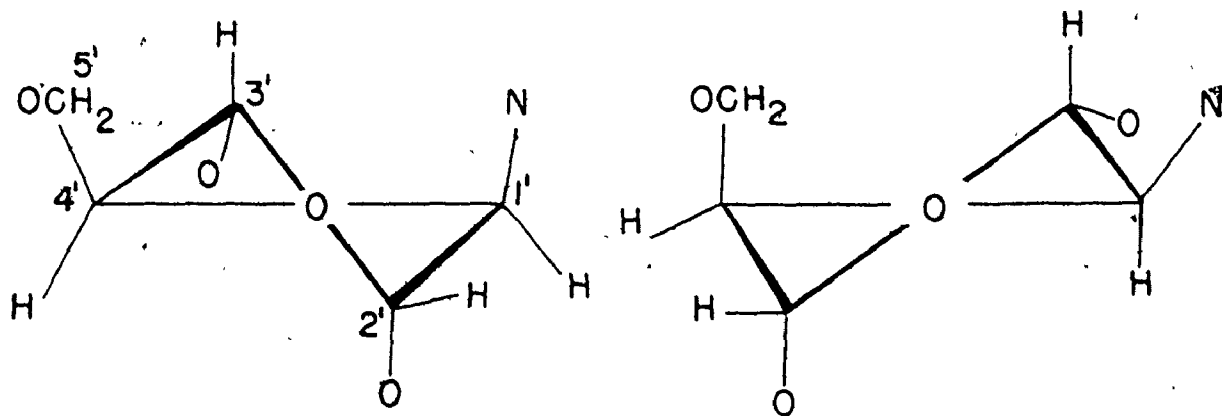
^c Accurate to ± 0.1 Hz

^d Lines too broad for coupling to be observed.

solvent, the H-5 signal appeared as a quartet with the additional coupling being 2.5 Hz. This splitting was removed when D₂O was added. Four bond coupling to the exchangeable proton on N-3 would account for this observation.

In order to define the conformation of the ribose ring two approaches can be used. The first considers the ribose ring existing as an envelope of conformations rapidly interconverting by pseudorotation in solution. This permits the ribose conformation to be described by a two-state equilibrium between the C-3' endo and C-2' endo forms (103) (Figure 18). Altona and Sundaralingam (104) have derived an alternative scheme in which the phase angle of pseudorotation and the degree of ring pucker determine a specific ribose conformational state on a pseudorotation circuit. These conformers exist in a dynamic equilibrium with the more favoured states being either the C-3' endo (Type N) or C-2' endo (Type S). A detailed error analysis by Evans and Sarma (103) and Davies and Danyluk (105) revealed that the pseudorotation concept could not define the ribose conformation any more accurately than the two-state equilibrium proposal. Since a two-state equilibrium provides a more simplified analysis of the ribose conformation, this approach will be used. The equilibrium distribution of these two conformations is determined by the magnitude of the coupling constant $J_{1',2'}$.

Computation of the ²E and ³E conformer populations involves determining the sum $J_{1',2'} + J_{3',4'}$ and using this in calculating the percentage of each conformer: $\% ^2E = 100 \times J_{1',2'} / (J_{1',2'} + J_{3',4'})$ (89). From the data in Table 15 the average value of $J_{1',2'} + J_{3',4'}$ for the diastereomers is 9.5 ± 0.1 Hz. The percentage of C-2' endo conformers



C - 3' ENDO (³E)
TYPE N

C - 2' ENDO (²E)
TYPE S

FIGURE 18. Conformations of the ribose ring.

was found to be 70% and 47% for 57 and 58, respectively, and 44% for uridine (100). These results indicate that substitution at the C-2' oxygen can have a considerable effect on the ribose conformation, especially in 57. Molecular models of 57 show that the S configuration of the THP C-1 causes nonbonded interactions between the THP H-1 and the H-2' and H-3' on the ribose ring. This steric crowding can be relieved by adopting the C-2' endo conformation. In the case of the R stereoisomer 58 the THP ring is in a conformation which allows a very weak hydrogen bond to form between the C-3' OH and the THP oxygen. This interaction reduces the contribution of the C-2' endo form until there is a slight excess of the C-3' endo conformation. Additional evidence of the proximity of the THP ring to the C-3' OH is provided by the change in OH chemical shift: 57, 5.218 ppm; 58, 5.033 ppm. The S configuration of the THP ring in 57 makes the C-3' OH more accessible for hydrogen bonding with the solvent. Since the THP group is much closer to the OH in 58, this hinders the interaction with solvent and causes the observed upfield shift.

The ^{13}C spectra of the two diastereomers were then recorded and these results are presented in Table 16 together with the data for uridine (106). Chemical shift assignments were made by reference to uridine and tetrahydropyran (21), and by selective proton decoupling experiments.

Placing the THP ring on the C-2' oxygen of uridine causes a number of chemical shift changes common to both diastereomers. Carbons 1' and 3' are both shielded by the γ effect of the THP C-1. The β THP

TABLE 16. ^{13}C chemical shifts^a of the diastereomers of 2'-O-tetrahydropyranyluridine^b and uridine^c (106).

Carbon	<u>57</u>	<u>58</u>	Uridine
2	150.8	150.6	152.5
4	163.2	163.2	164.8
5	102.1	101.9	103.1
6	140.8	140.4	142.3
1'	85.8	86.6	89.2
2'	77.0	78.0	74.9
3'	68.8	69.2	71.6
4'	85.8	85.0	86.0
5'	61.2	61.7	62.3
THP			
1	96.8	97.4	
2	29.7	30.2	
3	18.8	18.8	
4	25.0	25.0	
5	60.7	60.7	

^a Chemical shifts are in ppm from external TMS and are accurate to ± 0.1 ppm.

^b Concentrations in DMSO-d_6 : 57, 0.38 M; 58, 0.31 M.

^c Solvent: D_2O

C-1 deshields C-2' but the magnitude of the β effect is reduced by the γ THP oxygen and C-2. Comparing the spectra of 57 and 58 shows carbons 1', 2', 3', and the THP C-1 all undergoing a slight deshielding with the change in THP configuration from S to R. Despite this deshielding the ^{13}C chemical shifts were not very definitive in distinguishing the relative configurational and conformational difference of these diastereomers.

Conformational data can be obtained from the ^{13}C - ^1H coupling constants. Lemieux *et al.* (107) have shown that a Karplus relationship exists for the three bond coupling between the ribose H-1' and the uracil C-2. The value of this vicinal coupling constant provides a measure of the torsion angle about the glycosidic linkage between the uracil and ribose rings. From the gated decoupled spectra, the uracil C-2 resonances had the coupling constants detailed in Table 17.

TABLE 17. Vicinal coupling constants^a and torsion angles for 57, 58 and uridine^b (107).

	$^3J_{^{13}\text{C}, ^1\text{H}}$	Torsion Angle ($^\circ$)
C-2, H-6 <u>57</u>	8.3	180
<u>58</u>	8.7	180
uridine	8.0	180
C-2, H-1' <u>57</u>	2.2	-45
<u>58</u>	1.7	-53
uridine	2.4	-45

^a Accurate to ± 0.2 Hz

^b Solvent: D_2O

The estimated torsion angles indicate the anti-conformation for the uracil rings. As the configuration at the THP C-1 changes from 57 to 58 there is an increase in the glycosyl torsion angle. These results are in full agreement with the NOE experiments (101). Triple irradiation of H-2' and H-3' causes a 17% increase in the intensity of the uracil H-6 resonance in 57 while in 58 the same experiment produced only a 10% NOE. The larger glycosyl torsion angle in 58 has increased the distance between H-3' and H-2' and the uracil H-6 and this accounts for the reduction in NOE.

4.2.2 2'-O-TETRAHYDROPYRANYLURIDYL[3'-PHENYL-5'] AND [3'-(2,2,2-TRICHLOROETHYL)-5'] 2'-O-TETRAHYDROPYRANYLURIDINE

The conversion of 57 into the phosphotriesters shown in Figure 19 produces a pair of neutral diastereomers which can be characterized by their different chromatographic R_f values (59 and 61, high R_f ; 60 and 62, low R_f). The 220 MHz ^1H chemical shifts and coupling constants are presented in Tables 18 and 19, respectively.

A combination of signal overlap and line broadening due to solvent viscosity prevented the definite assignment of the protons on carbons 4' and 5'. Double irradiation experiments confirmed the remaining ribose protons since the 3' phosphate deshielded the 1', 2', and 3' protons in the A uridine moiety while these protons in the B half of the dinucleotide were similar to those of 57. The assignment of the two pairs of uracil H-5 and H-6 resonances was made by spin decoupling and by the fact that the phosphate and its ester group should only affect the chemical shifts of the B uracil protons.

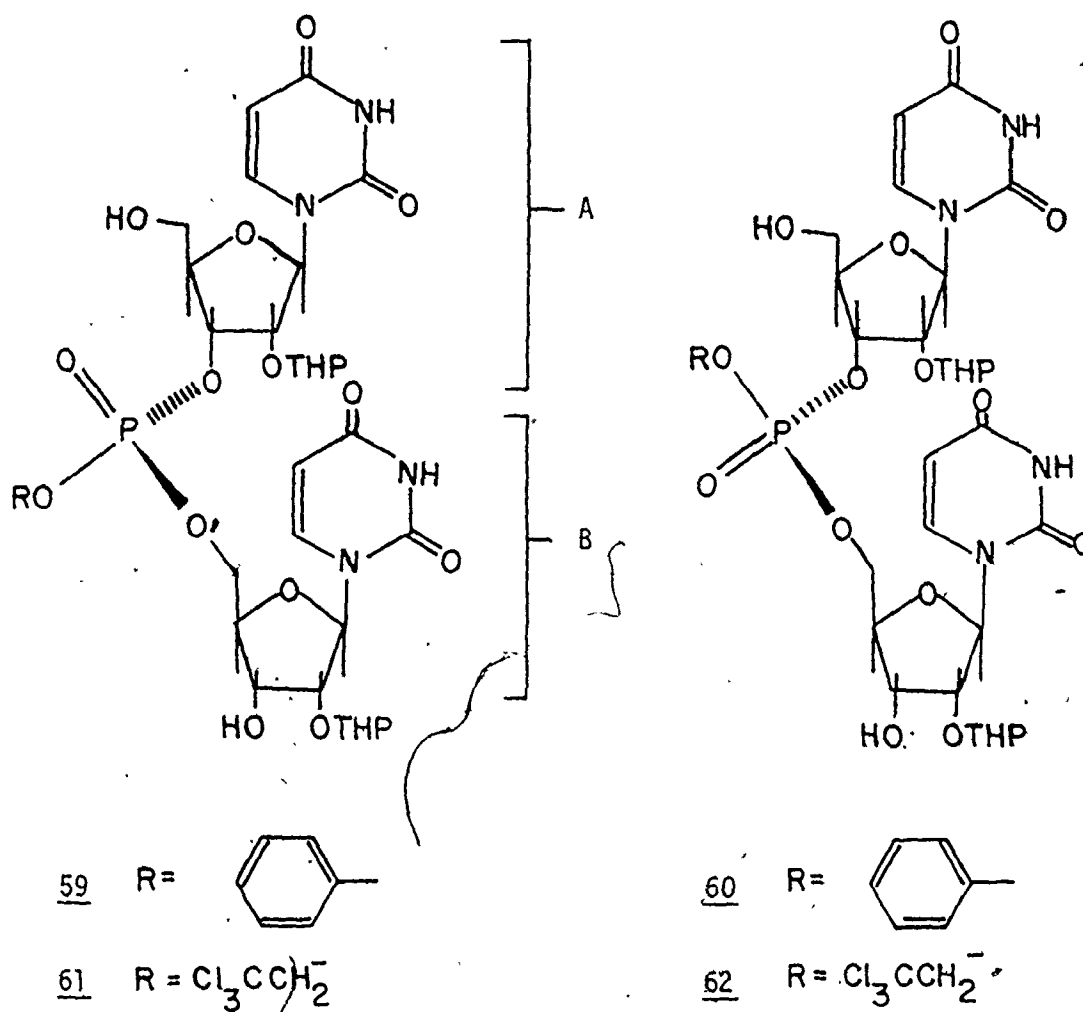


FIGURE 19. Structures of the UpU triesters. (To simplify the nomenclature, the uridine containing either the 3' phosphate or the 5' phosphate will be designated as either the A or B moiety, respectively, of the dinucleotide).

TABLE 18. ^1H chemical shifts^a of the phosphotriesters in DMSO-d_6^b

Triesters	1'	2'	3'	5	6	OC_6H_5	OCH_2CCl_3	THP H ₂ O
<u>59</u> Up	6.034	4.492	5.030	5.768	7.875	7.455, 7.273		4.723
pU	5.952	4.268		5.607	7.659			
<u>60</u> Up	6.075	4.495	5.086	5.676	7.864	7.398, 7.273		4.718
pU	5.927	4.180		5.589	7.511			
<u>61</u> Up	6.059	4.502	5.027	5.773	7.914		4.790	4.750
pU	5.964	4.245		5.677	7.728			
<u>62</u> Up	6.075	4.498	5.022	5.773	7.886		4.795	4.759
pU	5.961	4.273		5.689	7.700			

^a Chemical shifts are in ppm relative to internal TMS. The protons on carbons 3', 4', and 5' appear as broad multiplets in the region of 3.3-4.5 ppm. The THP protons on carbons 2-4 resonate at 1.3-1.7 ppm and the C-5 protons at 3.3-3.6 ppm.

^b concentrations: 0.09 M.

TABLE 19. J_{H} coupling constants^a (Hz) of the phosphotriesters

Triester		1',2'	2',3'	5,6	3',P
<u>59</u>	Up	8.0	5.0	7.5	8.0
	pU	6.0		8.5	
<u>60</u>	Up	8.1	5.0	8.0	7.5
	pU	5.5		8.0	
<u>61</u>	Up	8.5	5.0	8.0	7.5
	pU	5.5		8.0	
<u>62</u>	Up	8.0	5.0	8.0	8.0
	pU	6.5		8.5	

^a Accurate to ± 0.2 Hz.

The configuration of the phosphate in these diastereomers was determined by observing the differences in chemical shifts for the B uracil protons and by considering the results obtained by Ts'o and co-workers on the esters of TpT (97). Examination of the B uracil resonances in Table 18 shows that the H-5 and H-6 protons in 60 are shielded by -0.018 and -0.148 ppm, respectively, relative to 59. The phosphate configuration in 60 must therefore allow the phenyl ring to be close enough to be the B uracil in order to shield these protons. Molecular models confirmed this observation since an R configuration of the phosphate substituents directs the phenyl ring towards the centre of the dinucleotide and permits a weak stacking interaction with the B uracil. Alternatively, an S configuration directs the phenyl ring away from the dinucleotide and this would account for the deshielding of the B uracil protons in 59. In the S configuration the unsubstituted phosphate oxygen is pointed towards the A uridine. A slight deviation of the A 5' hydroxyl group from its gauche-gauche conformation (100) may result in an internal hydrogen bond between this hydroxyl and the phosphate oxygen. Thus a combination of the phenyl ring being on the outside of the dinucleotide structure and internal hydrogen bonding would reduce any polar interactions between the molecule and chromatographic adsorbent and result in a high R_f value. The 2,2,2-trichloroethyl esters are expected to have the same spatial arrangement of the groups around the phosphorus. However, the change in the Cahn-Ingold-Prelog priority ranking of the 2,2,2-trichloroethyl group causes the high R_f diastereomer 61 to have an R configuration and 62 to be S.

Comparison of the H-1' and H-2' coupling constant of 57 with those of the four triesters (Table 19) reveals a significant change in the ribose conformation especially for the A uridine portion of the dinucleotide. The $J_{1,2}$ value of the A uridine shows an increase of 1.4-1.9 Hz while the B uridine $J_{1,2}$ decreased by 0.1-1.1 Hz relative to 57. These results indicate that the A ribose ring exists predominantly in the C-2' endo conformation (ca. 84-90% 2E). In contrast, the B ribose ring remains similar to 57, as in 59 and 62, or shows a decrease in the percentage of the C-2' endo conformation (ca. 58-68% 2E). This difference is due to the A ribose ring being forced to adopt the C-2' endo conformation in order to minimize the steric interactions between the A THP group and the B uracil.

The ribose conformation also appears to be influenced by the phosphate configuration. In the phenyl diastereomers the change from 59 to 60 causes a reduction in the $J_{1,2}$ for the B uridine. The 2,2,2-trichloroethyl diastereomers exhibit a reversal of the above trend with the $J_{1,2}$ of the B uridine in 62 being larger. The exact nature of these conformational changes cannot be ascertained directly from the NMR data, however, these observations may result from the 2,2,2-trichloroethyl group being a bulky sp^3 two carbon unit which in the S phosphate configuration is situated approximately between the nucleotides and is forcing the nucleotides into a more unstacked conformation.

The ${}^{13}C$ chemical shift assignments (Table 20) were made by comparison with the data for UpU (91,93) and 57. In general the carbon shifts were insensitive to any changes in phosphate configuration as illustrated by the nearly identical shifts observed for the phenyl

TABLE 20. ^{13}C chemical shifts^{a, b} of the phosphotriesters in acetone- d_6 ^c

Carbon	<u>59</u>	<u>60</u>	<u>61</u>	<u>62</u>
Up 2'	150.9	151.0	150.9	150.9
4	163.0	163.3	163.0	163.1
5	102.5	102.5	102.5	102.6
6	140.9	140.8	140.9	140.9
1'	88.6	88.3	88.9	88.9
2'	76.4	76.3	76.4	76.4
3'	77.0	77.3	77.2	77.3
4'	84.8	84.8	84.8	84.8
5'	61.5	61.5	61.6	61.5
pU 2	151.3	151.4	151.3	151.3
4	163.0	163.3	163.1	163.1
5	102.7	102.7	102.8	102.6
6	140.9	140.9	141.4	141.3
1'	86.1	85.7	86.3	86.1
2'	77.5	77.7	77.6	77.3
3'	69.5	69.2	69.6	69.3
4'	82.7	82.8	82.8	82.8
5'	68.6	67.9	68.6	68.2
OC_6H_5 1	150.0	151.0		
2,6	120.8	120.6		
3,5	130.2	130.2		
4	125.7	125.7		

^a Chemical shifts in ppm relative to external TMS and are accurate to ± 0.01 ppm.

^b THP carbons showed essentially no change from those of 57 and are not included. The 2,2,2-trichloroethyl carbons could not be accurately assigned and are expected to have shifts similar to those in reference 108.

^c Concentrations: 0.12-0.13 M.

TABLE 21. ^{13}C - ^{31}P coupling constants^a of the phosphotriesters

Triesters	2',P	3',P	4',P	5',P	Phenyl C-2
<u>59</u> Up	2.6	4.1	5.3		4.9
pU			7.9	5.5	
<u>60</u> Up	2.3	3.4	4.7		4.3
pU			8.5	5.4	
<u>61</u> Up	3.8	3.6	5.1		
pU			7.6	6.5	
<u>62</u> Up	4.2	3.2	4.4		
pU			7.3	6.1	

^a Accurate to ± 0.3 Hz.

carbons in 59 and 60. The uracil resonances of the four triesters also showed very little change relative to 57. A definite assignment of the uracil signals to either A or B half of the dinucleotide could not be made. The carbons of the 2,2,2-trichloroethyl group in 61 and 62 were obscured by overlap with the ribose C-2' and C-3' resonances and by C-1 of the THP rings.

Assignment of the ribose carbons was facilitated by the deshielding effect of the phosphate and the presence of ^{13}C - ^{31}P spin-spin coupling (Table 21). Phosphorylation of either the 5' or 3' hydroxyl groups of 57 causes an average deshielding of +7.1 and +8.4 ppm, respectively. The 2' and 4' carbons were differentiated by the magnitude of the conformationally dependent three bond coupling to the phosphorus. Carbon-2' in the B uridine shows no coupling. The 4' carbons have significantly different values of $^3J_{\text{C},\text{P}}$ with that of the B uridine being larger than that of the A uridine (91,93). The ^{13}C chemical shifts are not indicative of the conformational change in the A uridine ribose ring to the C-2' endo form as was the case in the ^1H spectra.

CONFORMATIONAL ANALYSIS OF THE PHOSPHATE BACKBONE

Several physical and theoretical studies have demonstrated that the phosphate backbone is critical in determining the overall conformation of nucleic acids. Of the six torsion angles describing the conformation of the phosphate backbone, the angles ϕ' along the C_3 - O_3 bond and ϕ along the C_5 - O_5 bond can be examined by NMR. These angles are represented by the staggered rotamers in Figure 20 where ϕ' and ϕ define the angle between C-4' and the phosphorus. The angles in these rotamers can be determined

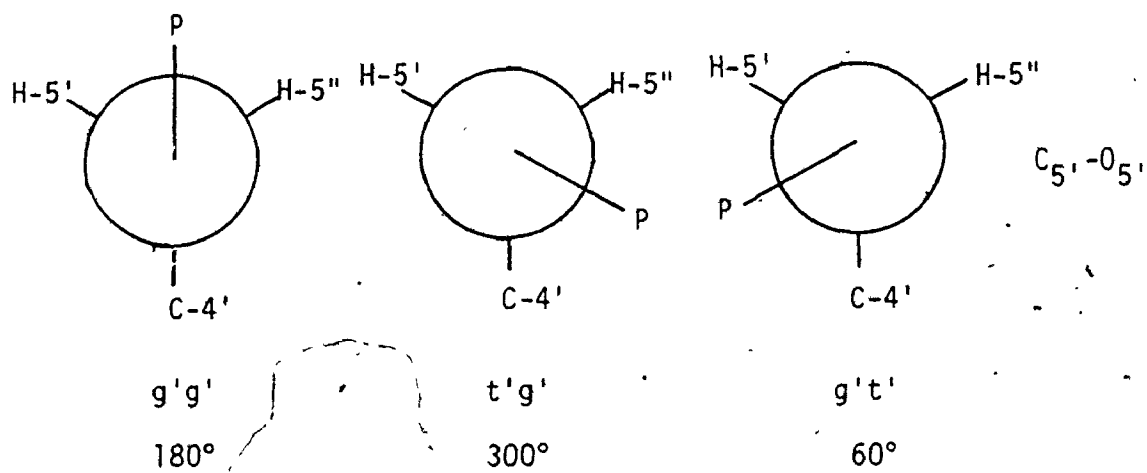
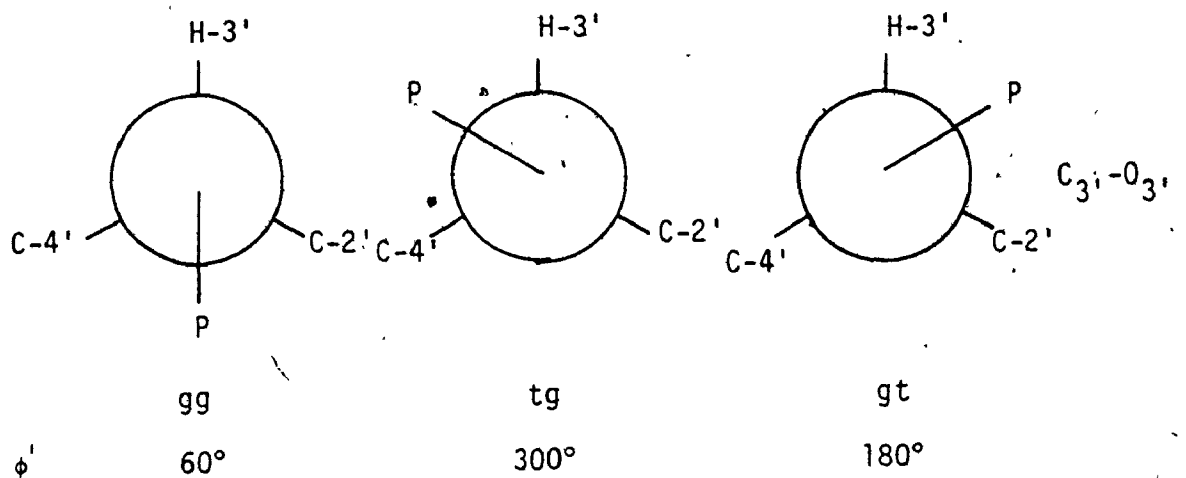


FIGURE 20. Staggered conformations of the $C_3'-O_3'$ and $C_5'-O_5'$ bonds.

from the vicinal coupling constants ${}^3J_{H_3,P_3}$, ${}^3J_{C_2,P_3}$, ${}^3J_{C_4,P_3}$, and ${}^3J_{C_4,P_5}$, by utilizing the appropriate Karplus equation.

Recent 1H (89) and ${}^{13}C$ (93) studies of ribodinucleotides indicate that the conformation about the C_3-O_3 bond involves a rapid equilibrium between the gt and tg forms with the ϕ' angles being 210° and 270° , respectively. This two rotamer model provides a better correlation between the conformer populations determined from the 1H and ${}^{13}C$ data. In addition this equilibrium is shifted towards the gt conformer where there is a high degree of base-stacking (93). The gg rotamer is the preferred conformation for the C_5-O_5 bond (89,91,93,109).

From the coupling constant data in Tables 19 and 21, the angles in Table 22 were calculated using the following Karplus equations:

$${}^3J_{H,P} = 18.1 \cos^2 \theta - 4.8 \cos \theta \quad (89)$$

$${}^3J_{C,P} = 9.5 \cos^2 \theta - 0.6 \cos \theta \quad (93)$$

The value of θ calculated from the vicinal 1H - ${}^{31}P$ coupling constants measures the dihedral angle between H-3' and P-3'. On the basis of X-ray and theoretical studies (89,93) the gg conformation of the C_3-O_3 bond is sterically unfavored and this allows the angles of $\pm 121.6^\circ$ and $\pm 123.1^\circ$ to be neglected. The remaining angles of $\pm 35.9^\circ$ and $\pm 37.8^\circ$ are nearly identical to the angle of $\pm 35.1^\circ$ determined for OpU (89). This places the phosphorus approximately half way between the H-3' and the P-3' in either of the staggered tg or gt rotamers in Figure 20 which is in accord with the two rotamer model (89,93).

TABLE 22. Phosphate torsion angles^a for the triesters.

Triester	H-3',P-3'	C-2',P-3'	C-4',P-3'	C-4',P-5'
<u>59</u>	± 35.9 ± 123.1	± 55.9 ± 119.3	± 38.8 ± 135.7	± 19.3 ± 151.8
<u>60</u>	± 37.8 ± 121.6	± 58.7 ± 117.4	± 42.3 ± 132.1	± 12.0 ± 156.2
<u>61</u>	± 37.8 ± 121.6	± 48.3 ± 127.0	± 40.1 ± 134.6	± 22.1 ± 149.7
<u>62</u>	± 35.9 ± 123.1	± 45.8 ± 129.4	± 44.8 ± 130.5	± 24.7 ± 147.7

^a θ measured in degrees.

When a molecular model is constructed using this torsion angle, placing the phosphorus in the gt conformation (Figure 20) results in a considerable amount of steric hindrance between the A uridine, THP group and the B uridine. It is only when the phosphorus is in the tg conformer that these steric interactions are relieved. The tg conformer also minimizes base-stacking and this is supported by the high percentage of C-2' endo ribose conformations. Therefore it may be concluded that the steric hindrance created by a large substituent on the 2' oxygen of the A uridine is one of the major factors influencing the overall conformation of the dinucleotide.

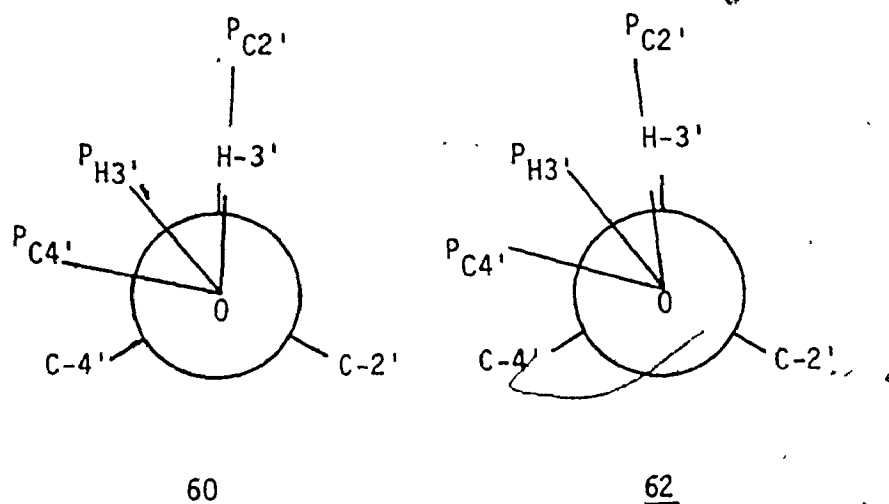


FIGURE 21. Calculated positions of the phosphorus atoms for the tg conformations of the C_3-O_3 bond of the triesters 60 and 62.

In order for the C_3-O_3 bond to be in the tg conformation, the angles calculated from the $^{13}C-^{31}P$ coupling constants must range from $\pm 119.3^\circ$ to $\pm 129.4^\circ$ relative to $C-2'$ and $\pm 38.8^\circ$ to $\pm 44.8^\circ$ relative to $C-4'$. These results are summarized in Figure 21 for the triesters 60 and 62. Although the position of the phosphorus predicted from the 1H and ^{13}C data do not exactly coincide, the angle- $P_{C4'}-O-P_{C3'}$ may be interpreted as specifying a region in space for the most probable location of the phosphorus. In this case the region within the limits of the tg conformer is more populated. The θ values of $\pm 147.7^\circ$ to $\pm 156.2^\circ$ for the C_4-O_5 bond places the phosphorus in the gg conformation (Figure 20).

Since these angles were determined from a Karplus relationship, it must be emphasized that these results only give a qualitative representation of the phosphorus conformation. As pointed out by Karplus (110), a number of factors such as substituent electronegativity, hybridization, and bond length will affect the vicinal coupling constant and produce inaccurate angle calculations if not properly taken into account. A major

source of error in the above calculations lies in the use of Karplus equations which were derived for a singly charged phosphorus. The triesters are neutral and the phosphorus now has a different electronic environment which may also be influenced by the type of ester group. These additional constraints will no doubt affect the vicinal coupling constants and a further refinement of the Karplus parameters in the equations that were used for these calculations will be necessary.

5. PROTON MAGNETIC RESONANCE STUDIES ON SHORT DUPLEXES OF OLIGORIBONUCLEOTIDES

5.1 HELIX FORMATION IN THE DUPLEX SET GpApGpC:GpCpUpC¹

5.1.1 INTRODUCTION

In order to probe the solution properties of t-RNA, considerable effort has recently been expended on the NMR analysis of base-pairing in short strands of nucleic acids (111-116). The first definitive study of helical ribonucleic acids was reported by Kearns and Shulman (112) who examined the NH protons of N-3 (uracil) and N-1 (guanine) which are involved in the hydrogen bonding required for base pair formation (Figure 22). At low temperatures these protons show pronounced downfield chemical shifts and their shift changes with respect to temperature have given useful information on the helix-coil transition for self-complementary nucleotides (113,115). At higher temperatures chemical exchange causes extensive line broadening and the utility of the NH protons is lost. It should also be noted that the NH chemical shifts contain very little information about the conformation of the helical duplex.

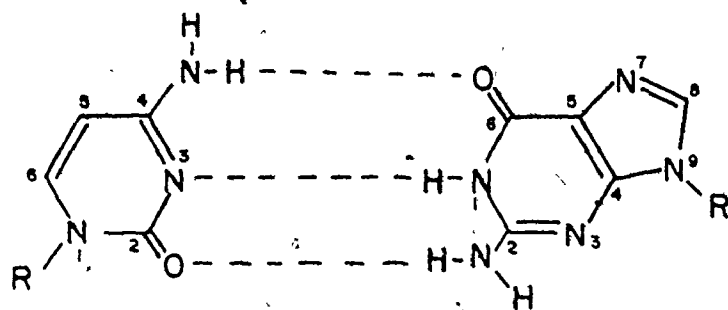
The work of Borer et al. (114) on the self-complementary hexaribonucleotide AAGCUU has shown that the carbon bound protons of the bases and the anomeric protons of the ribofuranoside ring may be used to define the helix-coil transition. Moreover, the observed chemical shift changes of the base protons were consistent with the duplex adopting either the A or A'-RNA helical structure.

¹ Abbreviations used: GAGC, ribosyl 5'-GpApGpC-3'.

Oligoribonucleotides are written in the normal 5' → 3' sequence and in the duplex the base pairs are numbered from left to right:

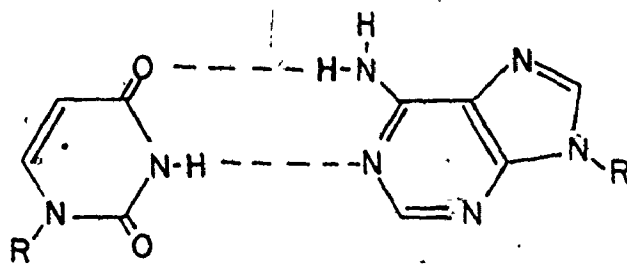


1234



CYTOSINE (C)

GUANOSINE (G)



URIDINE (U)

ADENINE (A)

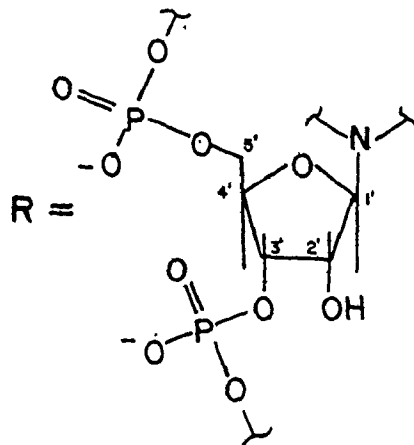


FIGURE 22. Watson-Crick base-pairs in ribonucleic acids.

A proton magnetic resonance study was undertaken to investigate the duplex formation by the complementary nucleotides GAGC and GCUC. These sequences were chosen because they correspond to natural sequences common to several t-RNA molecules; in particular they represent a proposed partial recognition site for yeast phenylalanyl-t-RNA ligase (117). In addition the duplex formed by the GAGC-GCUC set is the first simple example of a duplex formed from synthetic non-self-complementary tetranucleotides containing an internal A-U base pair. Since the proton spectra were obtained at 90 MHz, it was only possible to assign the lowfield aromatic protons of GCUC; the anomeric ribose ring protons were too complex to resolve adequately. It was possible however to completely assign the aromatic protons and the anomeric protons for all four units in GAGC at 65°C.

England and Neilson (118) have used ultraviolet and circular dichroism studies on these two tetranucleotide sequences to show that duplex formation occurs, and the authors have employed melting temperature (T_m) versus concentration studies to evaluate the enthalpy change occurring for the single strands through the helix-coil transition. It was of interest to determine if the NMR experiments would produce a T_m similar to that obtained from extrapolation of the optical data.

5.1.2 RESULTS

The chemical shift assignments for the lowfield protons of GAGC were made by comparison with spectra of GA and GAG which were recorded at 65°C. These data are presented in Table 23 which also includes the shifts of GCUC and the mixture of the two tetranucleotides.

TABLE 23. Chemical shifts^a and coupling constants^b for the derivatives of GAGC, GCUC and duplex. at 65°C.

Proton	GA ^c	GAG ^c	GAGC	GCUC	GAGC CUCG
G(1)H-8	7.789	7.802	7.871		7.870
A(2)H-8	8.347	8.393	8.257		8.264
A(2)H-2	8.243	8.252	8.146		8.142
G(3)H-8		7.948	7.890		7.890
C(4)H-6			7.738		7.729
C(1)H-6				7.779	7.786
U(2)H-6				7.829	7.829
C(3)H-6				7.779	7.786
G(4)H-8				7.965	7.965
G(1)H-1'	5.734	5.752	5.729		
A(2)H-1'	6.102	6.129	5.983		
G(3)H-1'		5.916	5.870		
C(4)H-1'			5.780		
C(4)H-5			5.848		
J _{1',2',G(1)}	6.0	5.0 ^d	4.1		
J _{1',2',A(2)}	5.2	5.5 ^d	3.8		
J _{1',2',G(3)}		6.0 ^d	3.4		
J _{1',2',C(4)}			5.1		
J _{5,6,C(4)}			7.5		

^a Chemical shifts in ppm from DSS using internal *t*-butyl alcohol-OD as reference (± 0.005 ppm).

^b Accurate to ± 0.2 Hz.

^c From spectra-recorded at 220 MHz.

^d Couplings not well resolved and accurate to ± 0.5 Hz.

Prior to recording the spectrum of the mixture of the tetranucleotides, the temperature dependence of the aromatic resonances in each tetranucleotide was obtained over the range of 65° to 15°C. These results are shown in Figure 23. In both cases linear and predominantly upfield chemical shift changes were observed. Of the anomeric protons only A(2)H-1' and G(3)H-1' in GAGC could be followed to lower temperatures. There was a considerable reduction in the magnitude of $J_{1',2'}$ for these resonances until at 15°C they appeared as broad singlets (Table 24).

The aromatic portion of the spectrum of the mixed tetranucleotides (concentration 6.7×10^{-3} M) at 65°C is shown in Figure 24. These resonances displayed both non-linear behaviour and rapid line broadening at lower temperatures. Thus a spectrum which bore a satisfactory signal/noise ratio at 65°C could be accumulated in 250 pulses, but required over 2000 pulses at 25°C. The A(2)H-2 proton remained relatively sharp throughout the entire temperature range while the remaining aromatic protons displayed a line-broadening at lower temperatures of 5-20 Hz. The shift changes with respect to temperature of the mixed tetranucleotides are shown in Figure 25.

The melting temperature, T_m , of the GAGC-GCUC duplex was estimated from the mid-point of the chemical shift-temperature curves when they were reasonably complete. The values all lay within the $42 \pm 1^\circ\text{C}$ range which is in good agreement with the T_m of 43.5°C predicted from ultraviolet absorption studies (118).

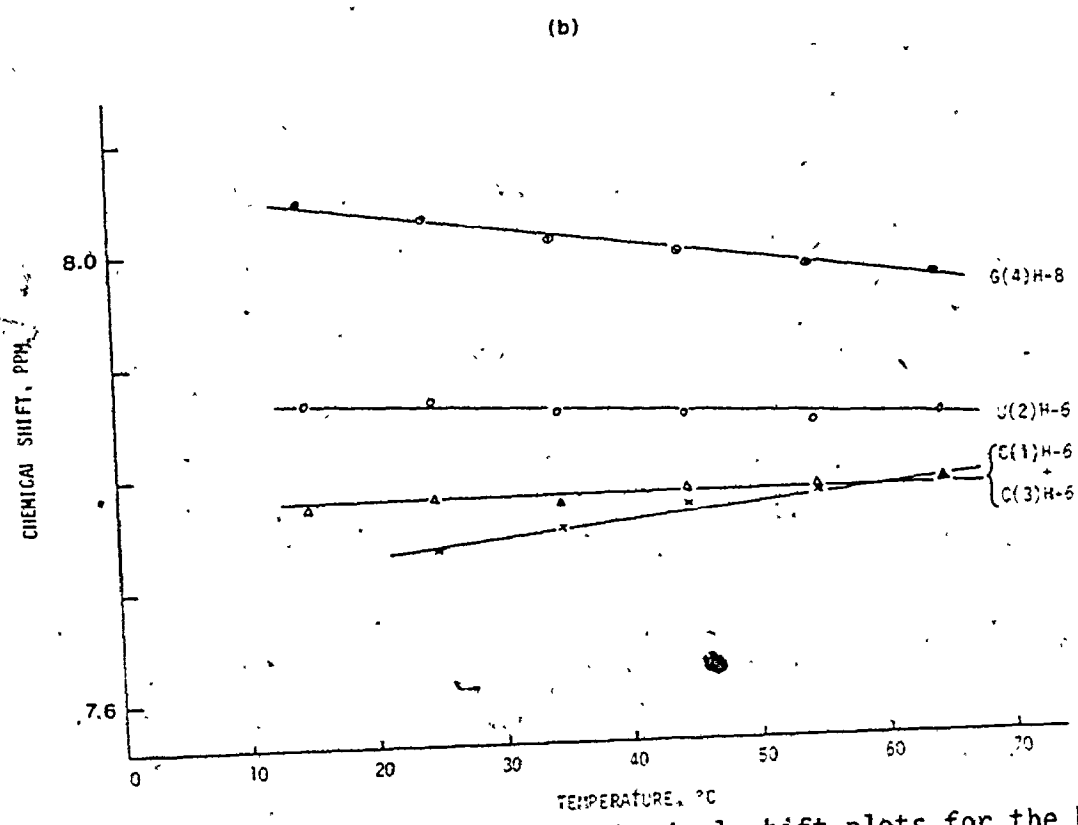
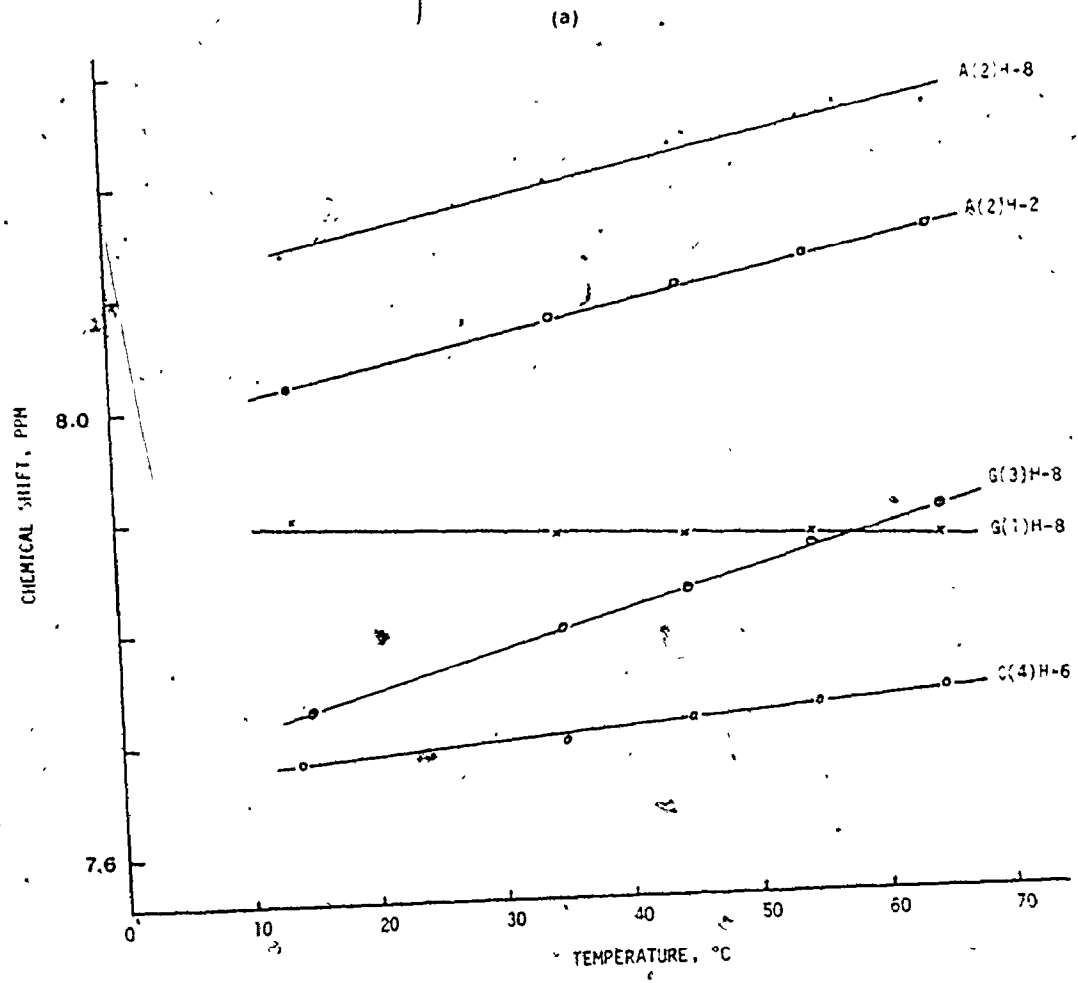


FIGURE 23. Variable temperature versus chemical shift plots for the base of (a) and (b)

TABLE 24. GAGC ribose ring $J_{1',2'}$ coupling constant changes with respect to temperature.

Temperature (°C)	$J_{1',2'}$ (Hz) ^a			
	G(1)	A(2)	G(3)	C(4)
65	4.1	3.8	3.4	4.7
55	3.5	3.8	3.0	4.0
45	... ^b	2.9	2.5	... ^b
35	...	2.2	2.4	...
15	...	< 1.0	< 1.0	...

^a \pm 0.2 Hz.

^b Lines too broad for coupling to be observed.

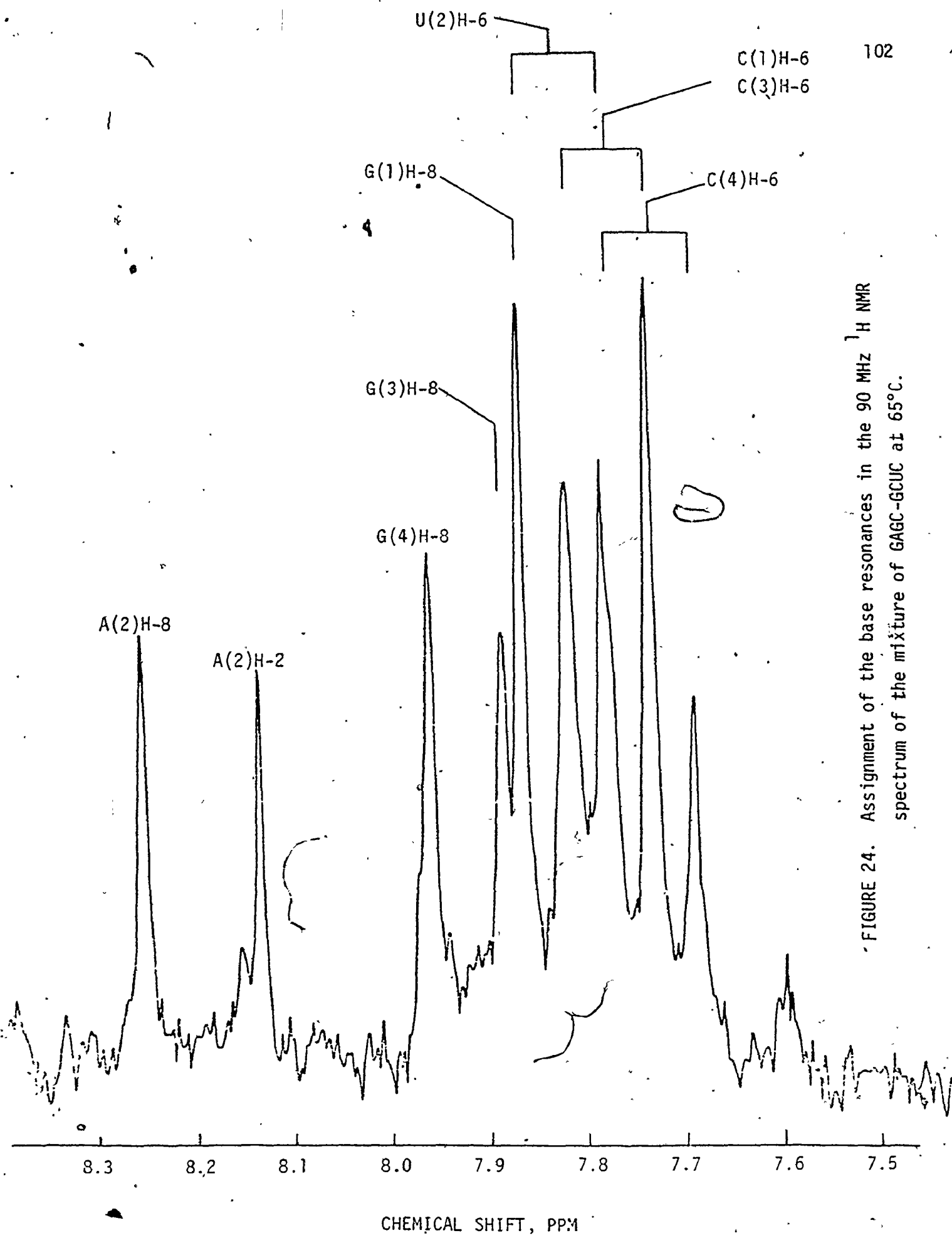


FIGURE 24. Assignment of the base resonances in the 90 MHz ¹H NMR spectrum of the mixture of GAGC-GCUC at 65°C.

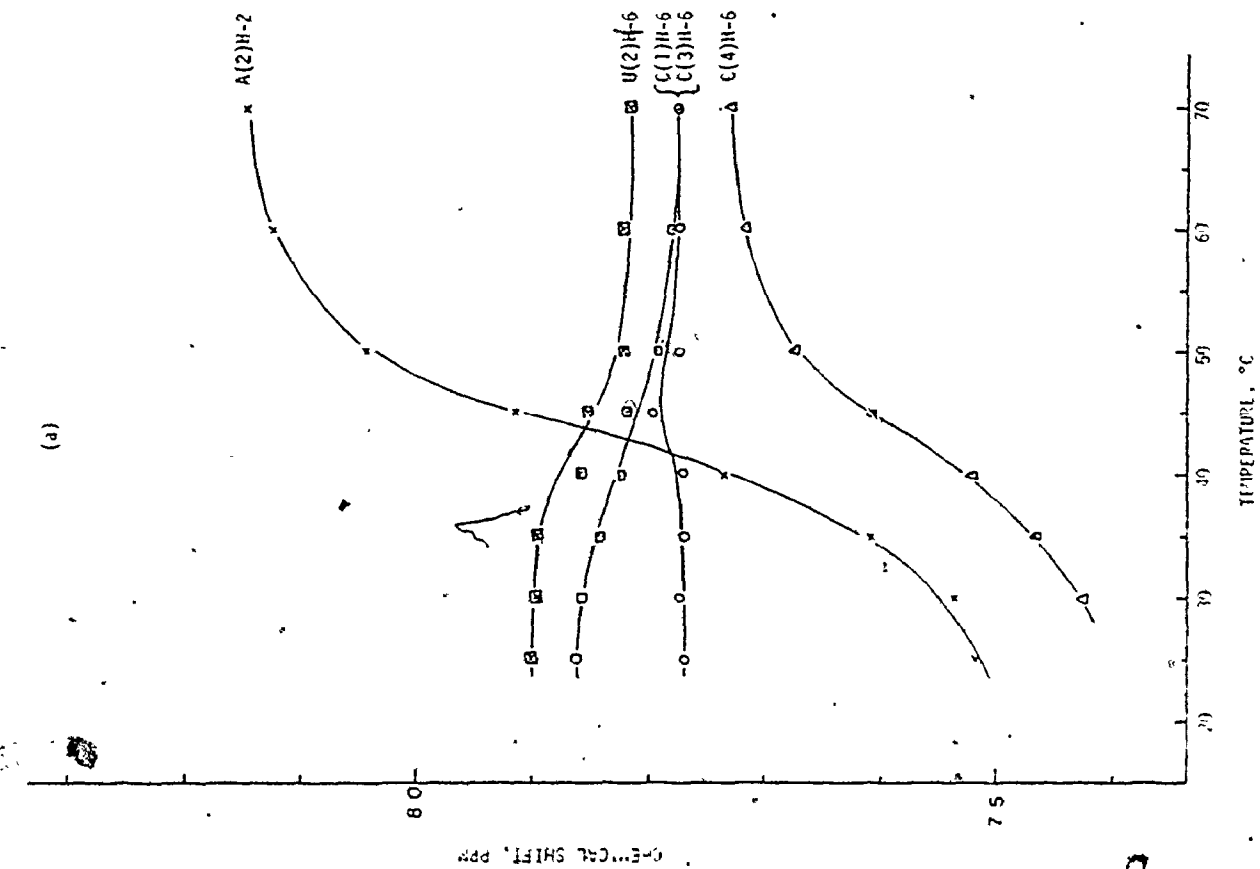
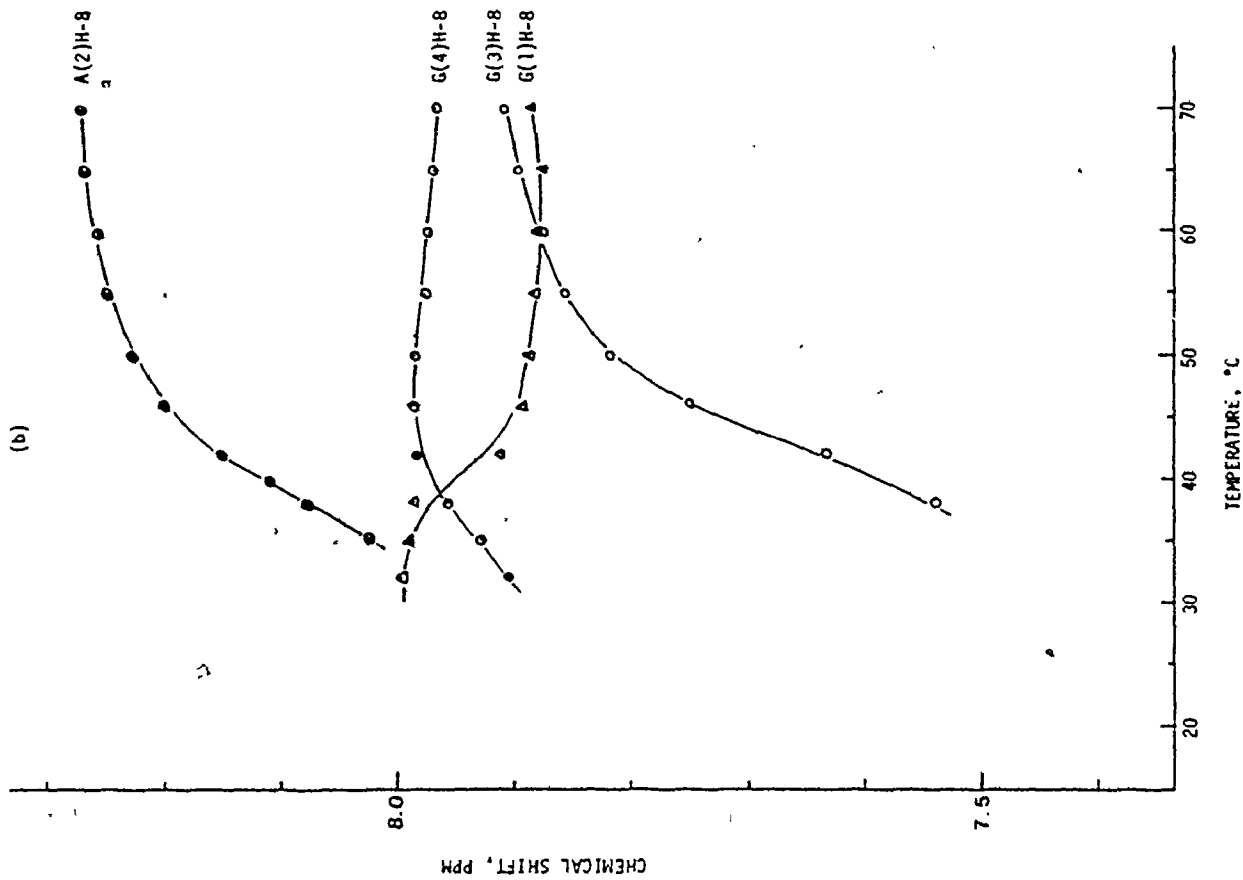


FIGURE 25. Variable temperature plots for (a) the non-exchangeable and (b) the exchangeable protons of the bases in the mixture of GAGC-GCUC.

5.1.3 DISCUSSION

The assignment of the lowfield resonances of GAGC was undertaken following the method of incremental analysis (114,119). This method assumes that as fragments are added to a molecular species, the chemical shifts of the protons already present will remain essentially constant since the spectra are recorded at temperatures high enough to minimize inter- and intra-strand effects. That this assumption is reasonably valid in the present case is evident from the chemical shift correlation diagram of GA, GAG, and GAGC shown in Figure 26. The shift assignments for GA were consistent with those reported by Lee *et al.* (89) and the positions of G(1)H-8 and A(2)H-8 were confirmed by a deuterium isotope exchange experiment (120). In GAG three of the signals in the aromatic region were virtually identical with those of GA and the new signal at 7.948 ppm was therefore assigned to G(3)H-8. Further confirmation of this assignment was obtained from a relaxation time (T_1) measurement in which the line at 7.948 ppm showed a shorter relaxation time (ca. 3 sec.) than the signal at 8.252 (ca. 5 sec.) which was assigned to A(2)H-2 (97). Similarly the anomeric proton doublet of G(3)H-1' was clearly discernable at 5.916 ppm ($J_{1',2'} = 6.0$ Hz) in the presence of the doublets for G(1)H-1' and A(2)H-1'.

The anomeric region of GAGC was complicated by the overlap of the C(4)H-5 doublet at 5.848 ppm onto both of the C(4)H-1' and G(3)H-1' doublets. However, the lowfield C(4)H-6 doublet at 7.725 ppm ($J_{5,6} = 7.5$ Hz) was well separated from the remaining four aromatic signals and a double irradiation experiment was sufficient to locate clearly the C(4)H-5 doublet.

As the temperature was decreased the A(2)H-8, A(2)H-2, G(3)H-8, and C(4)H-6 protons showed linear, upfield shifts while the G(1)H-8 proton

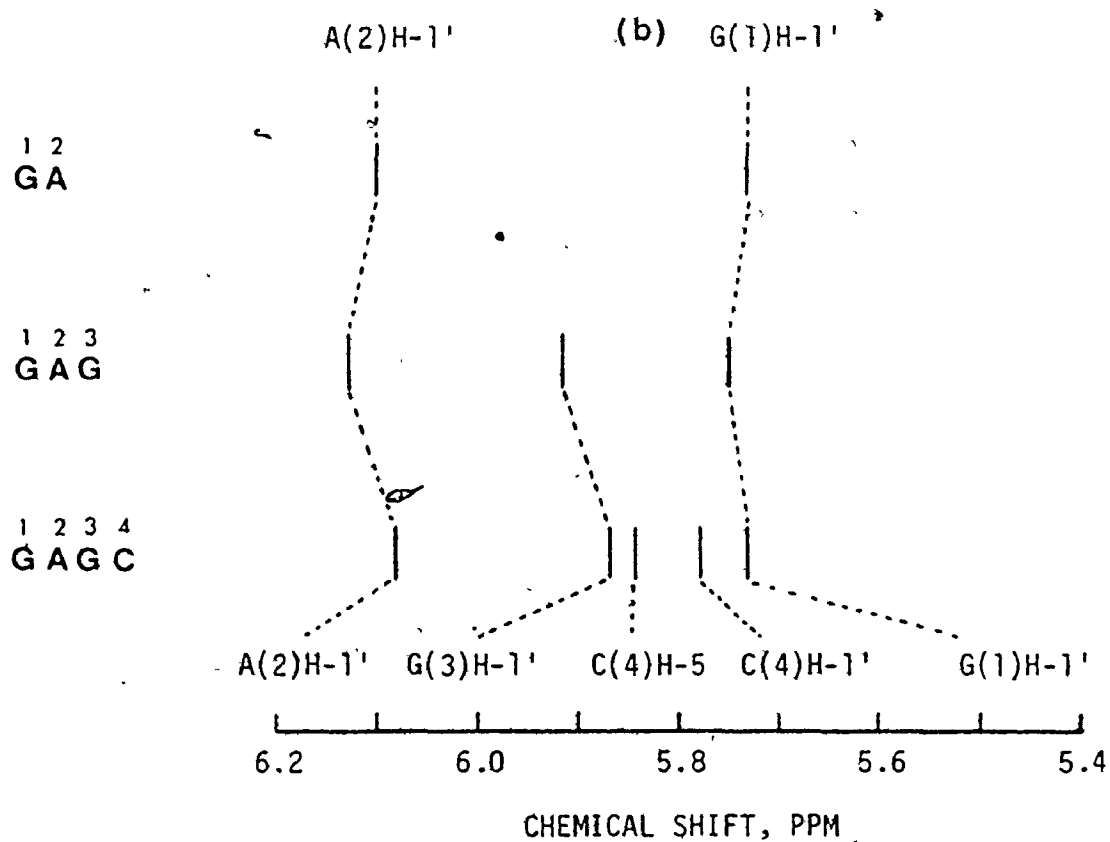
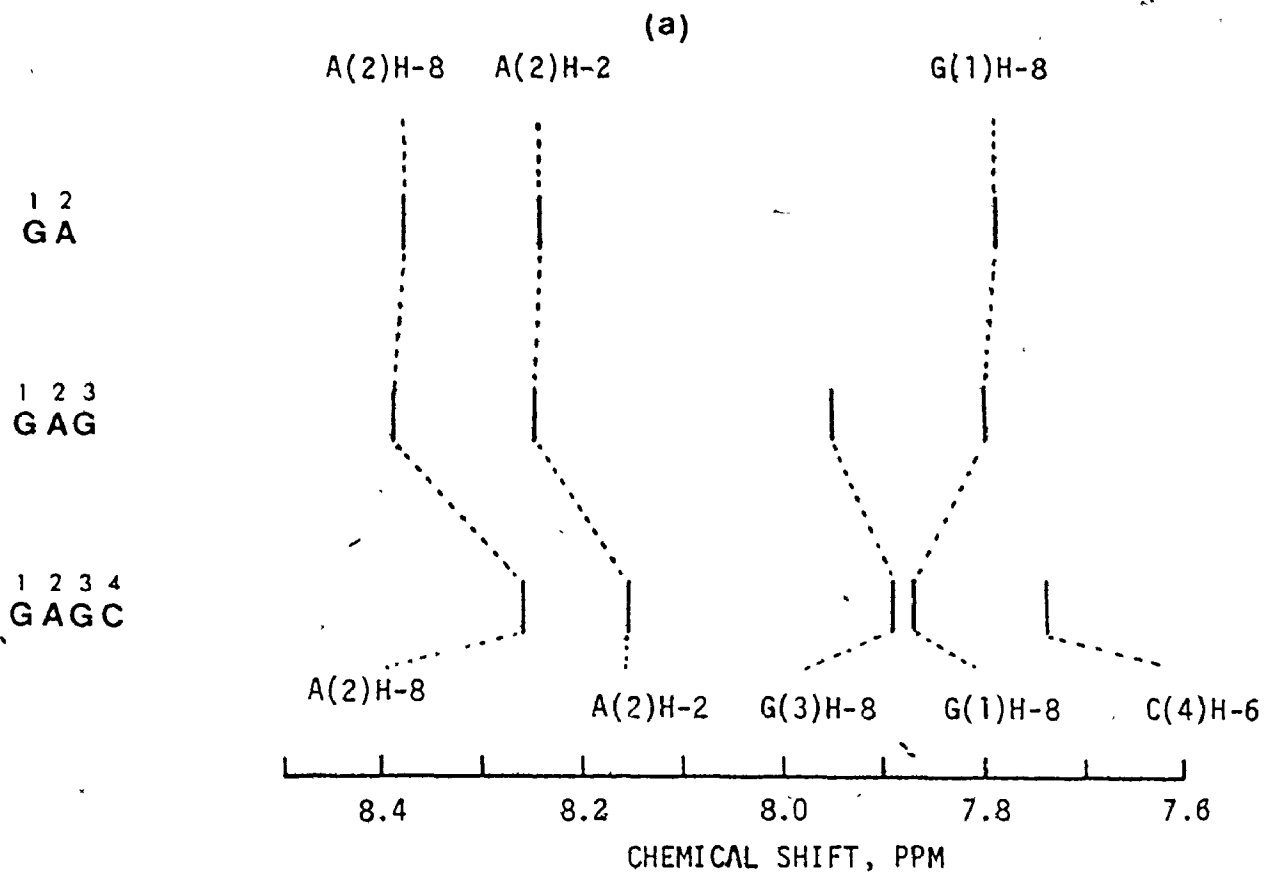


FIGURE 26. Chemical shift correlation of the ^1H resonances for GA, GAG, and GAGC.

was shifted downfield. These changes are attributed to single strand base-stacking. Further evidence of base-stacking is provided by the reduction of $J_{1,2}$ for the A(2)H-1' and G(3)H-1' in which the base-stacking causes the ribose rings to adopt the ³E or C-3' endo conformation. This is consistent with the molecule having either the A- or A'-RNA structure. Although the anomeric protons were not adequately resolved in GCUC and the duplex, it is expected that the ribose conformational changes in these systems will parallel the trend observed in GAGC.

The anomeric region of the spectrum of the tetranucleotide GCUC showed a complex overlapping set of lines derived from the four anomeric protons plus the three H-5 protons of C(2), U(3), and C(4), and assignment of these resonances was not attempted. The aromatic region however was simpler and showed only a singlet at 7.965 ppm (assigned G(4)H-8) and four lines between 7.7 and 7.9 ppm. Assignment of U(2)H-6 at 7.839 ppm ($J_{5,6} = 7.6$ Hz) and C(3)H-6 and C(1)H-6 at 7.780 ppm ($J_{5,6} = 7.4$ Hz) was based on intensity ratios and coupling constants expected for the uracil and cytosine residues.

The GCUC strand exhibited more variable changes with temperature. The U(2)H-6 and C(3)H-6 barely moved while G(4)H-8 moved downfield and C(1)H-6 shifted upfield (Figure 23). Presumably a process such as intermolecular end-to-end base stacking may be responsible for these latter shifts. Although the equivalence of the C(3)H-6 and C(1)H-6 signals was removed at lower temperatures, no unambiguous assignments could be made. However, it is probable that the signal showing the greater upfield shift

at lower temperatures (7.729 ppm at 25°C) belongs to C(3)H-6 as any stacking interaction between G(4) and C(3) would be expected to result in a diamagnetic shift of the C(3) protons.

The spectrum of the mixture of GAGC and GCUC at 65°C (aromatic region shown in Figure 24) was quite close to the sum of the spectra of the two separate strands and emphasized the complete absence of inter- and intra-strand effects at this temperature. It was only by comparison of the spectra where the G(1)H-8, A(2)H-8, G(3)H-8, and G(4)H-8 protons had undergone deuterium exchange (120) to the spectra of the fully protiated species that reasonable assignments of the remaining aromatic protons could be made particularly at the lower temperatures. The shifts of the aromatic protons varied widely with decreasing temperature, with those of A(2)H-2 being the most dramatic. Unfortunately, because of the severe line-broadening experienced at lower temperatures, the full sigmoidal curves of only C(1)H-6, G(1)H-8, A(2)H-2, U(2)H-6, C(3)H-6, and C(4)H-6 were visible. These lines with the exception of C(3)H-6 all gave T_m values lying within the range $42 \pm 1^\circ\text{C}$. The agreement between this T_m and the extrapolated value expected on the basis of variable concentration-UV studies (118) is remarkable but in conjunction with the similar correspondence in T_m values noted by Arter *et al.* (113) and Borer *et al.* (114) it must be concluded that NMR is a valid tool for the measurement of T_m values.

The three protons A(2)H-8, G(3)H-8, and G(4)H-8 whose resonances could not be followed down to 25°C because of excessive line broadening coupled with the problem of intensity loss arising from deuterium exchange, showed a differential behaviour. The resonance for G(3)H-8 probably has

a T_m close to 43°C, but both A(2)H-8 and G(3)H-8 had barely begun the expected upfield movement at 42°C. Although these low T_m values appear at first to be unusual, it must be pointed out that the aromatic protons are experiencing a variety of local diamagnetic and paramagnetic effects which are exerting their influence over a spatial region that is close to these protons. Factors such as base ring current shieldings or deshieldings, furanose ring conformations, glycosyl-base ring conformations, phosphate group anisotropies, and inter-strand hydrogen bonding are all contributing to the screening constant of each hydrogen. In addition, as the T_m is approached, there is an averaging effect arising from the dynamic interconversion between the various intermediate states where only some of the bases are hydrogen bonding. With these factors in mind it is not so much surprising that A(2)H-8 and G(4)H-8 show low T_m values, but rather that the remaining seven protons should show T_m values so closely grouped together.

From the data obtained on the GAGC-GCUC duplex there is no evidence of the fraying process noted by Borer et al. (114) and Ts'o et al. (119) in their examination of the self-complementary sequence A_2GCU_2 . It is reasonable to suggest that with the weaker A·U interaction being an interior one in the present duplex, the tendency for G·C end fraying is reduced.

The line broadening observed in the duplex spectra appear to be characteristic of oligonucleotides at high concentrations and low temperatures. In the base-paired duplex the correlation time for molecular motion would be much greater than that of the single strands. This results in a considerable reduction in the relaxation time of these protons and would contribute to the line broadening. It has also been suggested by

Borer et al. (114) that the high salt concentrations promote end-to-end interduplex base-stacking. Since guanosine exhibits a high degree of base-stacking with cytosine (89), end-to-end aggregation would be favoured in this case. The even longer correlation time for these aggregates would further increase the line broadening.

5.2 THE STABILIZING EFFECT OF DANGLING BASES ON A SHORT RNA DOUBLE HELIX

5.2.1 INTRODUCTION

The secondary structure of native RNA is composed of short helical regions separated by hairpin or bulge loops consisting of non-complementary bases. The stability of these helical regions is considered to arise from a combination of two interactions. The first is the Watson-Crick hydrogen bonding which contributes a free energy upon base pair formation. A second stabilizing factor is the sequence dependent base-stacking interaction. This is a form of van der Waal's interaction between the bases which are fixed in roughly parallel planes separated by 3.0 Å.

Attempts to predict the most stable secondary structure of an RNA from its primary sequence have relied on maximizing the base pairing interactions (121) while base stacking was originally thought to have only a minor contribution. However, as the primary sequence of the RNA got longer, it became increasingly more difficult to determine which of a number of possible secondary structures was the most stable. This was due to the fact that the effect of loop regions or dangling bases on helix stability was not well understood.

Early experiments designed to quantify these effects of loops and dangling bases were carried out by Uhlenbeck et al. (122). They showed by optical methods that the terminal dangling bases in the block copolymers of

composition $(Ap)_n (Up)_{n-1} U$ increased helix stability. More recently, Crothers and co-workers, utilizing temperature-jump relaxation, found the anticodon binding of yeast t-RNA^{Phe} and E. coli t-RNA^{Glu} to be a factor of 10^6 greater than the binding of the two corresponding trinucleotides (123). Crothers suggested that the dangling bases at the ends of the anticodon helix formed by the t-RNA's is one of the major contributors to this high degree of binding. It was further proposed that the binding of a t-RNA to the m-RNA in the ribosome is facilitated by the dangling bases along the m-RNA strand (123).

In order to further investigate this effect of a dangling base, a 1H NMR study of the helix formed by CAUG which contained either an unpaired U or A at each terminus was undertaken. A self-complementary sequence was chosen as a reference because the symmetry of the duplex reduces the number of resonances and this usually allows the complete assignment of the base and ribose anomeric proton chemical shifts. In addition to these sequences the complementary pentamers CAAUG and CAUUG were examined in order to compare the effectiveness of any helix stabilization provided by a dangling base relative to an additional internal A-U base pair.

Nuclear magnetic resonance was particularly useful in this study since the chemical shift and coupling constant data provides information about the conformational environment of individual nucleotides. Optical methods and temperature-jump only allow the overall conformational changes of the entire oligoribonucleotide to be observed.

5.2.2 CpApUpG

RESULTS

The base and ribose anomeric proton resonances of CAUG were assigned by comparison with the spectra of CA, CAU and AUG all of which were recorded at 70°C. These data are presented in Tables 25 and 26. The 90 MHz spectrum of CAUG at 70°C is shown in Figure 27 to illustrate the chemical shift assignments.

The effect of temperature variation on the proton resonances of CAU and AUG was examined, and the results are summarized in Figure 28. The trinucleotide resonances varied linearly with temperature over the range of 17° to 70°C. In CAU all the protons were shielded with decreasing temperature, except for CH-6 which was deshielded. Similar results were obtained for AUG with all the resonances being shielded. At high temperatures the UH-1' and GH-1' signals were equivalent but began to separate near 50°C with UH-1' being tentatively assigned to the more shielded resonance.

At high temperatures the proton spectrum of CAUG showed essentially a linear variation with temperature but at 45°C and lower, non-linear behaviour was observed (Figure 29). There was a rapid broadening of the resonances as the temperature was decreased below 35°C. The AH-2 signal showed the largest chemical shift change and also remained relatively sharp throughout the temperature range. A reduction in the magnitude of the ribose H-1' and H-2' coupling constant was observed until at 20°C these resonances appeared as broad singlets.

The average melting temperature, T_m , of the CAUG helix as determined from the temperature-chemical shift curves for AH-8, AH-2, and GH-8 was found to be $24 \pm 1^\circ\text{C}$.

TABLE 25. Chemical shifts^a of the oligoribonucleotides in D₂O^b at 70°C.

Proton	CA	CAU	CAUG	AUG
CH-6	7.660	7.687	7.662	
AH-8	8.377	8.382	8.346	8.276
AH-2	8.260	8.250	8.196	8.198
UH-6		7.744	7.692	7.730
GH-8			7.962	7.963
CH-1'	5.779	5.768	5.765	
AH-1'	6.093	6.088	6.039	6.024
UH-1'		5.856	5.845	5.841
GH-1'			5.813	5.841
CH-5	5.958	5.925	5.912	
UH-5		5.746	5.738	5.772

^a Chemical shifts are in ppm relative to DSS using *t*-butyl alcohol-OD as an internal reference and are accurate to ± 0.005 ppm.

^b pD = 7.0; concentrations: CA, 1.6×10^{-2} M; CAU, 1.0×10^{-2} M; AUG, 1.3×10^{-2} M; CAUG, 9.2×10^{-3} M.

TABLE 26. Coupling constants^a ($J_{1,2}$) for the oligoribonucleotides at 70°C.

Proton	CA	CAU	CAUG	AUG
CH-1'	4.4	4.0	3.8	
AH-1'	4.6	3.7	4.4	5.0
UH-1'		4.6	4.8	4.6
GH-1'			5.3	4.6

^a Accurate to ± 0.2 Hz.

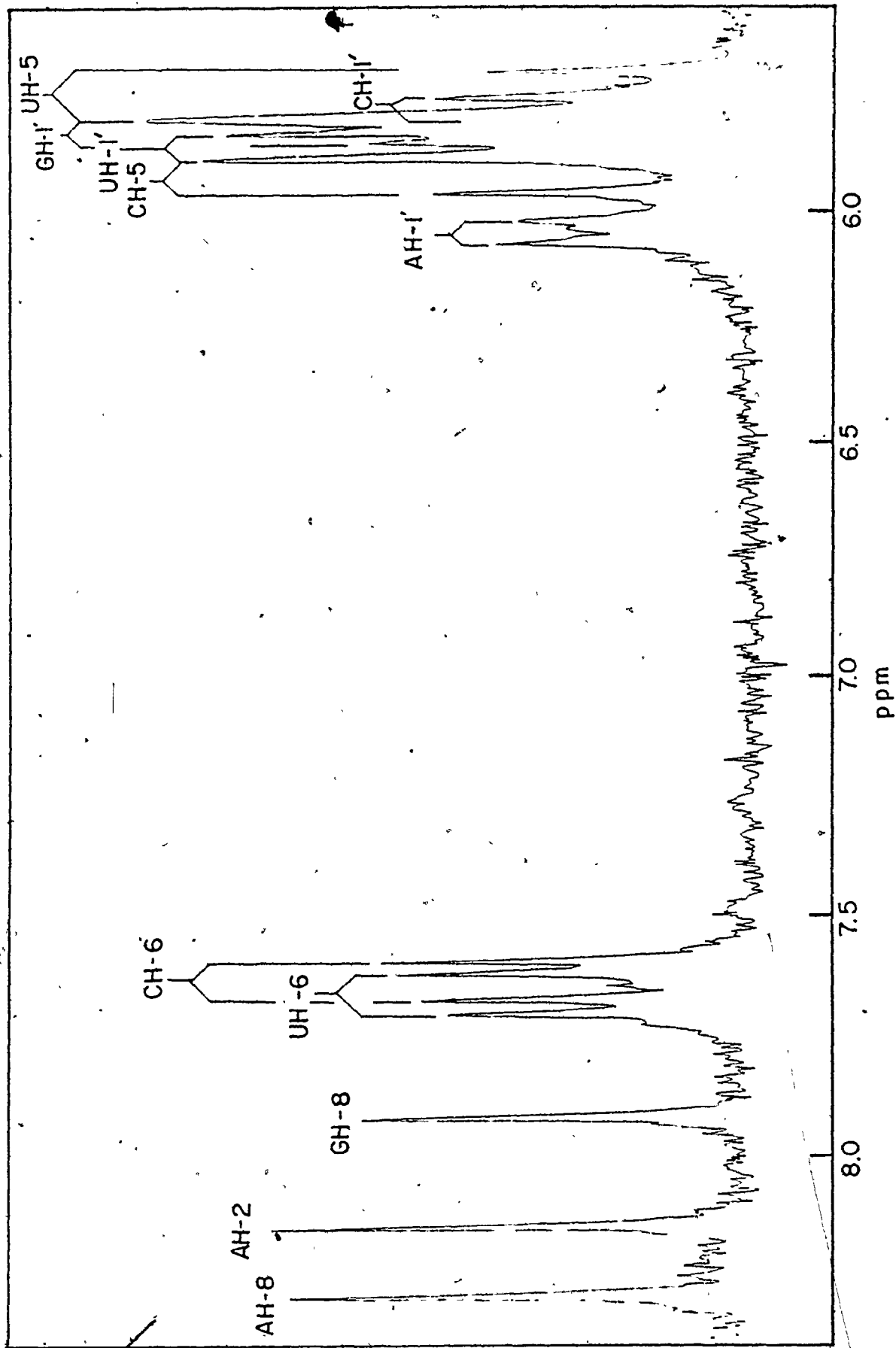


FIGURE 27. The assignment of the base and anomeric protons in the 90 MHz ^1H NMR spectrum of CAUG at 70°C.

FIGURE 28. Chemical shift versus temperature plots for (a) CAU and (b) AUG.

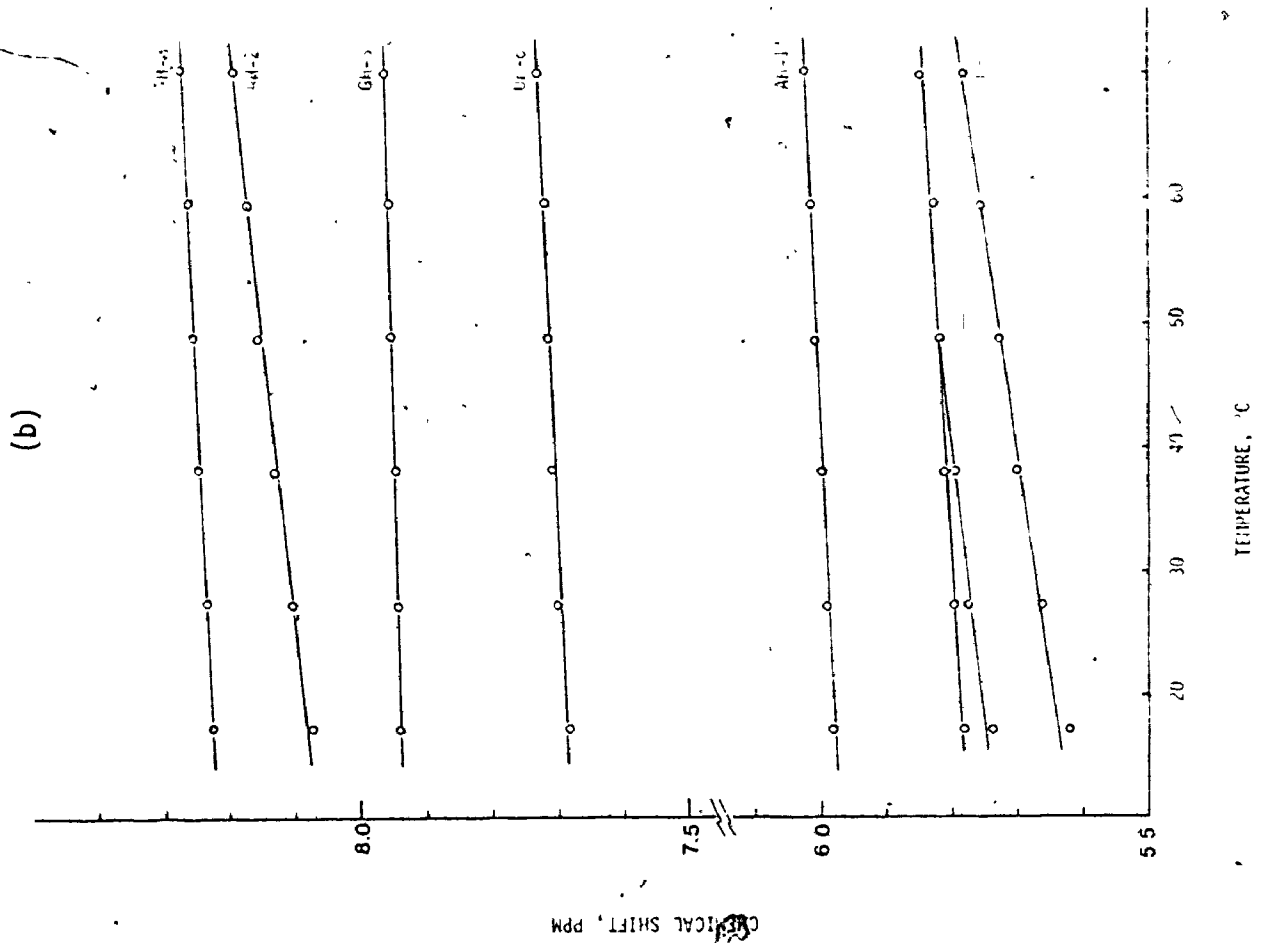
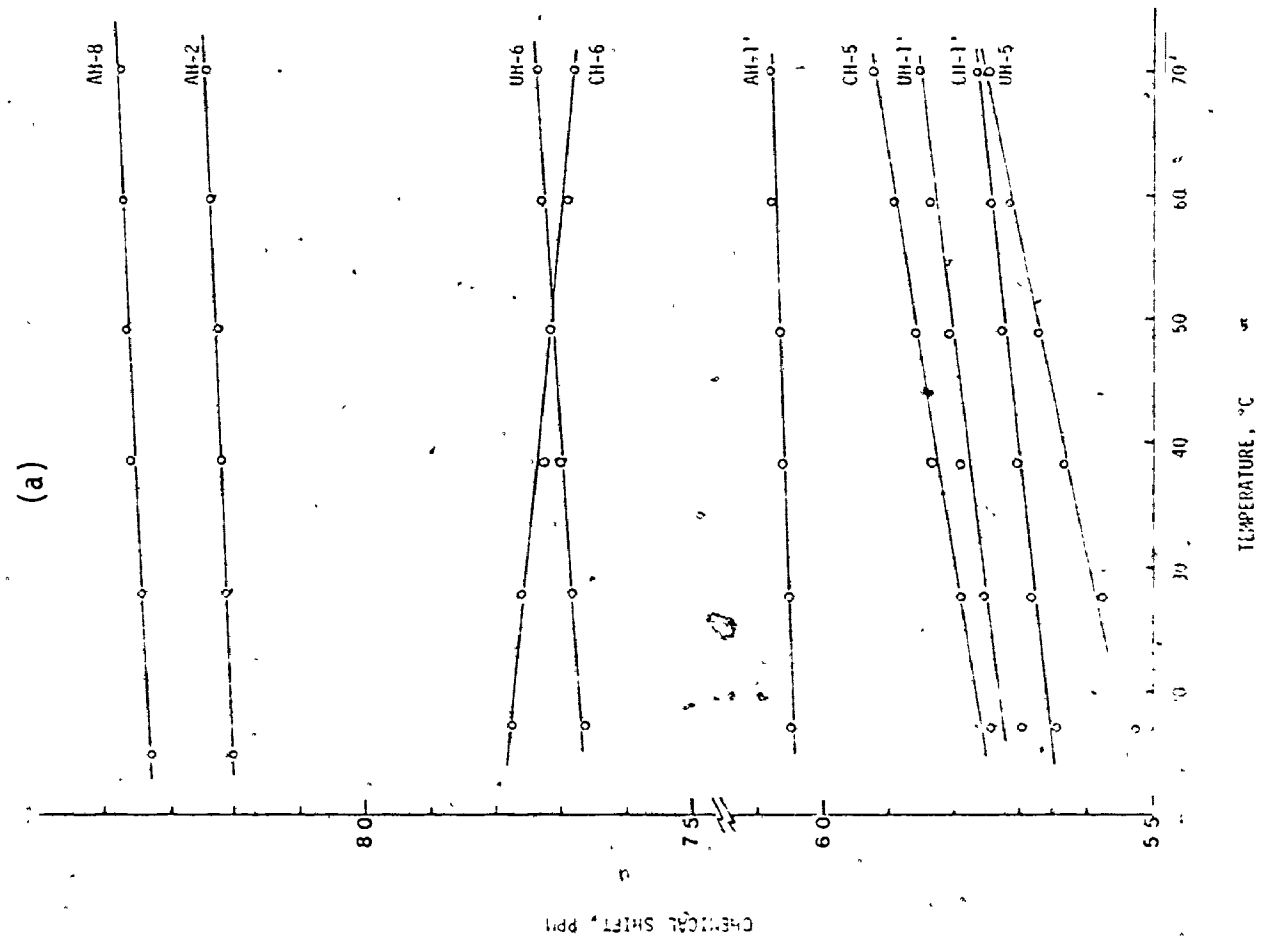
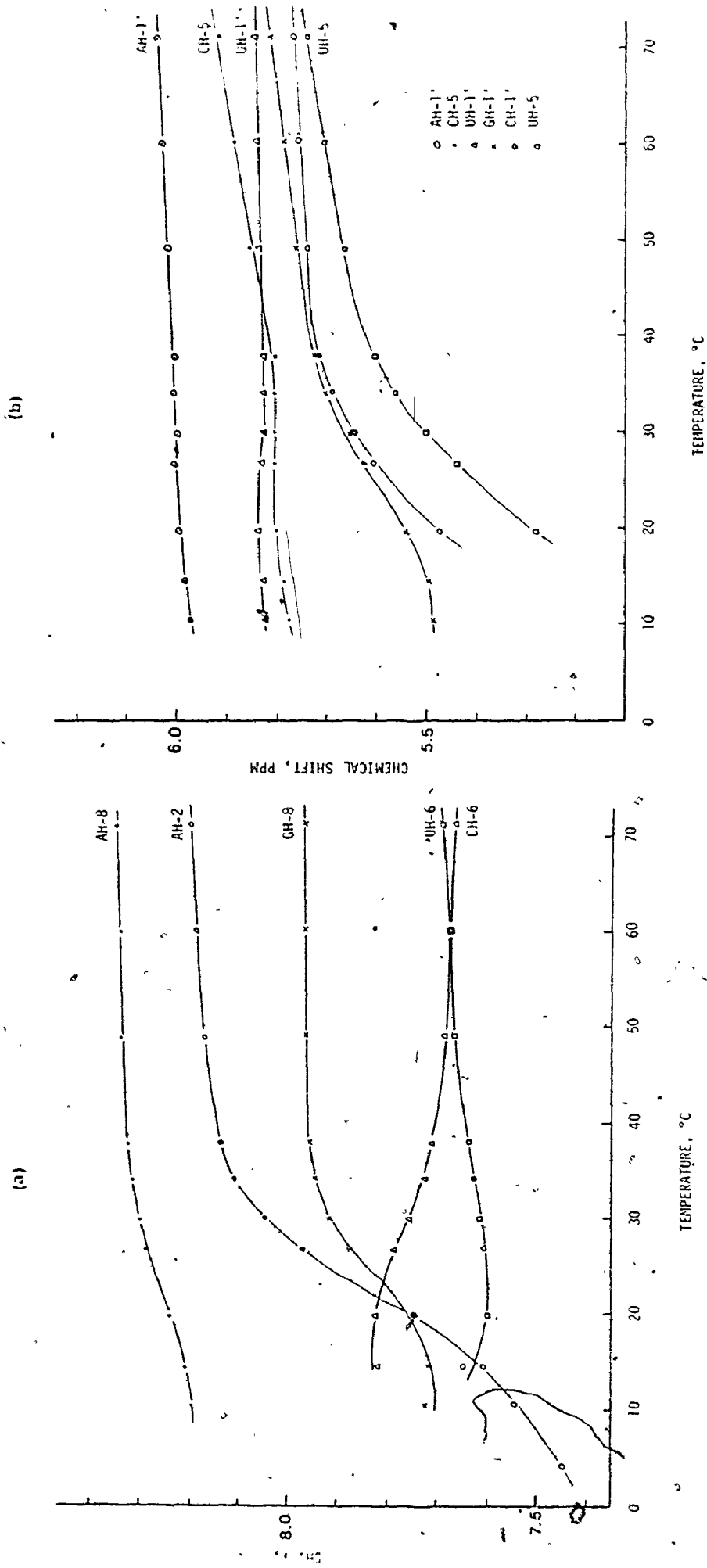


FIGURE 29. Chemical shift versus temperature plots for (a) the base and (b) the ribose anomeric protons of CAUG (concentration 9.2×10^{-3} M).



DISCUSSION

Chemical shift assignments were determined by incremental analysis in which the base and ribose anomeric protons of CA, CAU, and AUG were correlated with those of CAUG. The CA shifts were in agreement with the results published by Ezra *et al.* (89). Addition of uridine to form CAU resulted in three new doublets appearing at 7.744 ppm (UH-6, $J_{5,6} = 8.2$ Hz), 5.746 ppm (UH-5, $J_{5,6} = 8.2$ Hz) and 5.856 ppm (UH-1', $J_{1',2'} = 4.6$ Hz). The cytidine and uridine aromatic protons were again differentiated by the magnitude of the H-5 and H-6 coupling constant: cytidine, $J_{5,6} = 7.6$ Hz; uridine, $J_{5,6} = 8.2$ Hz. The uridine H-5 resonance was distinguished from the anomeric protons by irradiation of H-6 which caused the collapse of the doublet at 5.746 ppm.

The lowfield signals of AUG were assigned by comparison to AU and UG (89). The anomeric region of the high temperature spectrum was complicated by the overlap of the UH-1' and GH-1' doublets and it was only at lower temperatures that these resonances separated. The lower field signal was tentatively assigned to GH-1' since this proton should only be slightly shielded due to the weak stacking interaction between the U and G bases (89).

Using the chemical shift assignments of the trimers, the aromatic resonances of CAUG could be readily determined (Table 25 and Figure 27). Assignment of the anomeric protons was made difficult by the overlap of CH-5 (5.912 ppm) and UH-1' (5.845 ppm), and GH-1' (5.813 ppm) with CH-1' (5.765 ppm) and UH-5 (5.738 ppm). The observation that CH-6 and UH-6 become equivalent near 60°C allowed the simultaneous irradiation of both pyrimidine H-6 resonances and the collapse of both H-5 doublets facilitated the analysis of the anomeric region of the spectrum. A

direct result of this double irradiation experiment was that the UH-1' and GH-1' signals were found to be non-equivalent in the tetranucleotide as they were in AUG.

The variable temperature experiments on CAU and AUG produced linear and predominantly upfield chemical shift changes (Figure 28) which are the result of intramolecular base-stacking and are not characteristic of base-pairing (113,114). The degree of base-stacking can be monitored by the reduction of $J_{1,2}$ (89,109). This corresponds to a shift in the ribose conformational equilibrium towards the 3E or C-3' endo structure. CAU displayed the largest conformational changes since at 17°C all the anomeric doublets had collapsed to broad singlets with $J_{1,2}$ less than 1.0 Hz. In contrast, the AUG anomeric couplings at 17°C were still well resolved with a range of 2.0 to 4.5 Hz.

The behaviour of the CAUG resonances with respect to temperature was quite different from that of the trimers. Above 45°C there was a linear change with decreasing temperature for the base and anomeric protons which is attributed to single strand intramolecular base-stacking. Below 45°C there was a general non-linear variation which is associated with the formation of the following base-paired duplex:



Of the aromatic protons, AH-8, AH-2 and GH-8 all produced well defined sigmoidal curves. The average T_m was determined to be $24 \pm 1^\circ\text{C}$. It is interesting to note that the pyrimidine H-6 resonances follow essentially the same trend that was observed in CAU. This appears to be a result of the similarity in base-stacking interactions in CAU and

CAUG.- In the anomeric region of the spectrum the AH-1', CH-5, and UH-1' resonances all undergo relatively small shielding changes when compared to GH-1', CH-1', and UH-5. Although the curve for GH-1' is not as well defined as those of the aromatic protons, a T_m of $26 \pm 1^\circ\text{C}$ was estimated which is close to the value obtained for the aromatic protons.

Two aspects on the stability of the duplex formed by CAUG arise from these data. The first is the similarity in T_m values for the majority of resonances of both the terminal and interior base-pairs. This may be an indication that the presence of terminal G-C base pairs has reduced any fraying effects. Secondly, increasing the number of A-U base pairs in the interior of the duplex causes a lowering of the T_m value. This is demonstrated by comparison to the duplex formed by GAGC and GCUC ($T_m = 42 \pm 1^\circ\text{C}$) which has only one internal A-U base pair.

The large reduction in the coupling constant of the anomeric protons as the temperature was lowered ($J_{1,2}$, less than 1.0 Hz at 20°C) is indicative of a high percentage of the C-3' endo conformation of the ribose rings. This conformational change is associated with a high degree of base-stacking which appears to be an integral process involved in double helix formation and may make a significant contribution to helix stability (124).

5.2.3 CpApApUpG AND CpApUpUpG

RESULTS:

The chemical shifts and ribose anomeric proton coupling constants for CAAUG and CAUUG and their mixture along with those of CAUG are presented in Tables 27 and 28. The spectra of the separate pentanucleotides

and the mixture at 70°C are shown in Figures 30 and 31, respectively.

As the temperature of the mixed sample was reduced the purine resonances displayed linear and upfield shift changes until at 40°C nonlinearity was observed (Figure 32). The line broadening and signal overlap became so severe that the low temperature spectra had to be obtained at 270 MHz before the temperature-chemical shift curves could be completed. The doublets corresponding to the H-1' signals collapsed to broad singlets below 30°C.

The average T_m determined from the plots of the purine base protons was $28.4 \pm 2.1^\circ\text{C}$.

TABLE 27. Chemical shifts of the oligoribonucleotides^a in D₂O at 70°C

Proton	CAUG	CAAUG	CAUUG	CAAUG GUUAC
C(1)H-6	7.662	7.623		7.630
A(2)H-8	8.346	8.268		8.274
A(2)H-2	8.196	8.134		8.141
A(3)H-8		8.255		8.261
A(3)H-2		8.079		8.089
U(4)H-6	7.692	7.654		7.661
G(5)H-8	7.962	7.942		7.945
C(5)H-6			7.659	7.661
A(4)H-8			8.359	8.362
A(4)H-2			8.206	8.209
U(3)H-6			7.731	7.736
U(2)H-6			7.716	7.718
G(1)H-8			7.978	7.981
C(1)H-1'	5.765	5.777		5.780
A(2)H-1'	6.039	5.974		5.989
A(3)H-1'		5.924		5.940
U(4)H-1'	5.845	5.831		5.837
G(5)H-1'	5.813	5.796		5.806
C(5)H-1'			5.770	5.780
A(4)H-1'			6.062	6.065
U(3)H-1'			5.858	5.863
U(2)H-1'			5.888	5.884
G(1)H-1'			5.818	5.821
C(1)H-5	5.912	5.865		5.875
U(4)H-5	5.738	5.695		5.704
C(5)H-5			5.917	5.922
U(3)H-5			5.764	5.765
U(2)H-5			5.855	5.857

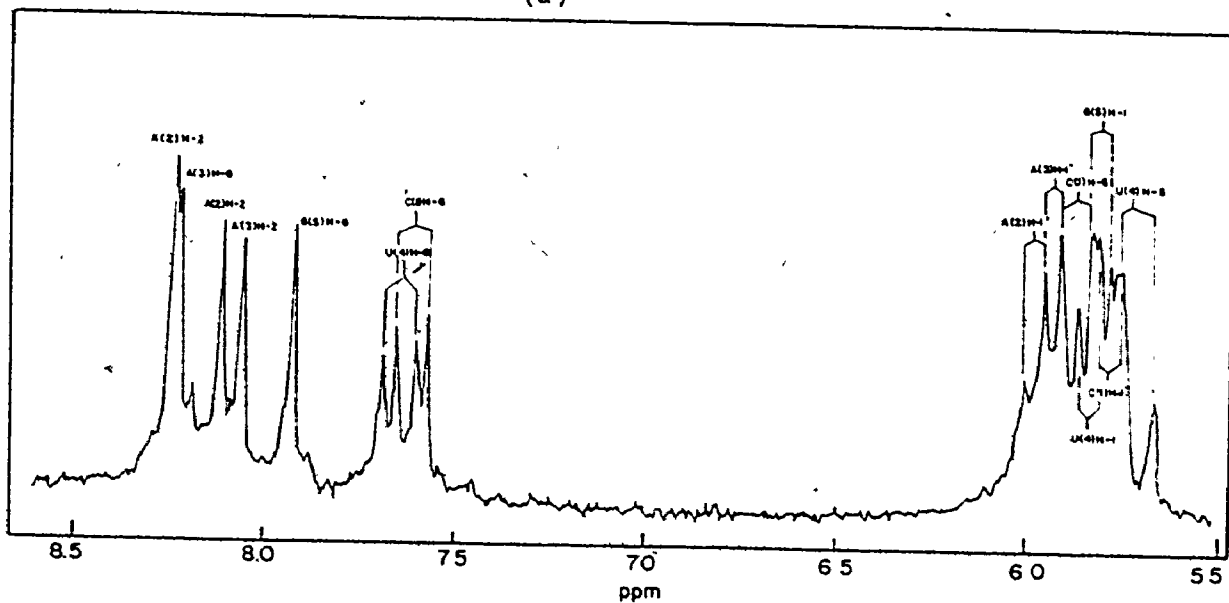
^a pD = 7.0; Concentrations: CAAUG, 1.1×10^{-2} M; CAUUG, 1.1×10^{-2} M

TABLE 28. Coupling constants ($J_{1,2}$)^a of the oligoribonucleotides, at 70°C

	CAUG	CAAUG	CAUUG	¹²³⁴⁵ CAAUG GUUAC
C(1)H-1'	3.8	4.7		5.3
A(2)H-1'	4.4	4.4		4.7
A(3)H-1'		3.8		4.1
U(4)H-1'	4.8	5.0		5.0
G(5)H-1'	5.3	4.7		4.7
C(5)H-1'			4.1	4.1
A(4)H-1'			4.4	4.4
U(3)H-1'			3.6	3.2
U(2)H-1'			3.0	3.5
G(1)H-1'			4.4	4.4

^a Accurate to ± 0.2 Hz

(a)



(b)

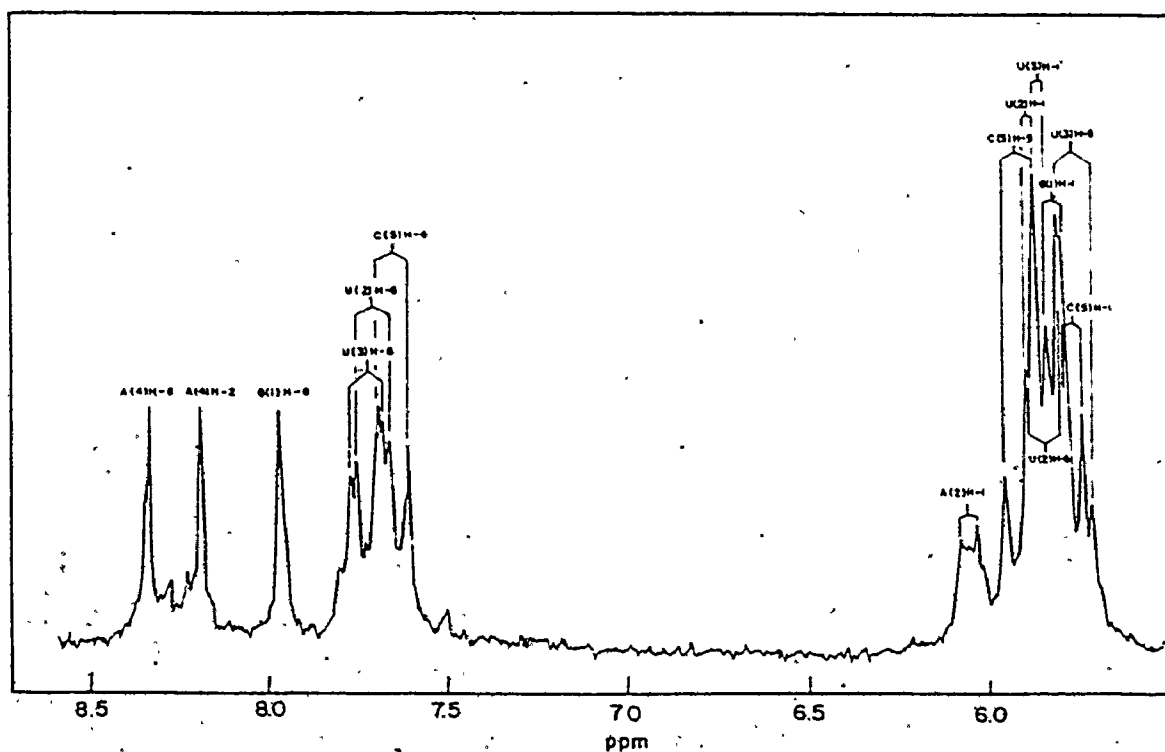


FIGURE 30. The 90 MHz ^1H NMR spectra of (a) CAAUG and (b) CAUG in D_2O at 70°C .

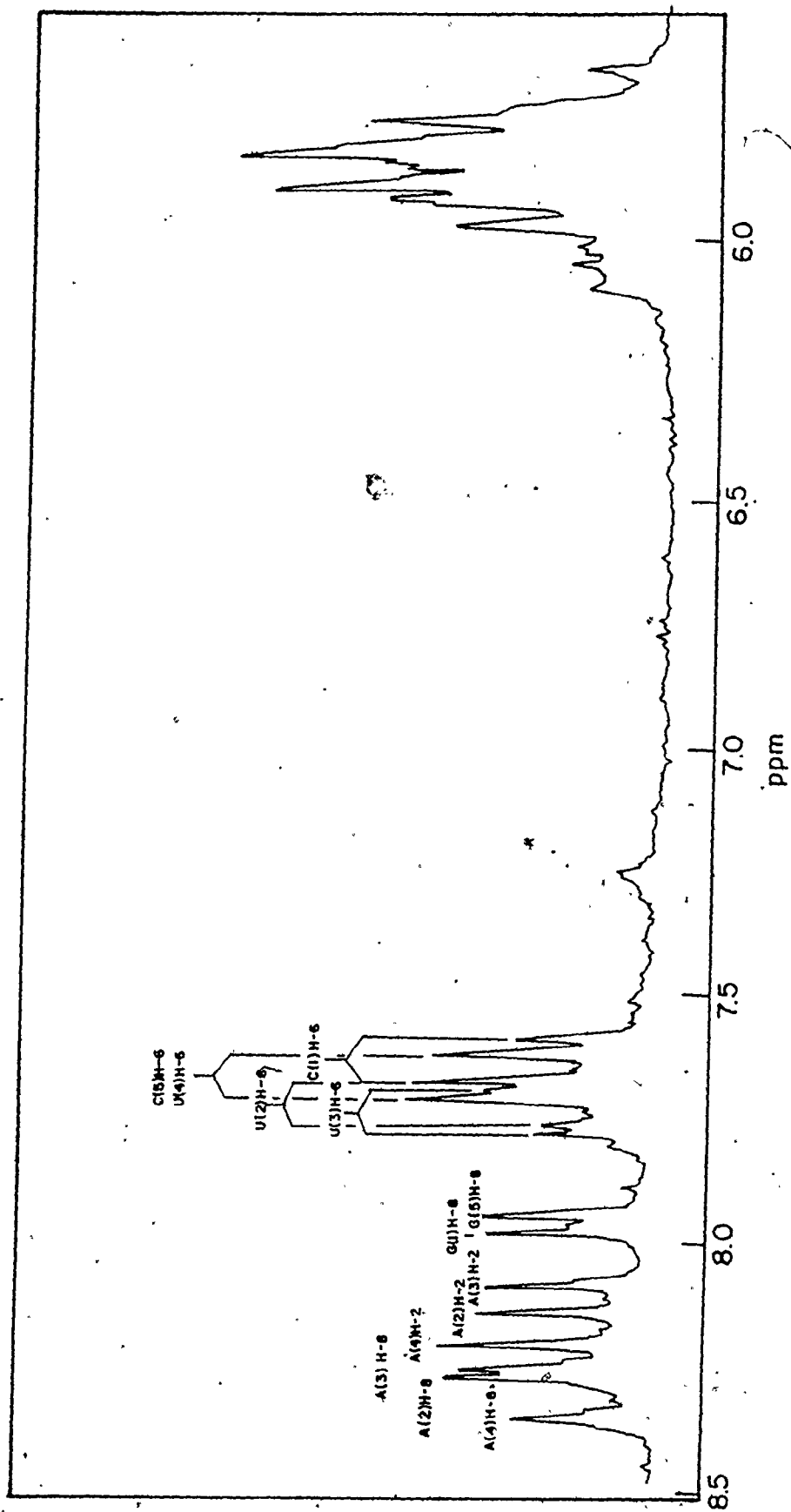


FIGURE 31. The 90 MHz ^1H NMR spectrum of the mixture of CAAUG and CAUUG at 70°C

DISCUSSION:

The low field proton chemical shifts of CAAUG and CAUUG were assigned by comparison to the data on CAUG. In CAAUG the presence of A(3) was indicated by two singlets at 8.255 ppm (H-8) and 8.079 ppm (H-2) and a doublet at 5.924 ppm (H-1', $J_{1',2'} = 3.8$ Hz). Since adenine has a strong ring current shielding effect this would account for the upfield shifts experienced by the neighbouring aromatic protons relative to CAUG. The appearance of three new doublets in the spectrum of CAUUG is attributed to the U(2)H-6 (7.716 ppm, $J_{5,6} = 8.2$ Hz), U(2)H-5 (5.855 ppm, $J_{5,6} = 8.2$ Hz) and U(2)H-1' (5.888 ppm, $J_{1',2'} = 3.0$ Hz). The remaining pentanucleotide protons showed little change in chemical shift.

When these complementary sequences were mixed and the spectrum recorded at 70°C the purine base protons displayed chemical shifts which were nearly identical to those of the single strands. However, the pyrimidine H-6 and H-5 signals and the ribose anomeric protons could not be assigned directly because of the overlap of these resonances (Figure 31). This problem was solved by the technique of difference spectroscopy. Computer subtraction of the separate pentanucleotide spectra from that of the mixture produced the difference spectra in Figure 33. Comparison of the difference spectra with those of the separate pentanucleotides allowed the complete assignment of all the pyrimidine H-6 and H-5 doublets as well as the ribose anomeric proton resonances of the mixture (Table 27). Spectral subtraction can only be used with high temperature spectra because the interstrand binding that would produce significant changes in chemical shift is at a minimum.

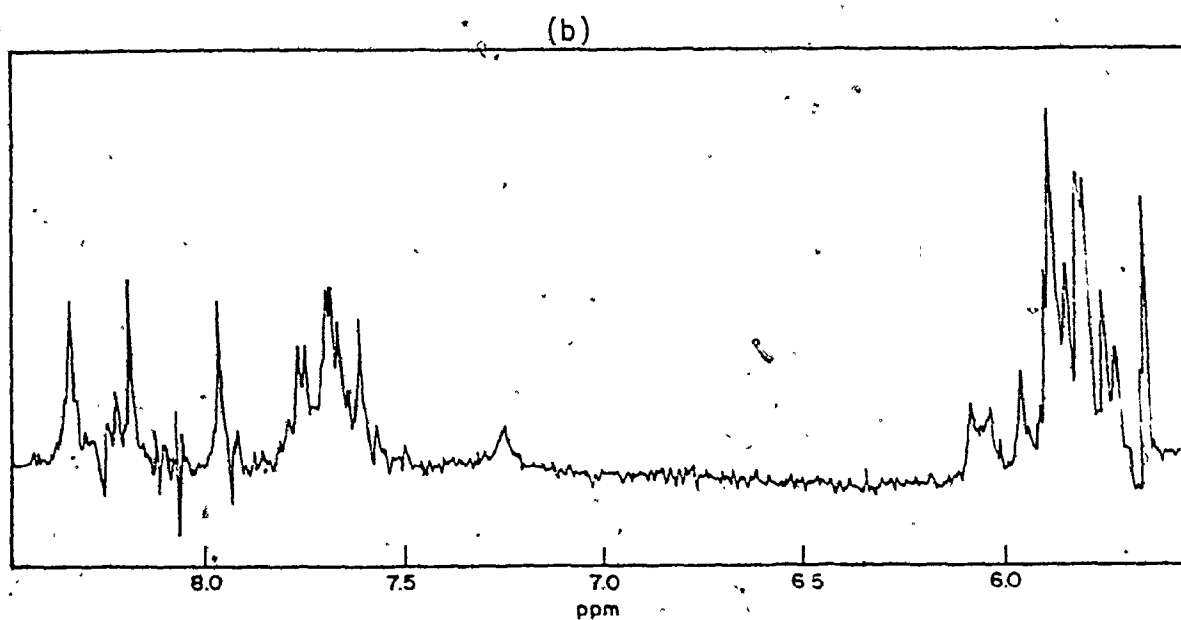
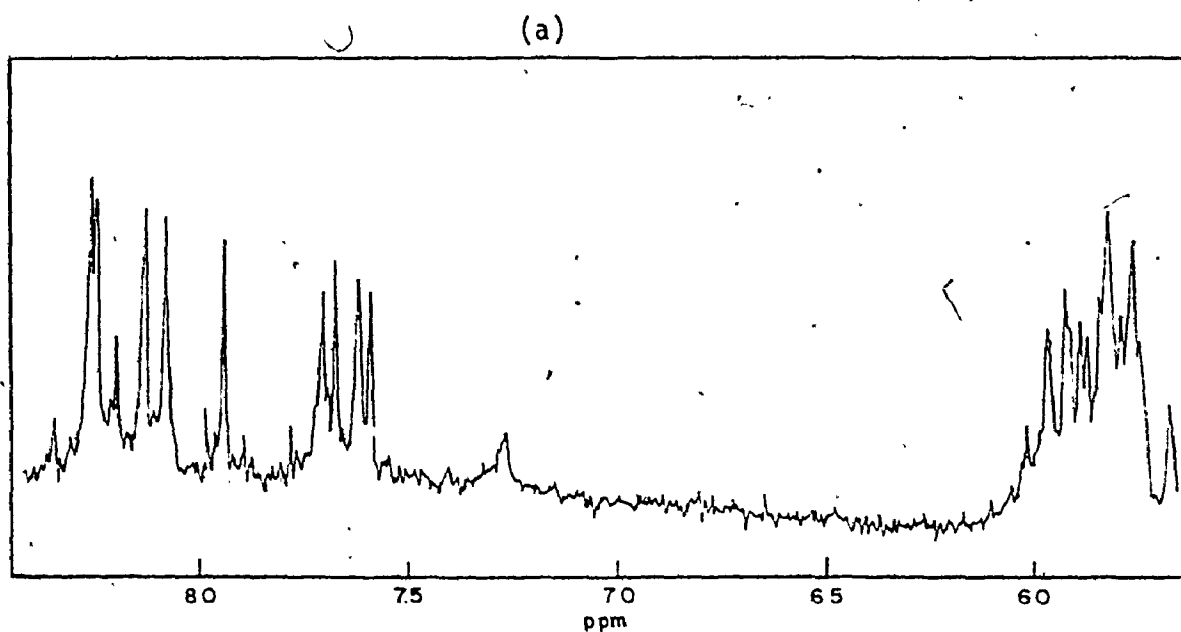


FIGURE 33. Difference spectra of (a) CAAUG and (b) CAUUG obtained by computer subtraction of the corresponding pentaribonucleotide spectra in Figure 30 from the mixture spectrum in Figure 31.

As the temperature of the mixture was reduced the purine aromatic resonances underwent linear changes in chemical shift associated with a spatial reorientation of the bases and a contribution from base stacking just prior to the non-linear behaviour. The first indication of base-paired duplex formation occurred at approximately 40°C as the shift changes became non-linear (Figure 32). The A(3)H-8 and H-2 showed the most significant change in chemical shift particularly at the higher temperatures and this would be due to a high degree of base stacking with A(2). A considerable amount of line broadening was observed at the lower temperatures even at 270 MHz. The combination of an increase in the correlation time for the molecular motion of these longer sequences and any end-to-end aggregation of the duplexes would contribute to the line broadening. All the purine aromatic protons gave well defined temperature-chemical shift plots from which an average T_m of $28.4 \pm 2.1^\circ\text{C}$ was determined.

The data acquired on this pentanucleotide duplex demonstrates the expected increase in T_m when the CAUG sequence is extended to include an additional internal A·U base pair. These results can now be used as a reference for comparing the effect of terminal dangling bases on the stability of the CAUG duplex.

5.2:4 CpApUpGpA AND CpApUpGpU

RESULTS:

The chemical shift assignments and ribose anomeric proton coupling constants for CAUGA and CAUGU are given in Tables 29 and 30. Figure 34 contains the 90 MHz ^1H spectra of these sequences at 70°C.

The variable temperature study of these pentanucleotides again produced linear chemical shift changes at the higher temperatures but at 48°C and lower non-linearity was observed (Figure 35). The appearance of line broadening did not occur until temperatures below 30°C were reached. In both cases the A(2)H-2 resonance underwent the greatest chemical shift change similar to that in CAUG. The H-8 and H-2 resonances of the A(5) in CAUGA and the H-6 and H-5 signals of U(5) in CAUGU displayed sigmoidal behaviour as a function of temperature. This is of particular significance since these residues are not involved in base pairing. A reduction in the magnitude of all the H-1', H-2' coupling constants was observed until the resonances appeared as broad singlets below 27°C.

The average melting temperatures of the duplexes were: CAUGA, $35.0 \pm 1^\circ\text{C}$ and CAUGU, $29.5 \pm 1^\circ\text{C}$.

DISCUSSION:

The incremental analysis method was used to assign the chemical shifts of the base and ribose anomeric protons of the pentaribonucleotides. As mentioned in section 5.1 the application of this procedure requires that the addition of the new residue to the sequence will have little effect on the protons already present. This was the case for CAUGU where the U(5) residue was clearly evident by the doublets centered at 7.783 ppm (H-6, $J_{5,6} = 8.2$ Hz), 5.813 ppm (H-5), and 5.853 (H-1', $J_{1',2'} = 3.2$ Hz) (Figure 34b). The majority of the remaining protons showed nearly identical chemical shifts to those of CAUG (Table 29).

However, for CAUGA the addition of the A(5) nucleotide caused a shielding of all the aromatic protons relative to CAUG even at 70°C (Table 29).

TABLE 29. Chemical shifts^a of the oligoribonucleotides in D₂O^b at 70°C

Proton	CAUG	CAUGA	CAUGU
CH-6	7.662	7.649	7.662
A(2)H-8	8.346	8.339	8.352
A(2)H-2	8.196	8.167	8.199
U(3)H-6	7.692	7.699	7.692
GH-8	7.962	7.890	7.958
A(5)H-8		8.316	
A(5)H-2		8.180	
U(5)H-6			7.783
CH-1'	5.765	5.721	5.772
A(2)H-1'	6.039	6.053	6.037
U(3)H-1'	5.845	5.779	5.849
GH-1'	5.813	5.764	5.796
A(5)H-1'		6.053	
U(5)H-1'			5.853
CH-5	5.912	5.897	5.912
U(3)H-5	5.738	5.741	5.749
U(5)H-5			5.813

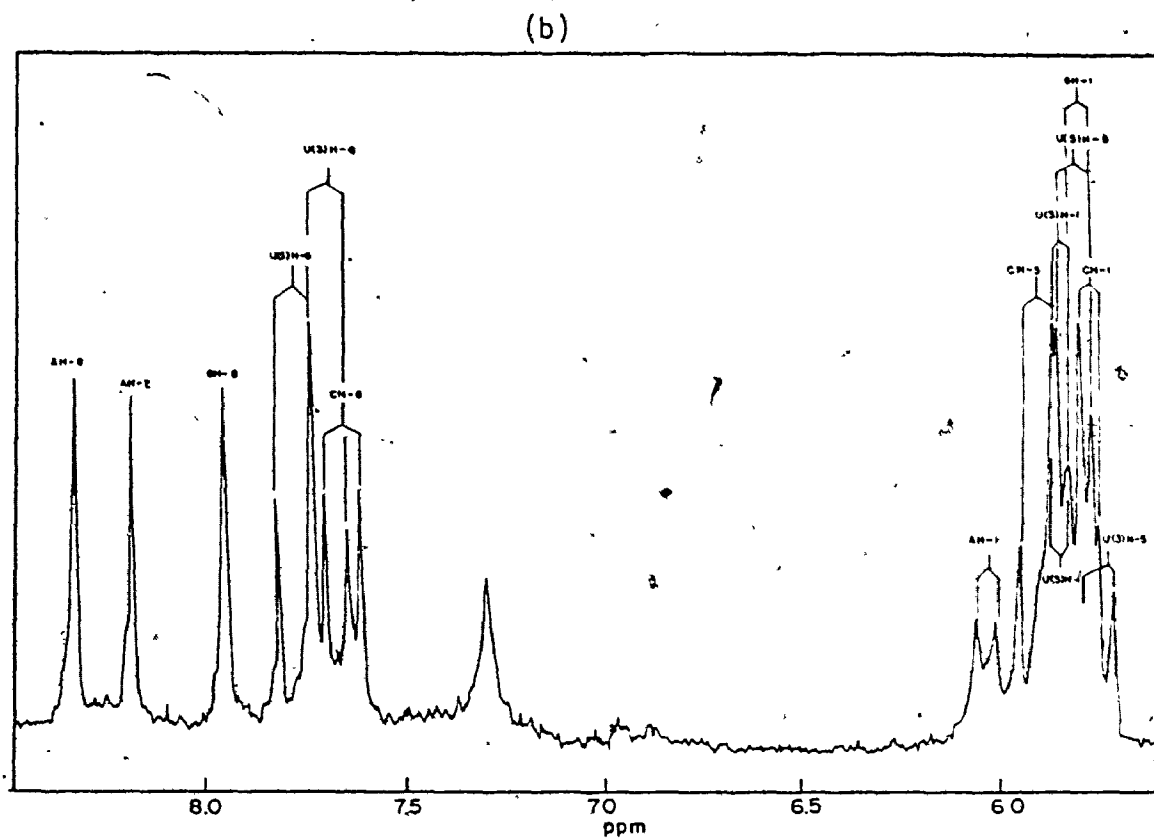
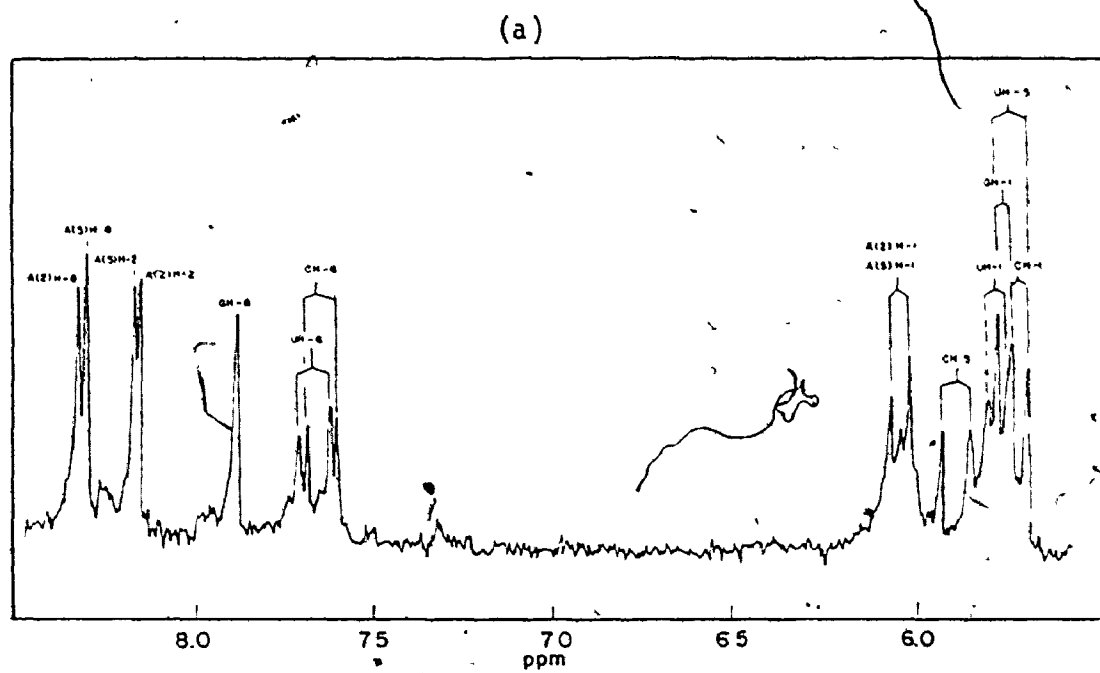
^a Chemical shifts are in ppm downfield from DSS using *t*-butyl alcohol-OD as an internal reference and are accurate to ± 0.005 ppm.

^b pD = 7.0; Concentrations: CAUG, 9.2×10^{-3} M; CAUGA, 9.2×10^{-3} M; CAUGU, 7.7×10^{-3} M.

TABLE 30. Coupling constants ($J_{1',2'}$)^a of the oligoribonucleotides at 70°C

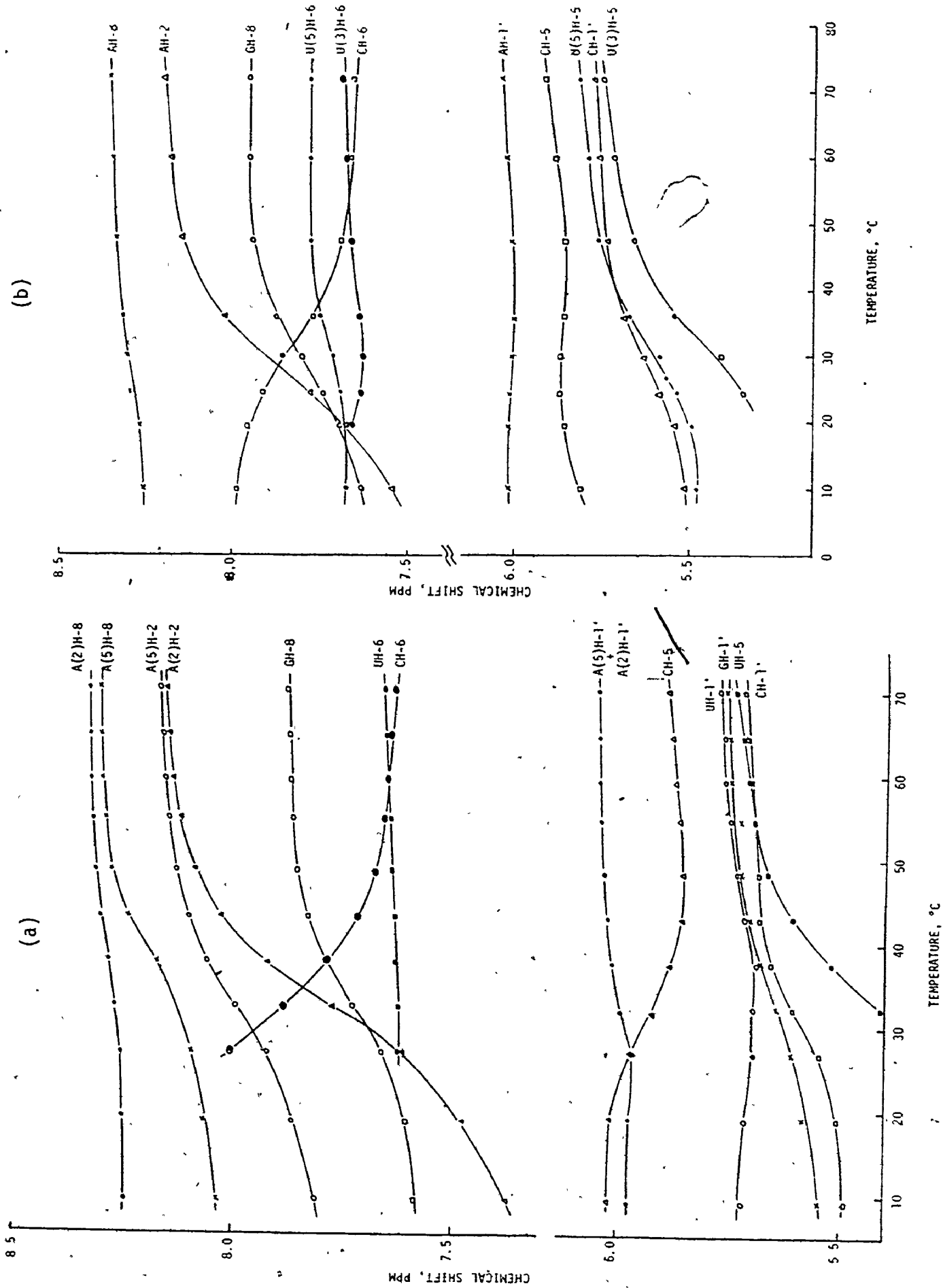
	CAUG	CAUGA	CAUGU
CH-1'	3.8	4.1	3.8
A(2)H-1'	4.4	4.7	4.4
U(3)H-1'	4.8	5.0	4.1
GH-1'	5.3	3.5	5.3
A(5)H-1'		4.7	
U(5)H-1'			3.2

^a Accurate to ± 0.2 Hz



• FIGURE 34. The 90 MHz ^1H NMR spectra of (a) CAUGA and (b) CAUGU in D_2O at 70°C .

FIG. 35: Chemical shift versus temperature plot for the base and ribose anomeric protons of (a) CAUGA and (b) CAUGU.



Although the GH-8 and pyrimidine H-6 resonances could be readily assigned by comparison to the CAUG spectrum, the major difficulty created by this increased shielding was in the differentiation of the A(2) and A(5) base protons. Assignment of the AH-2 signals was made by considering their variable temperature behaviour (Figure 35a). The resonance which undergoes the largest change in chemical shift was assigned to A(2)H-2. This is in agreement with the behaviour of the AH-2 signals in the A-U base pairs of the duplexes formed by GAGC-GCUC, CAUG, and CAUGU. The AH-8 resonances were also distinguished by their chemical shift versus temperature curves since the signal at 8.339 ppm experiences a relatively small chemical shift change. This resonance was therefore assigned to A(2)H-8 because of its similarity with the temperature behaviour of A(2)H-8 in CAUG and CAUGU (Figures 29 and 35b, respectively). The greater shielding observed for A(5)H-8 can also be rationalized from an examination of molecular models which will be commented on below.

Assignment of the ribose anomeric protons of CAUGA was complicated by the unexpected equivalence of A(2)H-1' and A(5)H-1' (6.053 ppm) and the overlap of U(3)H-1' (5.779 ppm), GH-1' (5.764 ppm), U(3)H-5 (5.741 ppm), and CH-1' (5.721 ppm). Since the CH-6 and U(3)H-6 resonances become equivalent at 60°C, simultaneous irradiation of the pyrimidine H-6 signals facilitated the assignment of both the H-5 and ribose anomeric protons. Similar decoupling experiments were performed on CAUGU.

Variation of the sample temperature over the range of 30°C to 10°C caused the general upfield and nonlinear chemical shift changes associated with the formation of based paired duplexes. The average melting temperatures of both the pentanucleotides and reference duplexes are summarized in Table 31.

TABLE 31. Melting temperatures and concentrations of the base paired duplexes.

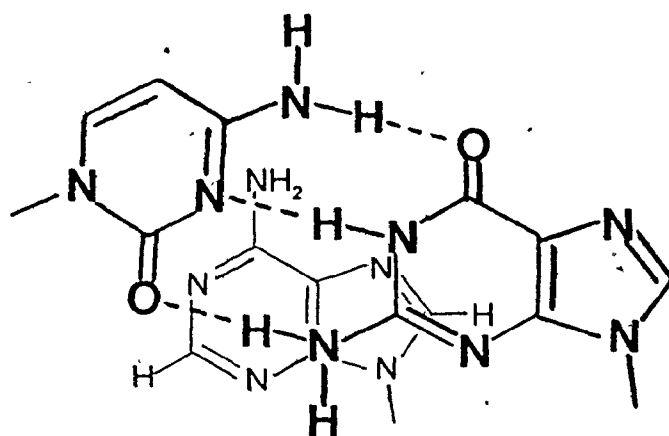
Duplex	T_m (°C)	Concentration (M)
$\begin{array}{c} \text{CAUG} \\ \cdot\cdot\cdot \\ \text{GUAC} \end{array}$	24.0 ± 1	9.2×10^{-3}
$\begin{array}{c} \text{CAUGU} \\ \cdot\cdot\cdot \\ \text{UGUAC} \end{array}$	29.5 ± 1	7.7×10^{-3}
$\begin{array}{c} \text{CAUGA} \\ \cdot\cdot\cdot \\ \text{AGUAC} \end{array}$	35.0 ± 1	9.2×10^{-3}
$\begin{array}{c} \text{CAAUG} \\ \cdot\cdot\cdot \\ \text{GUUAC} \end{array}$	28.5 ± 2.1	1.1×10^{-2}

The T_m 's were determined from only the sigmoidal upfield curves of the residues involved in base pairing. These results clearly indicate that a dangling base stabilizes a double helix. Comparison of these data to the T_m obtained for the duplex formed by the complementary pentanucleotides CAAUG and CAUUG shows the increase in T_m from an additional A-U base pair is similar to the increase provided by an unpaired U at each terminus, but less than the result from having a dangling A.

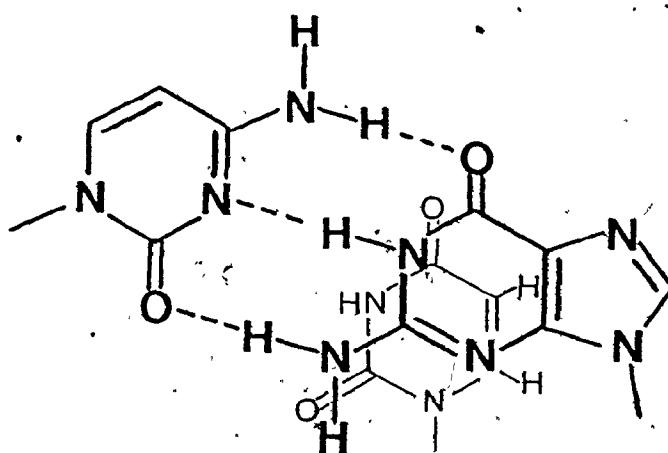
To account for this increased stability, Uhlenbeck (122) originally proposed that the dangling base increased the stacking interactions between the bases involved in base pairing. The most favourable conditions for the formation of a helical duplex require that the bases in the short oligonucleotide strand be close to a fully stacked conformation (124,125), while longer chains have a high percentage of base stacking. Thus any factor which increases base stacking will contribute to the stability of the duplex.

This study now provides direct evidence of a stacking interaction between the duplex and dangling base, while the previous optical work could only suggest the possibility of such an interaction.

Figure 35 shows that the temperature - chemical shift plots for A(5)H-8 and H-2 in CAUGA and U(5)H-6 and H-5 in CAUGU are sigmoidal in nature and exhibit an upfield shift with decreasing temperature. Prior to this work such behaviour was attributed to bases which were only involved in hydrogen bonding. Although the dangling A or U does not base pair, they are experiencing the rapid conformational changes associated with single strand stacking and duplex formation through their base stacking interactions with the neighbouring bases in the duplex. Further support for this base stacking is the rapid reduction in $J_{1,2}$ for all the anomeric protons as the temperature was lowered. This is attributed to an increase in the percentage of the C-3' endo ribose conformation upon base stacking (89,109). These results are also consistent with a helical duplex in the A or A' RNA conformation. The stacking interaction of the dangling base was also evident from its influence on the chemical shifts of the neighbouring bases. The CH-6 resonance in both CAUGA and CAUGU exhibited a more rapid deshielding than the corresponding proton in CAUG (Figure 29). A deshielding of CH-5 is observed in the pentanucleotide CAUGA which is the reverse of the chemical shift change in CAUG. In order to clarify these observations and determine the approximate position of the dangling base relative to the terminal G-C base pair, Dreiding molecular models were examined. These results are illustrated in Figure 36. In CAUGA the CH-5 and H-6 are approximately the same distance (6.5 Å) from the centre of



(a)



(b)

FIGURE 36. Diagrammatic representation of the base stacking interaction between the dangling base and terminal G-C base pair in (a) CAUGA (estimated distance of C(1)H-5 and H-6 from the centre of the six membered ring of A(5): 6.5 \AA°) and (b) CAUGU (estimated distances of C(1)H-5 and H-6 from the centre of the U(5) ring are 7.7 and 8.4 \AA° , respectively).

A(5) six membered ring and are most likely in the deshielding part of the A(5) ring current (126). These C protons are in a similar position to the U(5) residue but are affected to a lesser degree by the smaller uridine ring current. In addition to these ring current effects the terminal C protons will also be affected by changes in end-to-end aggregation and solvent effects when the CAUG sequence is extended to a pentanucleotide. The A(5)H-8 is in a position to experience a considerable shielding from the G (126) and this would explain the difference in temperature behaviour of the AH-8 signals in CAUGA (Figure 35a).

Other proposals have been made concerning the stabilizing effect of dangling bases. Kallenbach and Berman (125) suggested that the stacking of the dangling base stabilizes the terminal base pair by counteracting fraying effects. However, fraying of the terminal G·C base pairs was not observed from the study of CAUG and, therefore the increased stability in these shorter sequences must arise from a higher degree of single strand stacking. Another alternative was the possibility of a dangling base interacting with another dangling base in an interduplex fashion and increase the duplex stability by forming end-to-end aggregates. This can be discounted by the variable temperature study of the separate pentanucleotides CAAUG and CAUUG which showed the absence of sigmoidal behaviour down to 10°C, indicating the absence of U·U or A·A internal base pairs. Thus it is unlikely that a dangling U (or A) would hydrogen bond to another dangling U (or A). Consideration of the resonance line widths also does not comply with the aggregate proposal. As the temperature was lowered the signals in both CAUGA and CAUGU did not broaden as rapidly as they did in the CAUG and CAAUG-CAUUG spectra. This difference suggests that the presence of a dangling base reduces intermolecular end-to-end aggregation.

These results demonstrate that base stacking is an integral process in double helix formation and makes a significant contribution to the helix stability (124). Further study of the role of dangling bases in stabilizing a double helix will provide a better understanding of the binding interactions between various single stranded regions of nucleic acids, for example, tRNA and mRNA (123).

EXPERIMENTAL

1. ^{13}C NMR OF THE ISOQUINOLINE ALKALOIDS

Natural abundance ^{13}C nuclear magnetic resonance spectra were recorded in the Fourier transform mode on a Bruker WH-90 spectrometer at 22.62 MHz and a probe temperature of +35.0°C. Sample concentrations were 0.08 M to 0.45 M in CDCl_3 . Tetramethylsilane (TMS) was used as an internal reference. Field/frequency locking was provided by the deuterium signal of CDCl_3 . Routine spectra were obtained at a sweep width of either 6024 Hz (acquisition time, 1.359 sec) or 5000 Hz (acquisition time, 1.638 sec) using a 3.7 μsec (17°) pulse and 16K data points.

The ^{13}C spectrum of 10-oxodancentrine was recorded by Dr. K. Nakanishi of Columbia University.

Proton magnetic resonance spectra were obtained on either a Varian HA-100 or Varian EM-390 spectrometer in the frequency sweep mode. The 220 MHz ^1H magnetic resonance spectra were obtained at the Canadian 220 MHz Centre, University of Toronto, Toronto, Ontario. CDCl_3 and TMS were again used as solvent and internal reference, respectively.

Mass spectra were determined on a C.E.C. 21-110B mass spectrometer at an ionizing voltage of 80 eV and a source temperature of 200-250°C. Deuterium content was estimated by repeated scanning of the molecular ion and application of the appropriate corrections for the natural abundance of ^{13}C and the presence of M-1 and M-2 fragment ions. For high resolution work spectra were recorded on plates and accurate mass measurements were made by using perfluorokerosene as a marker (127).

The composition of all reported ions have been checked by high resolution mass spectrometry and agree with calculated values within ± 0.005 a.m.u.

Melting points were determined on a Kofler hot stage and are uncorrected. Infrared spectra were recorded on a Perkin-Elmer 337 or 283 spectrometer. A GCA/McPherson Instrument model 707D spectrometer was used for the U.V. spectra. Thin layer chromatography was performed on either silica gel (F-60₂₅₄) or alumina.

The following compounds were obtained from commercial sources: tetrahydroisoquinoline (6), β -hydrastine (11), veratrole (10), methylenedioxybenzene (15), phthalide (16), 1-indanone (34a), and 1,3-indandione (37). Dr. R.H.F. Manske of the University of Waterloo, Waterloo, Ontario provided generous samples of the following alkaloids: (+)-corlumine (13), (+)-adlumine (14), (+)-canadine (21), (+)-tetrahydropalmatine (23), (+)-corydaline (24), (+)-mesocorydaline (25), (+)-cavidine (26), and (+)-thalictrifoline (27).

All other compounds were synthesized by standard procedures or isolated from natural sources and gave satisfactory spectral and physical data:

6,7-dimethoxy-1,2,3,4-tetrahydroisoquinoline (1), (128,129), 6,7-dimethoxy-2-methyl-1,2,3,4-tetrahydroisoquinoline (2) (130), 6,7-dimethoxy-3,4-dihydroisoquinoline (3) (128), 6,7-dimethoxy-2-methyl-3,4-dihydroisoquinolinium iodide (4) (128), 7,8-dimethoxy-1,2,3,4-tetrahydroisoquinoline (5) (131), (+)- α -hydrastine (12) (132), 6,7-dimethoxyphthalide (19) (133), 6,7-methylenedioxyphthalide (20) (134), 6-nitrophthalide (17) (135), 6-aminophthalide (18) (135,136), phthalide-6-d (16b) (137), (+)-c-XXXXXXXXXX 9-¹³C₂H (137), (+)-nandinine (22) (138), 1-methyleneindane (32) (139), 4,5-dimethoxy-1-indanone (35) (140), 6,7-methylenedioxy-1-indanone (36)

(141), 2-phenyl-1,3-indandione (38) (142), 2-methylamino-2-phenyl-1,3-indandione (39) (143), spiro-diones (40) and (41) (75), spiro ketone (44) (144), (+)-sibiricine (47) (145), (+)-corydaine (48) (145), (+)-raddeanone (49) (145), (+)-yenusomidine (50) (145), (+)-yenusomine (52) (145), (+)-ochotensimine (43) (146), cancentrine (53a) (82,83), 10-oxocancentrine (53b) (147), 9,10-dihydrocancentrine methine-o-methyl ether (54) (86), and 10-oxocodeinone (55c) (147).

(+)-Canadine-8,14-d₂ (148,149):

To a stirred suspension of berberine chloride (0.89 g) in methanol (13.5 ml) and water (4 ml) was added in portions 0.11 g of sodium borodeuteride. When the addition of the sodium borodeuteride was completed the reaction mixture was then refluxed for 1/2 h, cooled, and the product (0.53 g, 64%) which precipitated from solution was filtered and recrystallized from absolute alcohol. Mass spectrum analysis indicated the following isotopic composition in the molecular ion region: d₂, 88.5%; D₁, 8.3%; d₀, 3.2%.

6-Deuterio-1-indanone (34b):

6-Amino-1-indanone (150) was diazotized and converted to its diazonium fluoborate (151). The solid fluoborate (210 mg) was added with vigorous stirring in portions to 4 ml of hypophosphorous acid-d₃ at -5 to 0°C. Stirring of the mixture was continued for fifteen minutes after addition was complete and the mixture was allowed to stand in a refrigerator for 48 hours before work up. D₂O (10 ml) was added to the reaction mixture and the mixture was extracted with chloroform, the extract dried and evaporated and the residue purified by t.l.c on alumina using CHCl₃ as eluent. The 6-deuterio-1-indanone (40 mg, 35%) so obtained gave

the following analysis by mass spectrometry: d_0 , 31%; d_1 , 69%.

^1H NMR: δ 2.75 2H,m, CH_2CO ; 3.21 2H,m, benzylic CH_2 ; 7.62 3H,m, aromatic H's.

2. NMR STUDY OF 2'-O-TETRAHYDOPYRANYLURIDYL[3'-PHENYL-5'] AND
[3'-(2,2,2-TRICHLOROETHYL)-5']2'-O-TETRAHYDOPYRANYLURIDINE:

The 220 MHz proton magnetic resonance spectra were recorded at the Canadian 220 MHz Centre, University of Toronto, Toronto, Ontario. Samples were made up in DMSO-d_6 at concentrations of 0.2 M for 57 and 58 and 0.09 M for the triesters 59-62. TMS was used as an internal reference.

Computer simulations of the ^1H spectra were performed on a Nicolet BNC-12 computer using the ITRCAL program.

Natural abundance ^{13}C spectra were obtained on a Bruker WH-90 spectrometer at 22.62 MHz. Compounds 57 and 58 were 0.38 and 0.31 M, respectively, in DMSO-d_6 . The triesters were 0.12-0.13 M in acetone- d_6 . Chemical shifts, referenced to external TMS spectra, were recorded with 16 K data points at a 5000 Hz sweep width (1.638 sec acquisition time) by using either a 3.7 μsec (17°) pulse or a 180° - τ - 90° sequence in order to eliminate the solvent peak.

Dr. T. Neilson of the Department of Biochemistry, McMaster University provided samples of the following compounds:
2'-O-tetrahydropyranyluridine (57 and 58), 2'-O-tetrahydropyranylyl-[3'-phenyl-5'] 2'-O-tetrahydropyranyluridine (59 and 60), and 2'-O-tetrahydropyranylyl[3'-(2,2,2-trichloroethyl)-5'] 2'-O-tetrahydropyranyluridine (61 and 62) (152).

3. PROTON MAGNETIC RESONANCE STUDIES ON SHORT DUPLEXES OF OLIGORIBONUCLEOTIDES:

The 90 MHz ^1H nuclear magnetic resonance spectra were recorded in the Fourier transform mode on a Bruker WH-90 spectrometer. All spectra, except those in Section 5.1, were obtained using quadrature detection and 8K data points at a 1200 Hz sweep width (3.411 sec acquisition time). The pulse width was 3 μsec (67.5° pulse angle). Probe temperatures were maintained to within $\pm 1^\circ\text{C}$ by a Bruker B-ST 100/700 variable temperature unit and were monitored by thermocouple measurements. Some spectra, mainly for confirmation purposes, were recorded at 220 MHz at the Canadian 220 MHz Centre, University of Toronto, Toronto, Ontario. The 270 MHz spectra of the mixture of CAAUG and CAUUG were obtained at the research laboratories of Eastman Kodak in Rochester, New York. Samples were lyophilized once or twice from 99.8% D_2O prior to use and were dissolved in 100% D_2O which contained 1.0 M sodium chloride and 0.01 M sodium phosphate buffer (pD = 7.0). Sample concentrations ranged from $6.1 \times 10^{-3}\text{M}$ to $1.7 \times 10^{-2}\text{M}$. *t*-Butyl alcohol- OD was used as an internal reference and the chemical shifts are reported relative to 2,2-dimethyl-2-silapentane-5-sulphonate (DSS). The deuterium signal of D_2O provided the field/frequency lock.

The following oligoribonucleotides were provided by the research group of Dr. T. Neilson of the Department of Biochemistry, McMaster University: GpA, GpApG, GpApGpC, GpCpUpC, CpA, CpApU, ApUpG, CpApUpG, CpApApUpG, CpApUpUpG, CpApUpGpA, and CpApUpGpU (153,154).

CONCLUSIONS

^{13}C nuclear magnetic resonance has been shown to be of considerable value in determining the overall structure and relative stereochemistry of several classes of isoquinoline alkaloids. The methodology of employing substituent effects, isotopic substitution, and model compound studies facilitated the assignment of the chemical shifts. The data acquired from these studies will be useful in the structural elucidation of new alkaloids and this was illustrated by the ^{13}C spectral analysis of 10-oxocantrine.

The NMR investigation of the phosphotriesters of UpU has provided information on one of the factors which affect the conformation and base stacking of a dinucleotide, namely the steric effect of large substituents on the ribose 2' carbon. This study also found evidence of a weak stacking interaction between the phenyl ester group and the uracil ring. Although NMR is one of the more effective methods for examining the solution structure of nucleic acids, precautions are still necessary in the interpretation of conformational data derived from the vicinal coupling constants.

Proton nuclear magnetic resonance can be used to follow the helix-coil transition of short strands of oligoribonucleotides. NMR is a valid method for studying this process because of the agreement between the melting temperature obtained from the NMR experiment and that predicted from extrapolation of the UV data. This also indicates that one is observing the same duplex formation over a 10^3 fold concentration range. These studies have clearly demonstrated the stabilizing effect of terminal dangling

bases. Evidence was presented to show that this stabilization arises from a base stacking interaction. This work represents the first attempt to quantify the effect of a dangling base on ribonucleotide double helix formation.

REFERENCES

1. I.I. Rabi, S. Millman, P. Kusch, and J.R. Zacharias. Phys. Rev., 55, 526 (1939).
2. F. Bloch, W.W. Hansen, and M. Packard. Phys. Rev., 69, 127 (1946).
3. F. Bloch. Phys. Rev., 70, 460 (1946).
4. F. Bloch, W.W. Hansen, and M. Packard. Phys. Rev., 70, 474 (1946).
5. E.M. Purcell, H.C. Torrey, and R.V. Pound. Phys. Rev., 69, 37 (1946).
6. W.D. Knight. Phys. Rev., 76, 1259 (1949); W.C. Dickinson, *ibid.*, 77, 736 (1950); G. Lindstrom. *ibid.*, 78, 817 (1950); W.G. Proctor and F.C. Yu. *ibid.*, 77, 717 (1950).
7. J.T. Arnold, S.S. Dharmatti, and M.E. Packard. J. Chem. Phys., 19, 507 (1951).
8. H.S. Gutowsky and D.W. McCall. Phys. Rev., 82, 748 (1951); E.L. Hahn and D.E. Maxwell. *ibid.*, 84, 1246 (1951); N.F. Ramsey and E.M. Purcell. *ibid.*, 85, 143 (1952).
9. E.L. Hahn. Phys. Rev., 80, 580 (1950).
10. R.R. Ernst and W.A. Anderson. Rev. Sci. Instrum., 37, 93 (1966).
11. T.C. Farrar and E.D. Becker. Pulse and Fourier Transform NMR. Academic Press, New York, 1971.
12. D.G. Gillies and D. Shaw. Annual Reports on NMR Spectroscopy. Vol. 5A. Edited by E.F. Mooney. Academic Press, London, 1972.
13. J.W. Cooper. Topics in Carbon-13 NMR Spectroscopy. Vol. 2. Edited by G.C. Levy. Wiley-Interscience, New York, 1976.
14. H.D.W. Hill and R. Freeman. Introduction to Fourier Transform NMR. Varian Associates, Analytical Instrument Division, Palo Alto, 1970.
15. P.C. Lauterbur. J. Chem. Phys., 26, 217 (1957).
16. C.H. Holm. J. Chem. Phys., 26, 707 (1957).

17. R.R. Ernst. *J. Chem. Phys.*, 45, 3845 (1966).
18. *Jeol News*. Vol. 12a(1). Jeol Ltd., Tokyo, 1975, p.6; *ibid.*, Vol. 13a(1), 1976, p. 3.
19. E.O. Stejskal and J. Schaefer. *J. Magn. Reson.*, 14, 160 (1974).
20. D.M. Wilson, R.W. Olsen, and A.L. Burlingame. *Rev. Sci. Instrum.*, 45, 1095 (1974).
21. J.B. Stothers. *Carbon-13 NMR Spectroscopy*, Academic Press, New York, 1972.
22. R. Ditchfield and P.D. Ellis. *Topics in Carbon-13 NMR Spectroscopy*. Vol. 1. Edited by G.C. Levy, Wiley-Interscience, New York, 1974.
23. D.M. Grant and B.V. Cheney. *J. Am. Chem. Soc.*, 89, 5315 (1967).
24. G.E. Maciel. *Topics in Carbon-13 NMR Spectroscopy*. Vol. 1. Edited by G.C. Levy, Wiley-Interscience, New York, 1974.
25. H. Beierbeck and J.K. Saunders. *Can. J. Chem.*, 53, 1307 (1975); *ibid.*, 54, 632, 2985 (1976); H. Beierbeck, J.K. Saunders and J.W. ApSimon, *ibid.*, 55, 2813 (1977).
26. D.G. Gorenstein. *J. Am. Chem. Soc.*, 99, 2254 (1977).
27. G.C. Levy and G.L. Nelson. *Carbon-13 Nuclear Magnetic Resonance for Organic Chemists*, Wiley-Interscience, New York, 1972.
28. N.K. Wilson and J.B. Stothers. *Topics in Stereochemistry*. Vol. 8. Edited by E.L. Eliel and N.L. Allinger, Wiley-Interscience, New York, 1974.
29. D.M. Grant and E.G. Paul. *J. Am. Chem. Soc.*, 86, 2984 (1964).
30. L.P. Lindeman and J.Q. Adams. *Anal. Chem.*, 43, 1245 (1971).
31. D.E. Dorman, M. Jautejat, and J.D. Roberts. *J. Org. Chem.*, 36, 2757 (1971).

32. G.E. Maciel. J. Phys. Chem., 69, 1947 (1965).
33. G.B. Savitsky, P.D. Ellis, K. Namikawa, and G.E. Maciel. J. Chem. Phys., 49, 2395 (1968).
34. D.K. Dalling and D.M. Grant. J. Am. Chem. Soc., 89, 6612 (1967).
35. F.A.L. Anet, C.H. Bradley, and G.W. Buchanan. J. Am. Chem. Soc., 93, 258 (1971).
36. T. Pehk and E. Lippmaa. Org. Magn. Reson., 3, 679 (1971).
37. J.D. Roberts, F.J. Weigert, J.I. Kroschwitz, and H.J. Reich. J. Am. Chem. Soc., 92, 1338 (1970).
38. F.J. Weigert and J.D. Roberts. J. Am. Chem. Soc., 92, 1347 (1970).
39. P.C. Lauterbur. J. Am. Chem. Soc., 83, 1846 (1961).
40. P.C. Lauterbur. Tetrahedron Lett., 274 (1961).
41. G.L. Nelson, G.C. Levy, and J.D. Cargoli. J. Am. Chem. Soc., 94, 3089 (1972).
42. D.H. Marr and J.B. Stothers. Can. J. Chem., 43, 596 (1965).
43. F.W. Wehrli and T. Wirthlin. Interpretation of Carbon-13 NMR Spectra. Heyden, New York, 1976.
44. G.A. Grey. Anal. Chem., 47, 546A (1975).
45. E.W. Hagaman. Org. Magn. Reson., 8, 389 (1976).
46. I.H. Sadler. J.C.S. Chem. Commun., 809 (1973).
47. J.B. Stothers. Topics in Carbon-13 NMR Spectroscopy. Vol. 1. Edited by G.C. Levy, Wiley-Interscience, New York, 1974; A.G. McInnes, J.A. Walter, J.L.C. Wright, and L.C. Vining. *ibid.*, Vol. 2, 1976.
48. O.A. Gansow and W. Schittgenhelm. J. Am. Chem. Soc., 93, 4294 (1971).
49. R. Freeman and H.D.W. Hill. J. Magn. Reson., 5, 278 (1971).
50. J. Feeney, D. Shaw, and P.J.S. Pauwels. J.C.S. Chem. Commun., 554 (1970).

51. B. Birdsall, N.M.J. Birdsall, and J. Feeney. *J.C.S. Chem. Commun.*, 361 (1972).
52. J.R. Lyerla, Jr., and G.C. Levy. *Topics in Carbon-13 NMR Spectroscopy*. Vol. 1. Edited by G.C. Levy, Wiley-Interscience, New York, 1974; F.W. Wehrli. *ibid.*, Vol. 2, 1976.
53. G.C. Levy. *Acc. Chem. Res.*, 6, 161 (1973).
54. E. Breitmaier, K.-H. Spohn, and S. Berger. *Angew. Chem. Internat. Ed.*, 14, 144 (1975).
55. G.C. Levy and I.R. Peat. *J. Magn. Reson.*, 18, 500 (1975).
56. R. Freeman, H.D.W. Hill, and R. Kaptein. *J. Magn. Reson.*, 7, 327 (1972).
57. W.O. Crain, Jr., W.C. Wildman, and J.D. Roberts. *J. Am. Chem. Soc.*, 93, 990 (1971).
58. T.T. Nakashima and G.E. Maciel. *Org. Magn. Reson.*, 5, 9 (1973).
59. E. Wenkert, B.L. Buckwalter, I.R. Burfitt, M.J. Gasic, H.E. Gottlieb, E.W. Hagaman, F.M. Schell, and P.M. Wovkulick. *Topics in Carbon-13 NMR Spectroscopy*. Vol. 2. Edited by G.C. Levy, Wiley-Interscience, New York, 1976.
60. T. Kametani, K. Fukumoto, M. Ihara, A. Ujiie, and H. Koizumi. *J. Org. Chem.*, 40, 3280 (1975).
61. G.S. Ricca and C. Casagrande. *Org. Magn. Reson.*, 9, 8 (1977).
62. E. Wenkert, J.S. Bindra, C. Chang, D.W. Cochran, and F.M. Schell. *Acc. Chem. Res.*, 7, 46 (1974).
63. K.S. Dhami and J.B. Stothers. *Can. J. Chem.*, 44, 2855 (1966).
64. S. Safe and R.Y. Moir. *Can. J. Chem.*, 42, 160 (1964).
65. C.K. Yu, D.B. MacLean, R.G.A. Rodrigo, and R.H.F. Manske. *Can. J. Chem.*, 48, 3673 (1970).

66. D.K. Dalling and D.M. Grant. *J. Am. Chem. Soc.*, 96, 1827 (1974).
67. D.K. Dalling, D.M. Grant, and E.G. Paul. *J. Am. Chem. Soc.*, 95, 3718 (1973).
68. R.T. LaLonde, T.N. Donvito, and A.I.-M. Tsai. *Can. J. Chem.*, 53, 1714 (1975).
69. T.T. Nakashima, P.P. Singer, L.M. Browne, and W.A. Ayer. *Can. J. Chem.*, 53, 1936 (1975).
70. M. Shamma. *The Isoquinoline Alkaloids: Chemistry and Pharmacology*, Academic Press, New York, 1972.
71. S. McLean and J. Whelan. *MTP International Review of Science*, Vol. 9, Alkaloids. Consultant editor D.H. Hey, Edited by K.F. Wiesner, University Park Press, Baltimore, 1973.
72. H.L. Retcofsky and R.A. Friedel. *Spectrometry of Fuels*. Edited by R.A. Friedel. Plenum Press, New York, 1970.
73. W. Adcock, B.D. Gupta, T.C. Khor, D. Doddrell, and W. Kitching. *J. Org. Chem.*, 41, 751 (1976).
74. S.H. Grover and J.B. Stothers. *Can. J. Chem.*, 53, 589 (1975).
75. R.H.F. Manske and Q.A. Ahmed. *Can. J. Chem.*, 48, 1280 (1970).
76. D. Zimmerman, R. Ottinger, J. Reisse, H. Christol, and J. Brugidou. *Org. Magn. Reson.*, 6, 346 (1974).
77. R.H.F. Manske, R. Rodrigo, D.B. MacLean, D.E.F. Gracey, and J.K. Saunders. *Can. J. Chem.*, 47, 3585 (1969).
78. Kh. Sh. Baisheva, D.A. Fesenko, B.K. Rostotskii, and M.E. Perel'son. *Khim. Prir. Soedin*, 6, 456 (1970).
79. T. Kametani, M. Takemura, M. Ihara, and K. Fukumoto. *Heterocycles*, 4, 723 (1976).

80. S.-T. Lu, T.-L. Su, T. Kametani, and M. Ihara. *Heterocycles*, 3, 301 (1975).
81. T.A. Crabb. *Annual Reports on NMR Spectroscopy*. Vol. 6A. Edited by E.F. Mooney, Academic Press, New York, 1975.
82. R.H.F. Manske. *Can. J. Res., Sect. B*, 7, 258 (1932).
83. G.R. Clark, R.H.F. Manske, G.J. Palenik, R. Rodrigo, D.B. MacLean, L. Baczynskyj, D.E.F. Gracey, and J.K. Saunders. *J. Am. Chem. Soc.*, 92, 4998 (1970).
84. D.B. MacLean, L. Baczynskyj, R. Rodrigo, and R.H.F. Manske. *Can. J. Chem.*, 50, 862 (1972).
85. Y. Terui, K. Tori, S. Maeda, and Y.K. Sawa. *Tetrahedron Lett.*, 2853 (1975).
86. R. Rodrigo, R.H.F. Manske, D.B. MacLean, L. Baczynskyj and J.K. Saunders. *Can. J. Chem.*, 50, 853 (1972).
87. P.O.P. Ts'o, N.S. Kondo, M.P. Schweizer, and P.D. Hollis. *Biochemistry*, 8, 997 (1969).
88. B.W. Bangerter and S.I. Chan. *J. Am. Chem. Soc.*, 91, 3910 (1969).
89. C.-H. Lee, F.S. Ezra, N.S. Kondo, R.H. Sarma, and S.S. Danyluk. *Biochemistry*, 15, 3627 (1976); *ibid.* 16, 1977 (1977).
90. I.C.P. Smith, H.J. Jennings, and R. Deslauriers. *Acc. Chem. Res.*, 8, 306 (1975).
91. T. Schleich, B.P. Cross, B.J. Blackburn, and I.C.P. Smith. *Structure and Conformation of Nucleic Acids and Protein-Nucleic Acid Interactions*. Edited by M. Sundaralingam and S.T. Rao, University Park Press, Baltimore, Md. 1975.

92. T. Schleich, B.P. Cross, and I.C.P. Smith. *Nuc. Acids Res.*, 3, 355 (1976).
93. J.L. Alderfer and P.O.P. Ts'o. *Biochemistry*, 16, 2410 (1977).
94. P.J. Cozzone and O. Jardetzky. *Biochemistry*, 15, 4853 (1976);
ibid. 4860 (1976).
95. D.G. Gorenstein, J.B. Findlay, R.K. Momii, B.A. Luxon and D. Kar. *Biochemistry*, 15, 3796 (1976).
96. P.O.P. Ts'o. *Basic Principles in Nucleic Acid Chemistry*. Vol. 2. Edited by P.O.P. Ts'o. Academic Press, New York, 1974.
97. P.O.P. Ts'o, J.C. Barrett, L.S. Kan, and P.S. Miller. *Ann. N.Y. Acad. Sci.*, 222, 290 (1973).
98. P.S. Miller, K.N. Fang, N.S. Kondo, and P.O.P. Ts'o. *J. Am. Chem. Soc.*, 93, 6657 (1971).
99. L.S. Kan, J.C. Barrett, P.S. Miller, and P.O.P. Ts'o. *Biopolymers*, 12, 2225 (1973).
100. B.J. Blackburn, A.A. Grey, I.C.P. Smith, and F.E. Hruska. *Can. J. Chem.*, 48, 2866 (1970).
101. R.A. Bell and J.K. Saunders. *Topics in Stereochemistry*. Vol. 7. Edited by E.L. Eliel and N.L. Allinger. Wiley-Interscience, New York, 1973.
102. P.H. Stothart, I.D. Brown, and T. Neilson. *Acta. Cryst.* B29, 2237 (1973).
103. F.E. Evans and R.H. Sarma. *J. Biol. Chem.*, 249, 4754 (1974).
104. C. Altona and M. Sundaralingam. *J. Am. Chem. Soc.*, 94, 8205 (1972);
ibid. 55, 2333 (1973).

105. D.B. Davies and S.S. Danyluk. *Biochemistry*, 13, 4417 (1974).
106. H.H. Mantsch and I.C.P. Smith. *Biochem. Biophys. Res. Commun.*, 46, 808 (1972).
107. R.U. Lemieux, T.L. Nagabhushan, and B. Paul. *Can. J. Chem.*, 50, 773 (1972).
108. E.M. Nottoli, J.B. Lambert, and R.L. Letsinger. *Org. Mag. Reson.*, 9, 499 (1977).
109. C. Altona. *Structure and Conformation of Nucleic Acids and Protein-Nucleic Acid Interactions*. Edited by M. Sundaralingam and S.T. Rao. University Park Press, Baltimore, Md. 1975.
110. M. Karplus. *J. Am. Chem. Soc.*, 85, 2870 (1963).
111. D.R. Kearns. *Ann. Rev. Biophys. Bioeng.*, 6, 477 (1977).
112. D.R. Kearns and R.G. Shulman. *Acc. Chem. Res.*, 7, 33 (1974).
113. D.B. Arter, G.C. Walker, O.C. Uhlenbeck, and P.G. Schmidt. *Biochem. Biophys. Res. Commun.*, 61, 1089 (1974).
114. P.N. Borer, L.S. Kan, and P.O.P. Ts'o. *Biochemistry*, 14, 4847 (1975).
115. L.S. Kan, P.N. Borer, and P.O.P. Ts'o. *Biochemistry*, 14, 4864 (1975).
116. T.R. Krugh, J.W. Laing, and M.A. Young. *Biochemistry*, 15, 1224 (1976).
117. B. Dudock, C. DiPeri, K. Scileppi, and R. Reszelback. *Proc. Nat'l. Acad. Sci. U.S.A.*, 68, 681 (1971).
118. T.E. England and T. Neilson. *Can. J. Biochem.*, 55, 365 (1977).
119. P.O.P. Ts'o, J.L. Alderfer, P.N. Borer, and L.S. Kan. *Structure and Conformation of Nucleic Acids and Protein-Nucleic Acid Interactions*. Edited by M. Saundaralingam and S.T. Rao, University Park Press, Baltimore, Md., 1975.

120. J.A. Elvidge, J.R. Jones, C. O'Brien, E.A. Evans, and H.C. Sheppard. J. Chem. Soc., Perkin II, 1889 (1973); *ibid.* 2138 (1973); *ibid.* 174 (1974).
121. I. Tinoco Jr., O.C. Uhlenbeck, and D.M. Levine. Nature, 230, 362 (1971).
122. F.H. Martin, O.C. Uhlenbeck, and P. Doty. J. Mol. Biol., 57, 201 (1971); *ibid.* 57, 217 (1971).
123. H. Grosjean, D.G. Söll, and D.M. Crothers. J. Mol. Biol., 103, 499 (1976).
124. D.W. Appleby and N.R. Kallenbach. Biopolymers, 12, 2093 (1973).
125. N.R. Kallenbach and H.M. Berman. Quart. Rev. Biophysics, 10, 138 (1977).
126. C. Giessner-Prettre, B. Pullman, P.N. Borer, L.-S. Kan, and P.O.P. Ts'o. Biopolymers, 15, 2277 (1976).
127. K. Biemann. Pure Appl. Chem., 9, 95 (1964).
128. W.M. Whaley and M. Meadow. J. Chem. Soc., 1067 (1953).
129. F.D. Popp and W.E. McEwen. J. Am. Chem. Soc., 79, 3773 (1959).
130. K. Knabe. Arch. Pharm., 292, 652 (1959).
131. G. Grethe, H.L. Lee, M. Uskokovic, and A. Brossi. J. Org. Chem., 33, 494 (1968).
132. M.A. Marshall, P.L. Pyman, and R. Robinson. J. Chem. Soc., 1315 (1934).
133. J.W. Wilson, C.L. Zirkle, E.L. Anderson, J.J. Stehle, and G.E. Ullgot. J. Org. Chem., 16, 792 (1951).
134. S.N. Chakravarti. J. Ind. Chem. Soc., 20, 382 (1943).
135. J. Tirouflet. Bull. Soc. Sci. Bretagne, 26, 7 (1951); Chem. Abstr. 47, 8692 g (1953).
136. C.W. Ferry, J.S. Buck, and R. Baltzly. Org. Synth. Coll. Vol. 2, 239 (1955).

137. D.W. Hughes, H.L. Holland, and D.B. MacLean. *Can. J. Chem.*, 54, 2252 (1976).
138. R.H.F. Manske, R. Rodrigo, D.B. MacLean, and L. Baczynskyj. *An. Quim.*, 68, 689 (1972), and references therein.
139. I.H. Sadler. *J. Chem. Soc. (B)*, 1024 (1969).
140. W.H. Perkin and R. Robinson. *J. Chem. Soc.*, 105, 2388 (1914).
141. B. Nalliah, Q.A. Ahmed, R.H.F. Manske, and R. Rodrigo. *Can. J. Chem.*, 50, 1819 (1972).
142. F. Nathanson. *Chem. Ber.*, 26, 2576 (1893).
143. E. Ya. Ozola, Ya.Ya. Ozol, A.K. Aren, and G. Ya. Vanag. *Zh. Org. Khim.*, 4, 88 (1968).
144. B. Nalliah, R.H.F. Manske, R. Rodrigo, and D.B. MacLean. *Tetr. Letters*, 2795 (1973).
145. B.C. Nalliah, D.B. MacLean, R.G.A. Rodrigo, and R.H.F. Manske. *Can. J. Chem.*, 55, 922 (1977).
146. R.H.F. Manske. *Can. J. Res.*, 18B, 75 (1940).
147. H.L. Holland, D.W. Hughes, D.B. MacLean, and R.G.A. Rodrigo. Submitted for publication to *Can. J. Chem.* In press.
148. I. Sallay and R.H. Ayers. *Tetrahedron*, 19, 1397 (1963).
149. R. Mirza. *J. Chem. Soc.*, 4400 (1957).
150. C.K. Ingold and H.A. Piggot. *J. Chem. Soc.*, 123, 1469 (1923).
151. D.T. Flood. *Org. Synth. Coll. Vol. 2*, 295 (1943).
152. E.S. Werstiuk and T. Neilson. *Can. J. Chem.*, 50, 1283 (1972).
153. T.E. England and T. Neilson. *Can. J. Chem.*, 54, 1714 (1976).
154. R.J. Gregoire and T. Neilson. *Can. J. Chem.*, 56, 487 (1978).